Child, Hannah (2012) Nanoparticles for biomedical applications. PhD thesis
http://theses.gla.ac.uk/3583/

Nanoparticles for Biomedical Applications

Hannah Winifred Child

For the degree of Doctor of Philosophy

June 2012
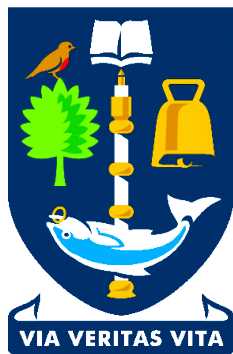
Centre for Cell Engineering

College of Medical, Veterinary and Life Sciences

University of Glasgow

UK, G12 8QQ

Abstract

Modern day medicine is on the brink of a new age of therapy, which aims to harness the natural power of molecular biology for disease treatment. This therapy could include replacement of dysfunctional genes that cause disorders such as cystic fibrosis (Lommatzsch and Aris, 2009), or silencing the over-expression of genes that cause disorders such as cancer (Pelengaris and Khan, 2003). In both examples, the treatment of these genetic diseases lies in the delivery of synthetic nucleic acids into diseased cells, the former being called gene replacement therapy (Dobson, 2006a), and the latter being called RNA interference (RNAi) therapy (Whitehead *et al.*, 2009). While these techniques have long been in use as genetic research tools for gene transfection or silencing *in vitro*, their translation for use in clinical disease treatment has yet to be achieved. The main problem facing the development of these novel therapies is the specific delivery of nucleic acids into diseased cells within the body. It is hoped that nanoparticles (NPs) can be used to overcome this problem, by acting as vehicles to transport nucleic acids through the body for specific delivery into diseased cells. This feat can be aided by the attachment of additional functional molecules such as cell penetrating peptides (CPPs), targeting peptides, additional drug types and molecules for imaging during treatment. Many different NP design strategies are currently under development. It is essential for new designs to be extensively tested for toxicity and efficiency in human cells before they can be successfully released into the clinic.

As part of this effort, this PhD project has investigated two different NP design strategies for drug delivery: 1) the use of a magnetic field (MF) and a CPP to increase the delivery of iron oxide magnetic NPs (mNPs) to cells grown in tissue-equivalent 3D collagen gels, and 2) gold NPs (AuNPs) for the delivery of siRNA to silence the c-myc oncogene for cancer treatment. In the first investigation, a MF and the CPP penetratin were found to increase mNP delivery to cells grown in 3D. In the second investigation, AuNPs were assessed in a range of different cell types (grown in 2D) for their performance in 4 main areas; cellular toxicity, cellular uptake, c-myc knockdown and effect on the cell cycle.

Table of Contents

Chapter 1 Introduction

Chapter 2 Materials and Methods

Chapter 3 Delivery of Iron mNPs to Cells in 3D

Chapter 4 Cellular Response to AuNPs

Chapter 5 c-myc Knockdown in HeLa Cells

Chapter 6 Discussion

List of Tables

List of Figures

Dedication

I would like to dedicate this thesis to my Dad, without whom it wouldn't exist. His love, kindness, support, wisdom, humour and bravery have been a joy to experience throughout my life. In particular, I am forever grateful for his unrivaled and selfless devotion to his children during my late teenage years during what was our darkest hour. His effort to fill our broken home with happiness and to put a hot and nutritious meal on the table every night after school undoubtedly saved us.

Acknowledgement

I would like to thank my supervisor Dr Catherine Berry for giving me the opportunity to do this PhD and for her patience and encouragement throughout. I would also like to thank Carol-Anne Smith for being the invaluable glue holding our lab together! She was a great technical support to me in every aspect of my PhD who never grumbled despite my head popping into her office nearly every day to ask her questions. She also provided great friendship to me and we shared wads of laughter while filling up the liquid nitrogen together.

Thanks to Dr Monica Tsimbouri for the huge amount of time and help she kindly gave me whenever I needed it. Her expertise in molecular biology greatly helped me on the long struggle to get my PCR and Western blots to work.

I would like to thank everyone else in CCE who made it such a fantastic and positive environment to work in. In particular I would like to thank Jemma and Diana for their friendship. We naturally formed a trio and our nights out, gym sessions and tea breaks made the last three years much sweeter for me.

Finally I would like to thank my fiancé David for his loving support during my PhD. This has included coming to get me and driving me home in the wee hours after late night experiments, listening to my endless scientific ramblings and letting me turn his living room into an office during my write up.

Author's Declaration

I hereby declare that the research reported within this thesis is my own work, unless otherwise stated, and that at the time of submission is not being considered elsewhere for any other academic qualification.

Hannah Child

20th June 2012

Abstracts and Publications

Original research publications authored by the candidate on work relating to this thesis.

Child HW, del Pino PA, De La Fuente J, Hursthouse AS, Stirling D, Mullen M, McPhee GM, Nixon C, Jayawarna V, Berry CC: Working together: the combined application of a magnetic field and penetratin for the delivery of magnetic nanoparticles to cells in 3D. ACS Nano. (2011) **5:** 7910-7919

Child HW, Hernandez Y, Conde J, Baptista PV, de la Fuente JM, Berry CC: Knockdown of c-myc in HeLa Cells; mRNA through to Cell Proliferation (manuscript in preparation)

Conde J, Ambrosone A, Sanz V, Hernandez Y, Marchesano V, Tian F, Child HW, Berry CC, Ibarra MR, Baptista PV, Tortiglione C, de la Fuente JM: Design of Multifunctional Gold Nanoparticles for *in vitro* and *in vivo* Gene Silencing. *Nature Nanotechnology* (submitted)

Conference Proceedings

2010   **Nanotoxicology**
             'A novel 3D model for the study of functionalised-nanoparticle penetration into human tissue'. *Edinburgh, UK* (poster presentation)

2010   **CDTM (Cellular Delivery of Therapeutic Macromolecules)**
             'A novel 3D model for the study of functionalised-nanoparticle penetration into human tissue'. *Cardiff, UK* (poster presentation)

2011   **TERMIS**
             'Working together: the combined application of a magnetic field and penetratin for the delivery of magnetic nanoparticles to cells in 3D' *Granada, Spain* (oral presentation)

Definitions

µg	microgram
µl	microlitre
µm	micrometer
Abs	absorbance
AFM	atomic force microscopy
AMD	age-related macular degeneration
AuNP	gold nanoparticle
BrdU	**5-Bromo-2'-deoxyridine**
BSA	bovine serum albumin
CFTR	cystic fibrosis transmembrane conductance regulator
CPP	cell penetrating peptide
CDP	cyclodextran-based polymer
c.m	c-myc
COOH	carboxylic acid
Da	Dalton
DLS	dynamic light scattering
DME	diabetic macular edema
DMEM	dulbecco's modified eagle medium
DMSO	dimethyl sulfoxide
dox	doxycycline
dsRNA	double stranded RNA
EBV	Epstein-Barr virus
ECL	enhanced chemical luminescence
ECM	extracellular matrix
EDTA	ethylenediaminetetraacetic acid
EGFP	enhanced green fluorescent protein
EGFR	epidermal growth factor receptor
EM	electron microscopy
EPR	enhanced permeability and retention
FACs	fluorescence-activated cell sorting
FBS	fetal bovine serum
FITC	fluorescein isothiocyanate
G'	elastic modulus

G″	viscous modulus
GAPDH	glyceraldehyde-3-phosphate dehydrogenase
GFP	green fluorescent protein
H&E	haematoxylin & eosin
HA	hyaluronic-acid
HEK	human epidermal keratinocytes
Hepes	4-(2-hydroxyethyl)-1-piperazineethanesulfonic acid
HIV	human immunodeficiency virus
HNP	hybrid magnetic nanoparticle
HRP	horseradish peroxidase
Hz	hertz
ICP-MS	inductively coupled plasma mass spectrometry
IFN	interferon
IgG	immunoglobulin G
kDa	kiloDalton
kPa	kiloPascal
Lipo	Lipofectamine 2000
MCS	myc core signature
MES	2-(N-morpholino)ethanesulfonic acid
MF	magnetic field
MRI	magnetic resonance imaging
mNP	magnetic nanoparticle
mRNA	messenger RNA
MSB	martius scarlet blue
MSCs	mesenchymal stem cells
mT	millitesla
MTT	(3-(4,5-Dimethylthiazol-2-yl)-2,5-diphenyltetrazolium bromide
N3	azide
NIR	near-infrared
nm	nanometer
NP	nanoparticle
n.s	nonsense
nt	nucleotide
PBS	phosphate buffered saline
PBS-T	PBT-Tween

PCR	polymerase chain reaction
PEB	protein extraction buffer
PEG	polyethylene glycol
PEI	polyethylenimine
PLA	polylactic acid
Pol III	RNA polymerase III
qRT-PCR	quantitative real-time PCR
QD	quantum dot
RES	reticuloendothelial system
RGD	arginine-glycine-asparagine tripeptide
RISC	RNA-induced silencing complex
RNAi	RNA interference
RSV	respiratory syncytial virus
SD	standard deviation
SDS	sodium dodecyl sulphate
SDS-PAGE	SDS-polyacrylamide gel electrophoresis
SEM	scanning electron microscopy
shRNA	short hairpin RNA
siRNA	small interfering RNA
SNALPs	stable nucleic acid lipid particles
sulfo-SMCC	sulfosuccinimidyl 4-[N-maleimidomethyl]cyclohexane-1-carboxylate
T	tesla
TEM	transmission electron microscopy
TNF	tumor necrosis factor
UWS	University of the West of Scotland
VEGF	vascular endothelial growth factor
w/v	weight (of solute) per volume (of solvent)
w/w	weight per weight

1 Introduction

1.1 Genetic Disease

Many human diseases are caused by incorrect expression of one or more genes. For example cystic fibrosis is an autosomal recessive disorder caused by mutations in the gene encoding the cystic fibrosis transmembrane conductance regulator (CFTR) (Lommatzsch and Aris, 2009). Similarly, Huntington's disease is an autosomal dominant disorder caused by mutations in the Huntingtin gene (Walker, 2007), and Duchenne muscular dystrophy is an x-linked recessive disorder caused by mutation in the dystrophin gene (Odom *et al.*, 2010). In addition to these quite rare single gene disorders, one of the most common genetic diseases is cancer; which accounts for approximately 13% of all deaths annually across the globe (Ferlay *et al.*, 2010). Curing diseases that have a known genetic cause is now one of the main targets of nanomedicine, and it is envisaged that nanoparticles (NPs) will play a major role by facilitating the delivery of novel oligonucleotide-based therapeutics into diseased cells to either replace dysfunctional genes or to reduce those that are expressed in overabundance. Whilst the number of genetic diseases that NPs can potentially target is extensive, this thesis will mainly focus on their use in the treatment of cancer.

1.1.1 Cancer

Cancer is a disease of unregulated cell growth, where cells divide and grow uncontrollably, resulting in the formation of tumours. The earliest written record of cancer dates back to 3000BC when a description of breast cancer was included in the Ancient Egyptian medical text, the Egyptian Edwin Smith Papyrus (Hajdu, 2011). Since then, many different theories have been proposed as to the causes of cancer, although after the discovery of DNA and the ensuing revolution of molecular biology, and in particular advances in proteomics and genomics, it is now clear that cancer is caused by genetic mutations in genes that regulate cell division. Of the 30,000 genes within the human genome, around 2% of these are involved in the formation of cancer (Santarius *et al.*, 2010). Such genes include those involved in cell cycle control, apoptosis, DNA repair, ageing and immortalisation, angiogenesis, invasion and metastasis (Pawaiya *et al.*, 2011).

These cancer-related genes can be split into two main categories; oncogenes and tumour suppressor genes. Genes that promote the cell cycle are termed proto-oncogenes, which induce cancer when they become oncogenes upon the acquisition of an upregulating mutation that leads to their overexpression. Around 90 oncogenes have so far been identified, including growth factors (*sis*), growth factor receptors (*K-sam*), tyrosine kinases (*Src*), G-protein coupled receptors, G-proteins (*gsp*), serine/threonine kinases (*akt*) and transcription factors (*c-myc*) (Pawaiya *et al.*, 2011).

Conversely, tumour suppressor genes inhibit the cell cycle, inducing cancer when they acquire a downregulating mutation that leads to their underexpression. Around 30 tumour suppressor genes have so far been identified, including those that function to control the cell cycle (Rb, PTEN, and APC), repair DNA damage (BRCA1, and BRCA2), and induce apoptosis (p53) (Pawaiya *et al.*, 2011).

1.1.2 The c-myc Oncogene

c-myc is one if the most studied oncogenes. It was first identified in early studies of chicken tumours caused by avian myelocytomatosis retroviruses. Publications emerged in 1979 reporting that the transforming gene found within the RNA genome of these retroviruses had been identified (Duesberg and Vogt, 1979; Hu *et al.*, 1979), and that this nucleotide sequence had homology to DNA and RNA from uninfected vertebrate cells (Sheiness and Bishop, 1979). After the discovery that cancer could be caused by viral myc (v-myc) in chickens, it was realised in 1982 that the homologous gene found in vertebrate cells (c-myc) was causally implicated in non-viral induced cancers in humans. This was based on the finding that human c-myc was consistently altered in Burkitt lymphoma by balanced chromosomal translocation (Dallafavera *et al.*, 1982; Taub *et al.*, 1982). Since then, c-myc has been found to be translocated in multiple myeloma and is one of the most highly amplified oncogenes identified in many different human cancers (Beroukhim *et al.*, 2010a).

c-myc encodes a transcription factor and has been described as an intermediate to mass signal transduction through the cell. In normal cells, the expression of c-

myc is tightly controlled throughout all stages of the central dogma. For example, the expression of c-myc is regulated at the levels of transcription by a host of transcription factors and DNA structures, translation by microRNA, protein by phosphorylation, and finally the cellular effect of c-myc is inhibited by feedback loops involving genes such as Arf and p53. Once transcribed, c-myc dimerises with another transcription factor called max, and the c-myc/max dimmer binds to DNA at the canonical c-myc E box 5'-CACGTG-3', which activates the expression of many target genes (Liao and Dickson, 2000) (see Figure 1-1). Genome wide studies have tried to determine the exact number of c-myc target genes. In 2003, Li *et al* described c-myc as a 'global transcription factor', after they used 4,839 promoter sequences to map c-myc-binding sites, and found that 15% bound to c-myc (Li *et al.*, 2003). This corresponds to another genome-wide study performed by Zeller *et al* in 2006, which used ChiP-PET to map c-myc binding sites, and found that although 6000 genes bound c-myc, only 700 of these responded to c-myc activation with alterations in their mRNA levels (Zeller *et al.*, 2006). This highlights that many of c-myc's targets also require the binding of other transcription factors in addition to c-myc before they can be activated. More recently, microarray analysis performed by Ji *et al* has identified a 50 gene c-myc core signature (MCS), which is considered to constitute the main targets of c-myc (Ji *et al.*, 2011). In his 2012 review of the literature, Dang concludes that the body of work that has aimed to identify c-myc targets suggests that c-myc functions as a master regulator affecting a broad spectrum of genes to coordinate energy metabolism with biomass accumulation in preparation for DNA replication and cell division (Dang, 2012). Due to the central role this oncogene plays in regulation of the cell cycle, teamed with the fact that it is so frequently found to be overexpressed in cancer cells, c-myc presents as a very promising candidate for targeted gene therapy to treat cancer, since normalising its expression should normalise the increased cell division associated with tumour formation.
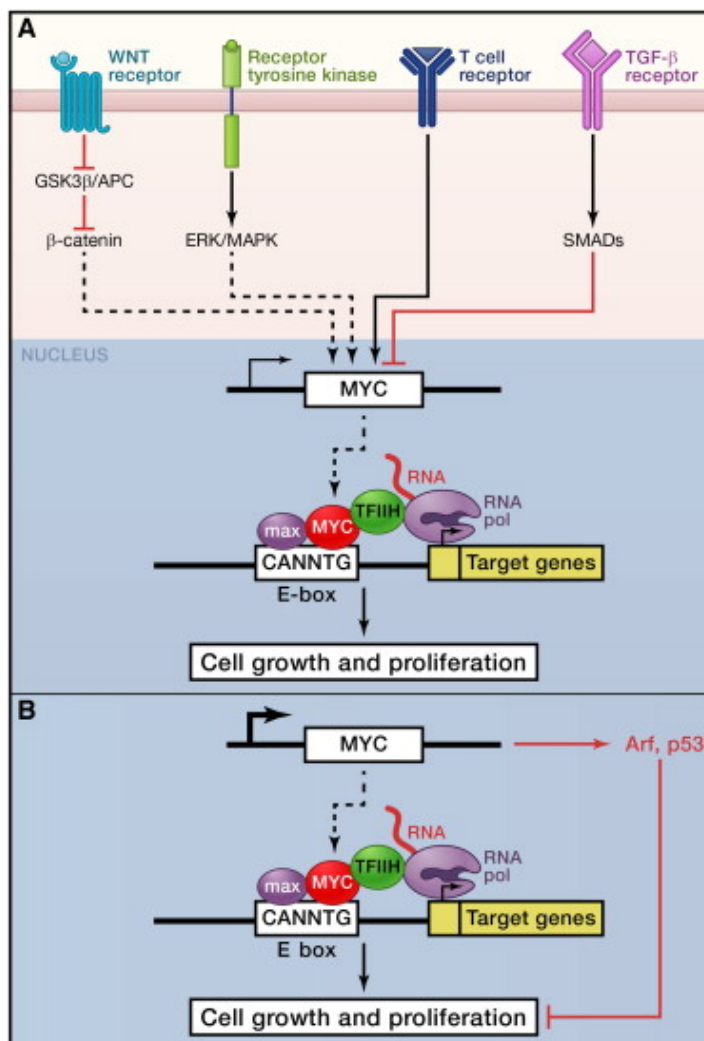
Figure 1-1 c-myc regulates cell growth and proliferation
A) Mitogenic signaling pathways, mediated by cell-surface receptors, regulate c-myc
expression. Once expressed, the c-myc protein acts as a transcription factor and dimerises
with max in order to bind the E-box domain of many target genes. c-myc/max activation
leads to the transcription of the target genes, many of which are involved in cell growth and
proliferation. B) The action of c-myc is negatively regulated by the tumour suppressor
genes Arf and p53. Image from (Dang, 2012).

1.1.3 Cancer Treatment

1.1.3.1 Traditional Approach

Due to increased understanding of the genes and pathways involved in regulating
the cell cycle and the formation of cancer, medical research now has a much
greater chance of curing this disease than in the past. The main goal of cancer
treatment is to either kill or arrest cancer cell division, without affecting
surrounding healthy cells and tissue. Traditional cancer treatment has involved
administering chemotherapeutic drugs into the patient's bloodstream.
Chemotherapy was first used to treat cancer patients in 1946, when Gilman *et al*

administered tris (ß-chloroethyl) amine hydrochloride (derived from mustard gas) to 6 cancer patients, which resulted in regression of the cancer (Gilman and Philips, 1946). Chemotherapeutic drugs work by killing rapidly dividing cells, such as cancer cells. However, the main drawback is that they are indiscriminate, and will also kill any other rapidly dividing cells found within the body including those in hair follicles, bone marrow and the digestive tract, which leads to undesirable side effects such as hair loss, immunosuppression and mucositis (inflammation of the digestive tract). Common chemotherapeutic drugs used in modern chemotherapy to date include docetaxel, doxorubicin, pacilitaxel and fluorouracil, all of which interfere with cell division.

1.1.3.2 Targeted Therapy

It is now understood that in order to overcome the deleterious side effects associated with chemotherapy drugs, new medications will need to be designed which are specific to cancer cells. This approach has been termed 'targeted therapy' and aims to inhibit the proliferation of cancer cells by interfering with specific molecules that are essential for tumour growth. This includes the use of oligonucleotide-based gene correction therapies such as RNA interference (RNAi), which aim to reduce cancer cell specific oncogene overexpression (e.g. c-myc), in addition to new small molecule drugs. The development of targeted therapeutics for the treatment of cancer has been advanced by the current knowledge base of cancer genetics, and also an increasing awareness of cancer cell behaviour. One of the most cited descriptions of cancer cell behaviour is that of Hanahan and Weinberg, who in 2000 published a list of the "6 hallmarks of cancer" (Hanahan and Weinberg, 2000), and in 2010, expanded upon this list by publishing a description of 10 acquired cancer cell capabilities necessary for tumour growth, which can thus pose as targets for new therapeutics. This included targeting cancer cells' sustained proliferative signaling with epidermal growth factor receptor (EGFR) inhibitors, their avoidance of immune destruction with immune activating anti-CTLA4 mAb, their induction of angiogenesis with inhibitors of vascular endothelial growth factor (VEGF) signaling and their resistance of cell death with proapoptotic BH3 mimetics (Hanahan and Weinberg, 2011). This highlights the clinical potential of developing new cancer drugs to target the unique physiological aspects of cancer cell behaviour caused

by the extensive alterations to gene expression within these diseased cells. All targeted therapeutics, including oligonucleotides and small molecule drugs, are candidates for NP-mediated delivery to cancer cells.

1.1.4 Oncogene Addiction

A recently proposed theory with big implications for targeted cancer therapy is that of oncogene addiction, whereby cancer cells become dependent on the expression of one main oncogene. This phenomenon has been described as the 'Achilles heel of cancer', and anticipates that rather than requiring correction of the many complex genetic pathways involved, cancer can instead be challenged by targeted therapy to reduce the expression of one key oncogene (Weinstein, 2002). Studies have shown that c-myc is one of the major oncogenes to which cancer cells can become addicted, and that in some cases, a brief suppression of c-myc is sufficient to reverse *in vivo* tumourigenesis. For example, Jain *et al* used a conditional transgenic mouse model for c-myc-induced tumourigenesis where c-myc transcription was activated upon doxycycline (dox) treatment, to investigate the effect of pharmacological inactivation of c-myc as a therapeutic strategy for cancer. They reported that brief inactivation of c-myc expression with dox treatment caused osteogenic sarcoma cells to differentiate into mature osteocytes. Interestingly, this study found that upon reactivation of c-myc expression by removing dox treatment, 99% of the tumour cells did not regain their neoplastic growth properties (Jain *et al.*, 2002). The authors hypothesise that this unexpected prolonged anti-cancer effect was due to the fact that brief oncogene inactivation can induce epigenetic changes that revoke its ability to maintain tumourigenesis. This experimental evidence, that cancer cells can be made to regress upon the reduction of c-myc expression, clearly identifies c-myc as a potential candidate for targeted therapy. Of course in a clinical setting, oncogenes cannot be inactivated by dox treatment, and so oligonucleotide-based gene correction therapies such as RNAi present as the best method for targeted inactivation of oncogenes, which can be facilitated by NP-mediated delivery to cancer cells.

1.2 RNAi for Targeted Therapy Against Oncogenes

RNAi is a naturally occurring cellular mechanism for gene silencing induced by RNA molecules that have complementarity to the target gene's mRNA. The action of RNAi is highly conserved across all species and is believed to have evolved from a defense mechanism against viruses and genetic instability arising from mobile genetic elements such as transposons *(Kurreck, 2009)*. In its natural context, RNAi is mediated by the transcription of double-stranded RNA (dsRNA), >30 nucleotides (nt) in length, which gets exported into the cytoplasm by the nuclear export receptor, Exportin-5 (Ohrt *et al.*, 2006; Lommatzsch and Aris, 2009). Once in the cytoplasm, these dsRNAs get cleaved by the ribonuclease enzyme, DICER, into 21-23nt fragments, thereafter named small interfering RNAs (siRNAs) (Bernstein *et al.*, 2001; Elbashir *et al.*, 2001). These siRNA molecules get loaded into the RNA-induced silencing complex (RISC) (Rand *et al.*, 2004), become single stranded (Matranga *et al.*, 2005), and bind complementary mRNA (Ameres *et al.*, 2007). Argonaute 2, a multifunctional protein found within RISC, cleaves the bound mRNA between nucleotides 10 and 11 (relative to the 5' end) (Whitehead *et al.*, 2009). This renders it unable to continue through the central dogma and be translated into protein. Thus the process of gene silencing by RNAi becomes complete (see Figure 1-2).
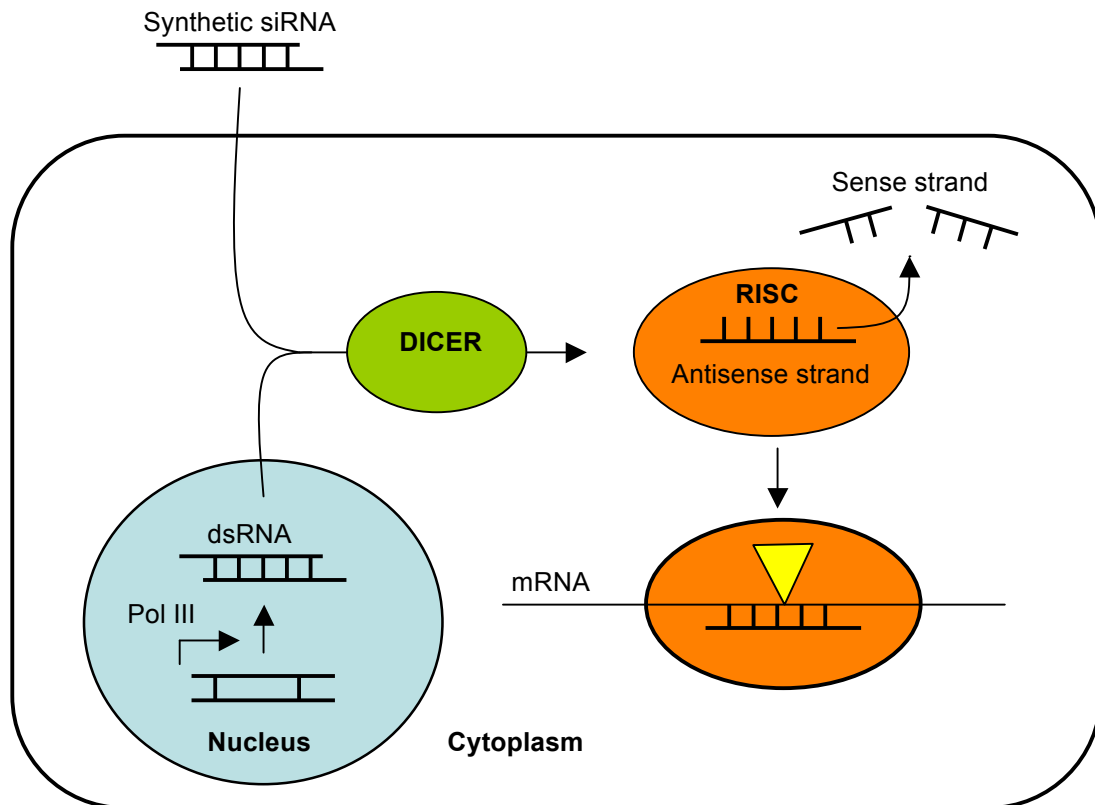
Figure 1-2 Simplified schematic of the mechanism of mammalian RNAi
Natural RNAi is mediated by the transcription of dsRNA in the nucleus by RNA Polymerase III. This dsRNA gets exported into the cytoplasm, cleaved by DICER, and incorporated into RISC. The sense strand is removed, and the remaining antisense strand activates RISC. Activated RISC then finds and cleaves mRNA with complementarity to the antisense strand. This cleavage prevents the mRNA from being translated into protein. Synthetic siRNA can be artificially transfected into the cytoplasm, where it gets processed by the natural RNAi machinery to prevent translation of a target mRNA. Image modified from (Kurreck, 2009).

The fact that RNA could induce gene silencing was first identified in plants in 1990, being originally termed 'co-suppression' and incorrectly attributed to the already established and similar mechanism of antisense gene silencing (Napoli *et al.*, 1990; Vanderkrol *et al.*, 1990). Eight years later, Fire and Mello proved that this RNA-based silencing phenomenon was in fact distinct from antisense gene silencing. They elucidated that eukaryotic cells perceive dsRNA as a sequence specific signal to inhibit expression of the corresponding mRNA (Fire *et al.*, 1998). In light of this discovery they were awarded the Nobel Prize in Physiology or Medicine in 2006 (Zamore, 2006). In their original experiments, Fire and Mello achieved potent and specific gene silencing in *C.elegans* after dsRNA molecules, 742nt in length, were injected directly into nematodes. In the immediate years following this pioneering work, many studies continued to demonstrate that long dsRNAs >30nt, similar to those used by Fire and Mello, could also induce gene silencing in other eukaryotic organisms, such as *D.melanogaster* (Kennerdell and Carthew, 1998), and plants (Hamilton and Baulcombe, 1999). This demonstrated

that RNAi was very highly conserved across species, which lead researchers to envisage that it could also be adopted to silence gene expression in humans. However, it was found that the long dsRNAs that had been used in the original group of RNAi studies invoked a severe interferon (IFN) immune response in mammalian cells (Manche *et al.*, 1992), rendering them useless for gene silencing in humans. This problem was solved in 2001, when Thomas Tuschl *et al,* discovered that artificial, synthetic dsRNA molecules of approximately 21nt in length were sufficiently long to perform gene silencing in mammalian cells, but small enough to prevent an IFN immune response (Elbashir *et al.*, 2001). This key finding demonstrated that RNAi could be exploited artificially to silence gene expression in human cells, facilitated by the transfection of synthetic, exogenous 21-23nt siRNA molecules.

Artificial RNAi has the potential to be used for many applications, and is already a multimillion dollar business (Castanotto and Rossi, 2009). Primarily, RNAi became a universal research tool for gene knockdown studies (Gondi and Rao, 2009), fueled by the fact that RNAi holds numerous advantages over traditional methods of gene knockdown. This includes having a broader target range than classical small-molecule inhibitory drugs (Whitehead *et al.*, 2009), since any gene of known sequence can be silenced by appropriately designed siRNA (Huang *et al.*, 2008). RNAi is also less toxic than chemical inhibitors, and less time-consuming than constructing dominant negative mutants (Huang *et al.*, 2008). These advantages have also led RNAi to emerge as an attractive therapeutic tool for targeted therapy of human genetic disease caused by abhorrent gene expression (Kurreck, 2009), such as cancer.

Therapeutic RNAi involves the transfection of mammalian cells with siRNA designed with complementarity to a target gene. These siRNA molecules can then use the inherent cellular RNAi machinery within the cytoplasm to silence that target gene by cleaving its mRNA (as depicted in Figure 1-2). Cells can alternatively be transfected with vector-based siRNA (shRNA), which provides a more stable and longer-lasting silencing effect (Shi, 2003; Huang *et al.*, 2008). As such, RNAi is now being heralded as a promising strategy that can meet the medical need for *in vivo* inactivation of key oncogenes such as c-myc for cancer treatment. The progress of clinical RNAi therapy from bench to bedside has

moved amazingly fast, with a gap of only 6 years between the initial discover of this technology in 1998 and the first RNAi-based clinical trial which was conducted in 2004 by Acuity Pharmaceuticals. This trial involved direct administration of a siRNA therapeutic (termed Cand5) into the eye, to reduce expression of the VEGF receptor as a treatment for patients with wet age-related macular degeneration (AMD), a leading cause of adult blindness. This siRNA treatment has since reached phase III clinical trials, and has been reported to improve near vision and lesion size (Bumcrot *et al.*, 2006). Acuity Pharmaceuticals have also since begun another clinical trial using Cand5 to treat patients with diabetic macular edema (DME). The eye has been a popular choice in the development of RNAi-based therapeutics, and siRNA against the VEGF receptor has also entered Phase II clinical trials under Merck-siRNA Therapeutics, with reports suggesting it to be well tolerated and to improve visual acuity. Another popular choice of disease target for RNAi has been the lungs, with siRNA (termed ALN-RSV01) to treat respiratory syncytial virus (RSV) infections entering Phase II clinical trials under Alnylam Pharmaceuticals. ALN-RSV01 aims to treat patients by reducing viral replication, and is the first antiviral siRNA to enter clinical trials (Castanotto and Rossi, 2009).

The reason why the eye and the lungs have been the main focus of pharmaceutical companies for RNAi therapeutics over other tissues, is that they present as easily accessible sites for direct administration of siRNA. Unfortunately, administering siRNA to less accessible sites within the body, such as deep solid tumours is more difficult since these sites cannot be reached by direct injection or inhalation. These sites must instead be reached by systemic delivery of siRNA *via* intravenous injection, after which the siRNA can be carried to the target site of disease within the body by the blood stream; a significant challenge to the success of this novel therapeutic strategy.

Systemic delivery of siRNA suffers from three main problems; 1) naked oligonucleotides have a short half-life inside the human body due to enzymatic degradation by nucleases within the bloodstream (Dykxhoorn and Lieberman, 2005); 2) they have no way of distinguishing between diseased and healthy cells, leading to nontargeted tissue distribution (Derfus *et al.*, 2007); and 3) they cannot easily cross cell membranes (Akhtar *et al.*, 1991; Wittung *et al.*, 1995).

Bumcrot *et al* attribute this lack of cellular uptake to the fact that siRNA molecules do not adhere to the 'Lipinski Rules'; a set of criteria that ascribes to most small-molecule pharmaceutical drugs. In particular, these rules state that drugs must have high lipophilicity and molecular weight less than 500 Dalton (Da) to be effective. In stark contrast, siRNA naturally lacks these drug-like properties due to their large size (two turns of a nucleic acid double helix), nearly 40 anionic charges provided by the phosphodiester backbone, and high molecular weight (over 13kDa) (Bumcrot *et al.*, 2006). siRNA also suffers from a range of more acute systemic delivery problems including rapid excretion by the kidney (Gao *et al.*, 2009), poor vascular permeability, difficult extracellular matrix (ECM) diffusion, and clearance by phagocytes of the reticuloendothelial system (RES) (Barry, 2008; Juliano *et al.*, 2008). At the subcellular level, siRNA delivery problems include poor endocytotic uptake and inefficient endosomal escape (Juliano *et al.*, 2008).

Unfortunately, due to this range of problems, naked siRNA molecules have very limited practical use in systemic delivery for disease treatment. Therefore, if widescale therapeutic RNAi is to become a reality, a protective and multifunctional delivery vehicle must be developed that can overcome these problems to administer siRNA molecules into human cells *in vivo*.

1.3 Delivery Vehicles for siRNA

The first clinical RNAi cancer trial in humans was conducted in 2006 and aimed to treat human glioblastoma multiforme brain tumors (Zukiel *et al.*, 2006). This study concluded that while direct, local injection of siRNA did successfully inhibit cancer, systemic siRNA administration *via* a delivery vehicle would maximize its therapeutic potential. Mounting evidence clearly shows that attachment to a delivery vehicle aids systemic siRNA administration, by imparting desirable pharmacokinetic properties to the siRNA molecule and promoting its cellular uptake in tissues (Bumcrot *et al.*, 2006). Various delivery vehicles have proved successful, including liposome delivery of siRNA to treat liver cirrhosis (Sato *et al.*, 2008), human papilloma-virus (Niu *et al.*, 2006) and ovarian cancer (Halder *et al.*, 2006). Also, atelocollagen delivery of siRNA has been used to treat bone cancer (Takeshita *et al.*, 2005).

In 2004, Soutschek *et al* reported that conjugation to cholesterol enhanced the pharmacokinetic and cellular uptake properties of systemically delivered siRNA in mice, resulting in reduction of the target mRNA (ApoB) by 57% and 73% in the liver and jejunum respectively, after intravenous injection (Soutschek *et al.*, 2004). However, following this success, in 2006 Zimmerman *et al* reported that conjugation to stable nucleic acid lipid particles (SNALPs) produced an even greater silencing of ApoB in mice than was attained in the earlier study using cholesterol-conjugated siRNA, demonstrating that NPs are a more effective type of siRNA delivery vehicle. In addition, the authors used SNALP delivery to achieve a 90% reduction in ApoB mRNA in non-human primates (Zimmermann *et al.*, 2006), proving the feasibility of using NP-mediated delivery of siRNA in humans.

Recent work by Kovtun *et al* reported that triple-shelled, biodegradable, calcium phosphate NPs carrying siRNA, enabled increased transfection and gene silencing compared to both naked siRNA and Polyfect (Kovtun *et al.*, 2009). This study further demonstrates the huge potential of NPs as an effective delivery vehicle for siRNA.

1.4 Nanoparticles (NPs)

NPs are defined as submicron colloidal particles ranging in size from 10 to 1000nm (Bosselmann and Williams; Rao *et al.*, 2004). Many types of NPs are currently being developed as prospective siRNA delivery vehicles. Those composed of organic polymers include liposomes (Torchilin, 2005), dendrimers (Lee *et al.*, 2005) and carbon nanotubes (Polizu *et al.*, 2006), while those composed of non-organic polymers include quantum dots (Medintz *et al.*, 2005), magnetic (Lu *et al.*, 2007) and gold NPs (Huang *et al.*, 2007; Sanvicens and Marco, 2008). NPs have many unique and advantageous chemical and physical properties inherently associated with their size. Sanvicens and Marco have listed these properties as optical, magnetic, catalytic, thermodynamic and electrochemical (Sanvicens and Marco, 2008). Furthermore, NPs have an advantageous high surface-volume ratio, are multivalent, and carry both inherent and tailored multifunctional properties, allowing them to overcome

many of the problems associated with systemic siRNA delivery. For example, NPs inherently extend the half-life of siRNA molecules circulating within the blood stream by preventing rapid excretion by the kidney - a fate that succumbs naked siRNA molecules (Soutschek *et al.*, 2004; Derfus *et al.*, 2007; Juliano *et al.*, 2008).

In 2010, Nature published results from the first human phase I clinical trial involving the systemic administration of siRNA to patients with solid cancers using a targeted, nanoparticle delivery system (Davis *et al.*, 2010). This study used a multifunctional delivery vehicle, featuring a cyclodextran-based polymer (CDP) NP, stabilised with polyethylene glycol (PEG), and functionalised with transferrin and siRNA. Biopsies revealed that after intravenous injection, the NPs accumulated within tumours, and were located intracellularly. In addition, quantitative real-time PCR (qRT-PCR) and Western blot analysis demonstrated reduced levels of the target mRNA and protein after treatment. The authors proved that this reduction in target gene expression was caused by siRNA-mediated mRNA cleavage, since they observed mRNA fragments of the correct size to support site-specific cleavage by RNAi. This pioneering study has proved that reduction of oncogene expression in tumours by RNAi is possible in humans, mediated by NP systemic delivery. Furthermore, it is an excellent example of how tailored NP multifunctionality can be used to improve the success of NP-mediated siRNA delivery.

1.4.1 Tailored Nanoparticle Multifunctionality

Aside from the inherent protection and increased half-life that attachment to a NP provides, NPs also offer a second level of systemic delivery assistance to siRNA molecules, as they can confer multifunctional properties *via* attachment of different surface groups. Popular functional groups that are currently used to aid NP delivery include cell-penetrating peptides (CPPs) (Meade and Dowdy, 2008), such as the human immunodeficiency virus (HIV)-1 Tat peptide (Berry, 2008), which enhance cell uptake. In addition, targeting ligands are used to allow cell selective recognition, by binding to receptors that are expressed on target cell membranes (Howard, 2009). Many targeting ligands against cancer cells are postulated, as cancer cells have a unique pattern of receptor

overexpression that is distinct from normal cells. Such targeting ligands include folate (Leamon and Low, 1991), transferrin (Davis *et al.*, 2010) and the integrin-binding Arg-Gly-Asp (RGD) tripeptide (Arap *et al.*, 1998; Singh *et al.*, 2009). The majority of NP designs include the attachment of organic oligomers, such as PEG, which increases NP stability and therapeutic efficiency (Howard *et al.*, 2008). The attachment of PEG (termed PEGylation) has been shown to inhibit phagocytotic clearance of NPs since it reduces opsonisation (the process of plasma protein adsorbtion to material, leading to its phagocytosis) (Juliano *et al.*, 2008).

The success of NP-mediated cell-targeted siRNA delivery was demonstrated by Kim *et al*, who reported that attachment of folate and PEG to polyethylenimine (PEI) NPs caused a ~3-fold increase in gene silencing compared to unmodified PEI NPs, when applied to folate-expressing cells (Kim *et al.*, 2006). Similarly, in an *in vivo* murine study, Schiffelers *et al* reported that PEI-PEG NPs, functionalised with RGD could deliver siRNA to cancer cells, resulting in silencing of the VEGF R2 oncogene and a subsequent reduction in tumour angiogenesis and growth rate (Schiffelers *et al.*, 2004). These studies exemplify that NP multifunctionality is a very useful tool to enhance the success of systemic siRNA delivery.

1.4.2 Multivalency

A further advantage of NPs, compared to other types of delivery vehicles, is that they are multivalent. This property allows NPs to be functionalised with many different siRNAs and peptides at once, potentially allowing multiple gene knockdowns, higher affinity for the target cell and ultimately more powerful disease treatment (Juliano *et al.*, 2008). Indeed, Paciotti *et al* believe that tailoring vectors to deliver multiple therapeutic agents is of the utmost importance to their effectiveness as a cancer treatment (Paciotti *et al.*, 2006). This is because, as has been discussed in earlier reports (Spremulli and Dexter, 1983; Dexter *et al.*, 1978), solid tumours are composed of heterogeneous cell populations. Therefore the future development of multi-targeting NPs is deemed necessary in order for them to effectively destroy the diverse populations of cells found within typical tumours (Paciotti *et al.*, 2006). This could entail the attachment of multiple siRNAs able to knockdown a range of oncogenes, possibly

in combination with the attachment of various anti-cancer drugs, such as paclitaxel (Iwase *et al.*, 2006), and tumor necrosis factor (TNF) (Helson *et al.*, 1975).

Interestingly, Derfus *et al* analysed the optimal number of siRNA and cancer targeting peptides that could be accommodated by covalent attachment on a single NP, in this case PEGylated quantum dots (QDs). They reported that one siRNA per particle in conjunction with >15 peptides, or two siRNA per particle in conjunction with <10 peptides gave optimal knockdown and targeting (Derfus *et al.*, 2007). This study highlights the importance of identifying the optimal load requirements of each NP when designed with multiple functional molecules.

A study by Song *et al* demonstrated the effectiveness of using multiple siRNAs for cancer treatment (Song *et al.*, 2005). This study targeted siRNAs against three oncogenes: MDM2, c-myc, and VGEF; which were all bound to a fusion protein for systemic murine delivery. MDM2 is an inactivator of p53 (Halaby and Yang, 2007), c-myc promotes cell proliferation (De Nigris *et al.*, 2006), and VGEF is a tumour secreted growth factor that mediates angiogenesis and metastasis (Grothey, 2006). This three-fold siRNA design resulted in reduced melanoma cell proliferation. This work was taken a step further in a recent study by Li *et al* that demonstrated the use of siRNAs against the same three oncogenes, this time bound to liposome-based NPs (Li *et al.*, 2008). These multi-siRNA NPs were injected into a murine lung cancer model, and caused simultaneous silencing of the three target genes. The authors compared the anti-cancer effect of NP-bound siRNA, to free siRNA. Remarkably, a ~70-80% decrease in lung metastasis was reported after siRNA-NP treatment, compared to little effect after free siRNA treatment. Secondly, the mice that were given the siRNA-NP injection showed a 30% increase in survival time compared to untreated controls. These results support the use of NPs to deliver siRNA, and the results from both Li *et al* and Song *et al* promote the effectiveness of using multiple oncogene knockdowns simultaneously.

1.4.3 Theranostics

In addition to the attachment of therapeutic molecules, such as siRNA; dyes and fluorescent molecules can also be attached to NPs, allowing imaging for diagnostics. Indeed, it is now becoming a widespread belief that multifunctional NPs can be used to supply both therapy and diagnosis, as a novel "theranostic" siRNA delivery platform (Derfus *et al.*, 2007; Lee *et al.*, 2009b). This approach is reliant on NPs being able to: 1) specifically target a disease site within the human body; 2) allow for that site to be diagnostically imaged; and 3) deliver a therapeutic treatment (e.g. siRNA).

In 2007 Medarova *et a*l reported the development of magnetic NPs that became localised inside tumours, delivered covalently attached siRNA into cancer cells, and were detectable by imaging (Medarova *et al.*, 2007). These NPs were functionalised with a myristoyl-coupled polyarginine peptide to facilitate membrane translocation. Subsequent imaging was two-fold; *via* attachment of a near-infrared dye (Cy5.5) to allow noninvasive near-infrared (NIR) imaging and also by magnetic resonance imaging (MRI), mediated by the magnetic nature of the NPs. The authors deduced that the NP tumour-accumulation observed during imaging was probably due to the enhanced permeability and retention (EPR) effect associated with the leaky vasculature of tumours. This study concluded that NPs further functionalised with tumour-targeting moieties would increase tumour localisation in order to deliver siRNA treatment.

Derfus *et al* have reported the development of theranostic quantum dot (QD) NPs, capable of tumour localisation, siRNA delivery and imaging (Derfus *et al.*, 2007). In this particular design, tumour targeting was facilitated by the attachment of a tumour-homing peptide (F3), which binds to nucleolin expressed on the surface of cancer cells (Christian *et al.*, 2003). This addition of F3 increased QD tumour cell uptake by 2 orders of magnitude compared to non-targeting QDs. Diagnostic imaging was facilitated by the photostable QD core with emission in the near-infrared (NIR). The attached siRNA silenced the enhanced green fluorescent protein (EGFP) gene, but the authors noted that their theranostic design could also be applied to silence oncogenes for cancer treatment. The siRNA conjugation chemistry was also investigated in this paper,

comparing a cleavable disulphide bond with covalent attachment. The former demonstrated higher knockdown, presumably due to an increase in siRNA-RISC interaction as the disulphide bond is cleaved once inside the reducing environment of the cell. This clarifies the importance of such acute attention to molecular design in the development of an efficient NP-based theranostic RNAi platform.

A recent study by Lee *et al* provides an example of another type of theranostic multifunctional NP that utilised the disulphide bond cleavage for siRNA release, in this case with a magnetic NP (Lee *et al.*, 2009b). In this design, tumour selectivity was facilitated by the attachment of a cyclic RGD peptide, and PEGylation of this targeting peptide increased NP stability. Diagnostic imaging was facilitated by the magnetic nature of the NP, which could be visualized by MIR, and further by the attachment of a Cy5 near-infrared dye that could be visualized by NIR. Treatment delivery was facilitated by the attachment of siRNA to silence the green fluorescent protein (GFP). Interestingly, the authors state that their magnetic NPs provided better targeting and reduced toxicity compared to the popular delivery vehicle polyethyleneimine (PEI), famous for its "proton sponge" method of endosomal escape. This study concluded that joining the tasks of diagnosis and treatment in future *in vivo* and clinical applications will reduce invasiveness and side effects (Lee *et al.*, 2009b).

1.4.4 Choice of NP Material

1.4.4.1 Gold NPs (AuNPs)

Gold has been used in medicine since ancient times to treat a range of ailments (Chen Pc, 2008). During the 19th century, gold was used to treat nervous disorders, depression, epilepsy, migraine and glandular problems (Richards *et al.*, 2002). In modern medicine, gold is commonly used in pacemakers, dental restoration and the treatment of rheumatoid arthritis (Chen Pc, 2008). Colloidal gold NPs (AuNPs) were first synthesised in 1857 by Michael Faraday (Faraday, 1857; Paciotti *et al.*, 2006), however the method described by Brust *et al* (Brust *et al.*, 1994) is traditionally one of the most popular methods for AuNP synthesis (De La Fuente *et al.*, 2006a). In 1950 it was discovered that AuNPs could bind

protein biologics without affecting their activity, leading to their later use in immunodiagnostics and histopathology (Chandler *et al.*, 2001). AuNPs were first used for biological applications in 1971, when Frank and Taylor devised the immunogold staining procedure (De La Fuente and Berry, 2005). In the 1990s, AuNPs found a role as scaffolds for DNA diagnostics and biosensors (Mirkin *et al.*, 1996). Paciotti *et al* have concluded that based on this historical data, and their own toxicology studies, AuNPs are relatively inert and biologically compatible delivery vehicles (Paciotti *et al.*, 2006). Due to this biological compatibility teamed with their distinct optical properties, AuNPs have become powerful tools in various nanomedical applications (Chen Pc, 2008). For example, a 2003 study by Hirsch *et al* demonstrated thermal ablation of solid tumors using gold coated silica NPs that had been tuned to absorb light in the near infrared (NIR) (Hirsch *et al.*, 2003). Once internalised inside cancer cells, exposure to NIR light caused localised AuNP heating that killed the surrounding cancer cells, a process now termed intracellular hyperthermia therapy (or thermal ablation).

Much research has highlighted the potential use of gold as a multi-functional NP for RNAi therapeutics. This potential is due to many factors, including low cytotoxicity (Connor *et al.*, 2005), easy size control (Daniel and Astruc, 2004), and well-developed surface chemistry for dense loading of functional groups (Love *et al.*, 2005; Lee *et al.*, 2009a). A study by Braun *et al* demonstrated gene silencing using AuNPs functionalised with the CPP Tat to enable cell entry, and siRNA against the reporter gene GFP (Braun *et al.*, 2009). The authors used a pulsed NIR laser for the dual purposes of both siRNA-NP detachment and subsequent endosomal escape, allowing the free siRNA to become incorporated into RISC for efficient gene silencing. It is considered that future studies on AuNPs for RNAi therapy should focus on investigation of oncogene knockdown efficiency, and also NP cytotoxicity. This latter point is deemed very important because, somewhat in contradiction to the reported biocompatibility of gold, organogold compounds such as auranofin have been associated with toxic side effects including proteinuria and skin reaction during its use in arthritis patients (Chen Pc, 2008). Indeed, Chen *et al* state that more needs to be done to better our understanding of the pharmacokinetics and toxicological profiles of AuNPs (Chen Pc, 2008).

1.4.4.2 Iron, Magnetic Nanoparticles (mNPs)

Iron is another excellent choice of material from which to fabricate therapeutic NPs, since the magnetism it bestows is very useful for systemic drug delivery. The main benefits of magnetism are that it allows the movement of mNPs to be controlled by an externally applied magnetic field, and it also enables mNPs to be imaged within the body by MRI. The literature suggests that mNPs composed of iron oxide are ideal for systemic drug delivery since they display good biocompatibility (Jain *et al.*, 2008), strong magnetism (Corchero and Villaverde, 2009), useful imaging properties (such as MRI) (Wu *et al.*, 2010), ease of functionalisation and have been extensively researched *in vitro* (Dobson, 2006a).

Magnetic targeting of drug delivery vehicles was first demonstrated by Widder *et al* in 1978, when they showed that iron oxide microspheres loaded with the chemotherapeutic drug adriamycin could be injected into rat tails, and directed to a target site elsewhere in the body where a magnet had been externally placed. This resulted in intracellular accumulation of the drug at the site of the magnet, which was comparable to that achieved by administration of a 100-fold higher dose of the free drug (Widder *et al.*, 1978a). This early study, and many more since, have demonstrated the huge potential of mNPs for magnetically targeted systemic drug delivery.

1.4.5 NP Uptake and Intracellular Processing

In order for therapeutic NPs to cause gene silencing by RNAi, their cellular internalisation and subsequent cytoplasmic delivery of siRNA are essential. This is because the RNAi machinery, with which the delivered siRNA must associate (DICER and RISC), is located in the cytoplasm. Endocytosis is the main route for NPs to achieve cell internalisation. Three types of this process can occur: 1) phagocytosis, 2) pinocytosis (a.k.a. fluid-phase endocytosis), and 3) receptor-mediated endocytosis (Berry *et al.*, 2004b) as shown in Figure 1-3.

Endocytosis
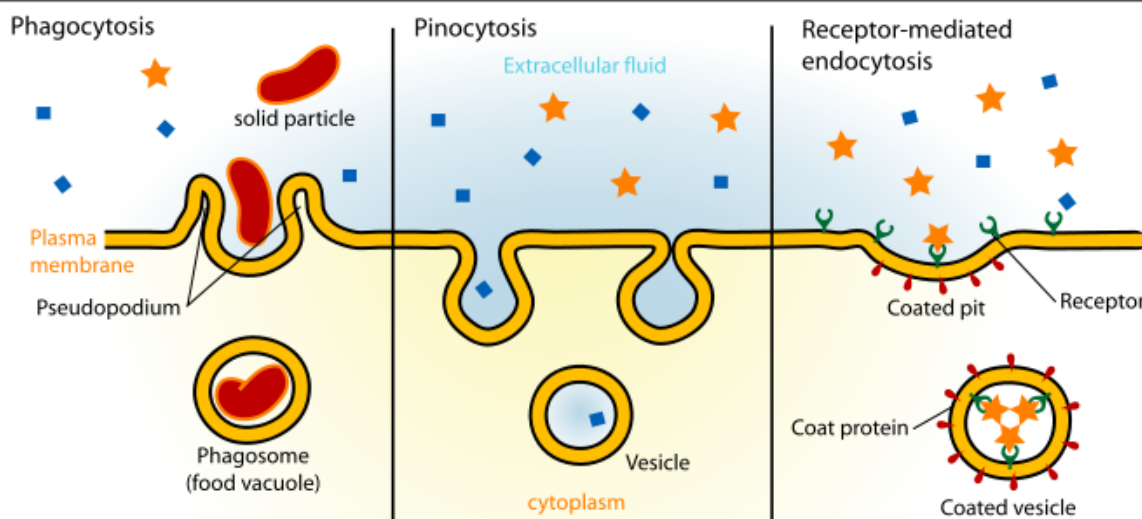
Figure 1-3 Mechanisms of endocytosis
This figure outlines the three main mechanisms of endocytosis; phagocytosis, pinocytosis and receptor-mediated endocytosis. These natural cellular uptake mechanisms can be exploited for the uptake of therapeutic nanoparticles. (Image freely available from Mariana Ruiz Villarreal).

All forms of endocytosis involve membrane invagination. In addition, pinocytosis and receptor-mediated endocytosis also involve clathrin- or caveolin- coated pit formation, detachment of the newly formed vesicle *via* the action of the small GTPase dynamin, and finally movement of the vesicle, termed the endosome, into the cytosol (Schafer, 2002). Endocytosis is a very efficient process; however, it can lead to undesirable fates for therapeutic NPs. For example, endosomes fuse with lysosomes, which have a destructive chemical environment that can degrade siRNA. Also, material contained within lysosomes is designated to be removed from the cell, in a process called exocytosis. Therefore, it seems clear that endosomal escape must take place before endo-lysosomal fusion, if therapeutic NPs are to deliver their siRNA payload into the cytoplasm (see Figure 1-4).
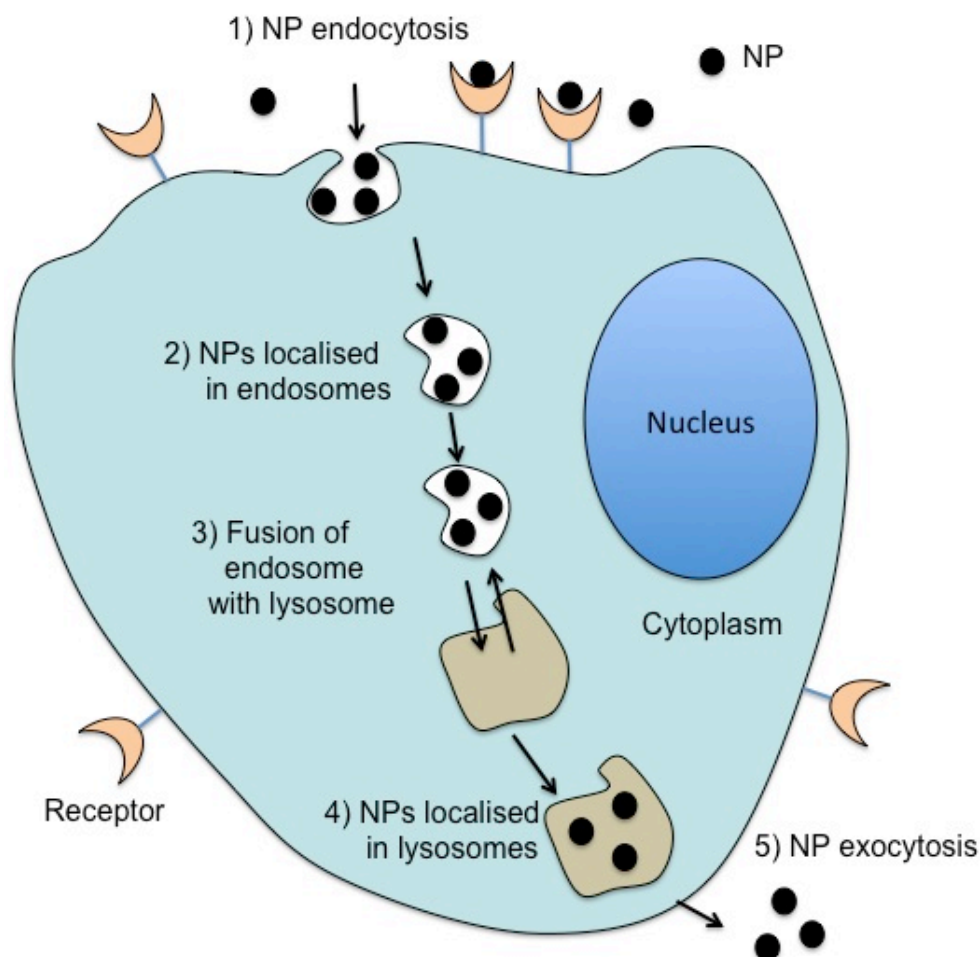
Figure 1-4 The cellular endo-lysosomal pathway of nanoparticles
This simplified schematic outlines the 5 main steps involved in the endo-lysosomal pathway of nanoparticles (NPs) through the cell. 1) Binding of NPs to cell-surface receptors causes membrane invagination. 2) This membrane invagination results in an endosome containing NPs. 3) Endosomes fuse with lysosomes. 4) This endo-lysosomal fusion results in a lysosome containing NPs. The destructive chemical environment of the lysosome can degrade siRNA. 5) Lysosomes fuse with the plasma membrane, expelling their contents out of the cell in a process called exocytosis. Therapeutic NPs must avoid/escape this endo-lysosomal pathway if they are to successfully deliver their siRNA payload into the cytoplasm to cause gene silencing by RNAi. Image modified from (Chithrani *et al.*, 2009).

The requirement for cytoplasmic siRNA delivery, coupled with interest in nanotoxicology, has lead to increased research into NP uptake and intracellular processing. It has been widely reported that NP uptake is dependent on size and surface properties (Chithrani *et al.*, 2009). For example, Verma and Stellacci reported that 50nm was the optimal NP size for efficient cellular uptake (Verma and Stellacci, 2010). In addition, they identified that spherical particles were taken up 500% more than rod-shaped particles of similar sizes. Cho *et al* found that NPs with a positive surface charge showed higher levels of endocytosis compared to both negatively and neutrally charged NPs (Cho *et al.*, 2009), as they display the highest affinity for the negatively charged plasma membrane,

encouraging membrane invagination. A series of studies by Berry *et al* have reported differing NP-cell interactions depending on NP surface moiety. For example, AuNPs aggregated if functionalised with tiopronin, induced endocytosis if functionalised with ethylenediamine, and adhered to cells if functionalised with PEG (De La Fuente *et al.*, 2006b). In a separate study, NPs functionalised with dextran induced deleterious alterations in cell behaviour and morphology, such as apoptosis and decreased cell motility, believed to be due to the large chains used in the study as dextran is typically inert (Berry *et al.*, 2004b). In another study, NPs functionalised with transferrin localised at the cell membrane, without instigating the expected receptor-mediated endocytosis, and produced positive increases in proliferation, cytoskelaton organisation, cell signaling and production of extracellular matrix (Berry *et al.*, 2004a). In a further study, AuNPs functionalised with a Tat-protein-derived peptide sequence localised inside the nucleus (De La Fuente and Berry, 2005). This string of studies demonstrates the considerable influence of NP surface groups on their uptake and intracellular processing.

The fact that Berry *et al* achieved NP localisation in the nucleus suggests that those NPs must have escaped the endo-lysosomal pathway. However, there are currently no reliable and well-understood methods to achieve this essential feat, and therefore endosomal escape remains a large hurdle preventing the success of NP-mediated siRNA delivery (Nativo *et al.*, 2008). Nativo *et al* investigated this problem by conducting a transmission electron microscopy (TEM) study of the uptake of 16nm surface-modified AuNPs into human fibroblast cells (Nativo *et al.*, 2008). They reported that the endosomal route of cellular uptake could be bypassed by delivering the NPs *via* 2 uptake strategies: 1) liposome delivery, and 2) functionalisation with cell penetrating peptides (CPPs). Both of these uptake strategies resulted in the presence of free NPs within the cytosol. NPs delivered in liposomes appeared to enter the cytosol either by caveolar-clathrin-dependent pathways, or directly across the plasma membrane. NPs functionalised with CPPs appeared to enter the cytosol either by endosomal escape, or directly through the plasma membrane. The observation that CPP-functionalised NPs allow endosomal escape was supported by the fact that NPs within the cytosol were found in association with membrane-like structures that the authors believed could be destroyed endosome. It should also be noted that

the observation that CPP-functionalised NPs directly cross the plasma membrane could possibly be an artefact of cell fixation. This is in relation to a study by Richard *et al,* which reported that cell fixation can lead to the artificial uptake of CPPs (Richard *et al.*, 2003).

Nativo *et al* concluded that further studies will be needed to optimise particle delivery. They believe that this optimisation will involve finding the ideal composition of NP surface moieties in order to facilitate therapeutic RNAi. It is essential that this optimisation strategy involves nanotoxicity testing of the functionalised NPs, in order to avoid the induction of deleterious cell responses, and to ensure NP safety for human administration.

1.4.6 Nanotoxicology

In 2004, The Royal Society and The Royal Academy of Engineering published a report on the opportunities and uncertainties regarding nanoscience and nanotechnologies. This report concluded that NPs should be treated as new chemicals from a risk point of view, as they can overcome the body's normal protective barrier due to their small size (Royalsociety, 2004). This type of cautious perspective has led to the emergence of nanotoxicology, a new discipline that aims to investigate the safety of nanotechnologies. This includes assessment of the risks involved with exposure to nanomaterials, investigations into the routes of NP entry into organisms, and studies into the molecular mechanisms of NP toxicity (Fischer and Chan, 2007; Oberdorster *et al.*, 2005). There is currently a huge demand for nanotoxicological studies to be completed as NP research is rapidly translating into clinical use. This demand is amplified by growing public concern and awareness regarding NPs in everyday life (e.g. in sunscreens and cosmetics) and their impact on human health (Miller, 2006). Sanvicens and Marco acknowledge that the few risk-evaluating studies that have been performed with NPs to date have yielded inconclusive results; reporting effects at the cellular, subcellular, protein and gene levels (Sanvicens and Marco, 2008). For example, Sayes *et al* found that nano-C60 particles disrupted the plasma membrane (Sayes *et al.*, 2005), whereas Lovric *et al* found that unmodified QDs damaged the plasma membrane, mitochondria and nucleus (Lovric *et al.*, 2005). In contrast to these studies, Qian *et al* reported no toxicity

or physiological complications when PEGylated AuNPs were administered to nude mice (Qian *et al.*, 2008). However, Su *et al* reported a dose-dependent toxic effect when Au-nanoshells were administered to BALBc mice (Su *et al.*, 2007). Conner *et al* have voiced concerns that due to the size similarity of AuNPs to biological matters, they could be disguised against cellular barriers and gain unintended entry into cells, leading to toxic side effects (Connor *et al.*, 2005). In relation to this idea, Pan *et al* have reported that AuNP cytotoxicity is size dependent (Pan *et al.*, 2007). This latter study systematically investigated the effect of AuNP size on four cell lines: HeLa cervix carcinoma epithelial cells, Sk-Mel-28 melanoma cells, L929 mouse fibroblast, and J774A11 mouse monocytic/macrophage cells. They found that AuNPs 1-2nm in size displayed cell type dependent cytotoxicity, whereas in another study, AuNPs 15nm in size did not (Chen Pc, 2008). Other investigations have suggested that NP toxicity is related to various factors, including cationic side chain attachment (Goodman *et al.*, 2004), concentration (Kirchner *et al.*, 2005), geometry (Cui *et al.*, 2005) and surface modifications (Hoshino *et al.*, 2007). In relation to AuNPs, Conner *et al* have concluded that their toxicity varies depending on the nature of the NP surface coating (Connor *et al.*, 2005; Sanvicens and Marco, 2008). Sanvicens *et al* conclude that NPs must be analysed on a particle-to-particle basis using a strategy that tests adsorption, distribution, metabolism and excretion, together with physiochemical and toxicological *in vitro* and *in vivo* studies (Sanvicens and Marco, 2008). Crosera *et al* conclude that the classic investigation protocols must be adapted and re-standardised to the new nanosized compounds (Crosera *et al.*, 2009).

1.4.7 3D Research

During the past decade, the majority of nanotoxicology research has focused on 2D cell culture systems (Fischer and Chan, 2007). However, Fischer *et al* suggest that the data from these studies could be misleading and will require verification from animal studies (Fischer and Chan, 2007). This is because 2D cell systems do not adequately mimic the 3D environment of healthy and tumour tissues (Balis, 2002). It is becoming apparent that understanding the relationship between the nanostructure and its *in vivo* behaviour are essential when assessing, and predicting nanotoxicity (Fischer and Chan, 2007). An elegant

solution to this requirement of lengthy and expensive *in vivo* nanotoxicity testing is to use human tissue equivalents as an alternative to animal testing. An established example of this strategy is the use of fibroblast-seeded collagen gels. Bell *et al* first published the use of fibroblast-seeded collagen gels in 1979, demonstrating the cell-mediated contraction of the matrix into a denser, 'tissue-like' structure (Bell *et al.*, 1979). Since then, many researchers have replicated these findings, including R.A. Brown (Hadjipanayi *et al.*, 2009; Marenzana *et al.*, 2002), M. Eastwood (Eastwood *et al.*, 1998), F. Grinnell (Grinnell *et al.*, 1999b; Grinnell *et al.*, 2003; Grinnell *et al.*, 1999a; Grinnell, 2003) and C.C. Berry (Berry *et al.*, 2003; Berry *et al.*, 2009b). It is only very recently, however, that such cell-seeded collagen gels have been adopted for use in nanotoxicity testing. For example, Mertsching *et al*, have developed a 3D skin equivalent model that is physiologically comparable to natural skin (Mertsching *et al.*, 2008) and suitable for toxicity studies. This model is composed of primary human keratinocytes on a collagen substrate containing human dermal fibroblasts. It is grown at the air-liquid interface, facilitating complete epidermal stratification and epidermal-dermal interactions to occur. The authors state that this *in vitro* skin equivalent will be an excellent model for toxicity testing, tumor modeling, infection testing, and wound healing (Mertsching *et al.*, 2008).

1.5 Future Perspective

With the advent of RNAi, gene replacement therapy and a host of new small molecule drugs, achieving the correct delivery of these novel therapeutics to diseased cells within a patient's body still remains a major hurdle to achieving targeted disease treatment. NPs are set to facilitate this delivery, since they provide inherent protection, tailored multifunctionality, multivalency and theranostics. These qualities are allowing the development of very complex and clever NP designs for systemic delivery, which can protect therapeutic cargo from degradation during circulation within the bloodstream, recognise the correct disease cells *via* the binding of targeting moieties, facilitate cell uptake by CPPs, provide imaging by dyes or MRI, induce thermal ablation of tumours by NIR, and promote drug release once inside diseased cells. Needless to say, the design of NP-delivery systems is progressing well. These designs now need to

undergo extensive testing within human cell lines and suitable *in vivo* models, to ensure they function as intended. Before NP-mediated delivery of novel therapeutics (such as siRNA) can be routinely performed in the clinic, much more needs to be learnt about the cellular interactions of NPs in terms of toxicity, uptake, drug efficiency and effect of treatment on disease progression. Once these issues are resolved, widescale NP-mediated targeted disease treatment will no doubt become a reality.

1.6 Aims

This PhD has involved two separate projects, each investigating a different NP delivery system in order to assess their potential to be used for *in vivo* drug delivery. The first project focused on iron mNP delivery in 3D, and the second project focused on AuNPs for c-myc knockdown by RNAi.

Aims of Project 1: Iron mNP Delivery in 3D
- To develop and characterise cell-seeded Type 1 collagen gels as a tissue-equivalent 3D cell culture system for the testing of NP delivery into tissue.
- To determine if a magnetic field and the CPP penetratin can be used to increase the delivery of 100 and 200nm iron oxide mNPs to cells growing within 3D collagen gels.

Aims of Project 2: AuNPs for c-myc Knockdown by RNAi
- To assess the therapeutic potential of a range of AuNP formulations, featuring stepwise addition of PEG, Tat and c-myc siRNA, as were synthesised by grant partners. AuNPs were assessed in 2D monolayer cell culture on the basis of 4 main criteria; cellular toxicity, cellular uptake, c-myc knockdown and effect on the cell cycle.

2 Materials and Methods

2.1 Materials

2.1.1 Atomic Force Microscopy (AFM)

Silica microsphere 4.8μm	**Microparticles GmbH, Berlin**
Tipless silicon nitride cantilever	**Arrow-TL1, NanoWorld**
UV curable glue	**Loctite 349**
AFM, NanoWizard II Bio	**JPK Instruments, Berlin**

2.1.2 Antibodies

Primary Antibodies

- Anti-c-myc antibody [9E10]   **Abcam**
  ChIP Grade (ab32) (murine)

Used in Western blot at 1:500

- Anti-GAPDH Rabbit Monoclonal   **Epitomics**
  antibody (clone EPR6256)

Used in Western blot at 1:10,000

- Amersham Monoclonal anti-   **GE Healthcare**
  Bromo-deoxyuridine
  (clone BU-1) (murine)

 Used to detect BrdU at 1:100

Secondary Antibodies

- Goat anti-mouse IgG-HRP (sc-2032)   **Santa Cruz Biotechnology**

Used in Western blot (c-myc) at 1:4000

- Goat anti-rabbit IgG-HRP (sc-2030)   **Santa Cruz Biotechnology**

Used in Western blot (GAPDH) at 1:4000

- Biotinylated anti-mouse   **Vector Laboratories, Inc**

Used in BrdU assay at 1:50

Tertiary Antibodies

- Streptavidin-FITC   **Vector Laboratories, Inc**

Used in BrdU assay at 1:50

2.1.3 Cell Culture

Trypsin	**Sigma**
Versine	**(made in house)**
Fetal Bovine Serum (FBS)	**Lonza**
10x DMEM	**Sigma**
Type 1 collagen	**First Link UK Ltd**
0.1M NaOH (liquid)	**Sigma**
Needle (1.2mm x 40mm)	**BD Microlance 3**
13mm glass coverslips	**(from stores)**
Incubator (CO_2 water jacketed incubator)	**Forma Scientific**
Dulbeco's Modified Eagle Medium (DMEM)	**Sigma**
Medium 199	**Sigma**
L-Glutamine 200mM (100x) liquid	**Invitrogen**
Sodium pyruvate	**Life Technologies, UK**
Penicillin streptomycin	**Sigma**
Opti-MEM® I Reduced Serum Media	**Invitrogen**

2.1.4 Electron Microscopy (EM)

Thermanox coverslips	**Thermo Scientific**
Gluteraldehyde (25% aqu Pure, EM Grade)	**Sigma**
Sodium cacodylate	**Agar Scientific Ltd UK**
Osmium tetroxide	**Agar Scientific Ltd UK**
Phosphate buffer	**VWR International Ltd**
Uranyl acetate	**Agar Scientific Ltd UK**
Propylene oxide	**VWR International Ltd**
Resin (812 Kit E202)	**TAAB Lab Equipment Ltd UK**
Methanol	**Sigma**
Reynolds lead citrate	**Agar Scientific Ltd UK**

Alcohol increments (30-100% (dry))	**AnalaR NORMAPUR, VWR BDH**
Molecular sieve	**Sigma**
Hexamethyl-disilazane	**TAAB Lab Equipment Ltd. UK**
Carbon coated grids	**Agar Scientific Ltd UK**

2.1.5 General Reagents

5-Bromo-2'-deoxyridine (BrdU)	**Calbiochem**
DMSO	**Sigma**
Ethanol absolute	**AnalaR NORMAPUR, VWR**
Lipofectamine 2000	**Invitrogen**
LIVE/DEAD® Viability/Cytotoxicity kit	**Invitrogen**
Methanol, analytical reagent grade	**Fisher Scientific**
MTT	**Sigma**
Nitric acid (70%), analytical reagent grade	**Fisher Scientific**
Rhodamine phalloidin	**Invitrogen Molecular Probes**
siRNA (c-myc and nonsense)	**Thermo Scientific Dharmacon**
PBS tablets	**Sigma**
Sucrose	**Fisher Scientific**
NaCl	**AnalaR NORMAPUR**
$MgCl_2$ (hexahydrae)	**AnalaR NORMAPUR**
Hepes	**Fisher Scientific**
Triton® X-100	**Sigma**
Formaldehyde (40%)	**Fisher Scientific**
BSA (Albumin, from Bovine serum)	**Sigma**
Tween® 20	**Sigma**
Sodium deoxycholate	**Sigma**
Sodium Dodecyl Sulphate (SDS)	**BDH**
Protease inhibitor (10X)	**Roche**
Phosphatase inhibitor (10X)	**Roche**
ß-mercaptoethanol	**BDH AnalaR**
Powdered milk (dried, skimmed)	**Marvel**
Glycine	**BDH**
KCl	**BDH AnalaR**
D-Glucose	**Fisher Scientific**

EDTA	**Sigma**
Phenol red	**Sigma**
NaOH (powder)	**Fisher Scientific**
TRIZMA® base	**Sigma**

2.1.6 Histology

Paraffin wax	**Leica UK**
Polysine coated slides	**CellPath, UK**
Oven	**Thermo, UK**
Xylene	**Genta Medical, UK**
Graded alcohols (100%, 70%)	**Genta Medical, UK**
Haematoxylin & Eosin (H&E)	
- Haem	**CellPath, UK**
- Eosin	**Sigma**
Martius Scarlet Blue (MSB)	**TCS Biosciences**
Perls Prussian blue	**Leica Microsystems**

2.1.7 Iron Nanoparticles (mNPs)

100 and 200nm, nano-screenMAG/G-PEA	**Chemicell GmbH**
MagnetoFACTOR-96 device	**Chemicell GmbH**

2.1.8 Microscopes

Axiovert 25 light microscope	**Zeiss**
Axiophot fluorescence microscope	**Zeiss**
Leitz DMRB fluorescence microscope	**Leica**
Observer A1 inverted optical microscope	**Zeiss**
LSM 510 META confocal microscope	**Zeiss**
Leo 912 AB TEM	**Zeiss**
Jeol 6400 SEM	**Jeol Ltd**

2.1.9 Quantitative Real-Time PCR (qRT-PCR)

RNeasy® Micro kit	**Qiagen**
QuantiTect® Reverse Transcription kit	**Qiagen**
Taqman® master mix	**Applied Biosystems**
Primers and Probes	**Eurofins MWG Operon**
Abi Prism 96-well plates	**Applied Biosystems**
Real-time PCR, 7500 System	**Applied Biosystems**

2.1.10 Scientific Instruments

ICP-MS	**THERMO X Series II**
NanoDrop-1000 V3.7.1	**Thermo Scientific**
Plate reader	**Dynatech MR7000**
Rheometer	**CSL$_{500}$ Carri-Med Rheometer**
Vortex	**Fisions Whirlimixer**
Zetasizer	**Malvern**

2.1.11 Western Blot

Medical X-ray film	**Kodak**
Light-proof cassette	**Harper LONDON**
Sponge pads	**Invitrogen**
Filter paper	**Whatman**
Transfer membrane	**Immobilon**
NuPAGE® 4-12% Bis-Tris gels	**Invitrogen**
NuPAGE® LDS Sample Buffer (4X)	**Invitrogen**
NuPAGE® Transfer buffer (20x)	**Invitrogen**
NuPAGE® MOPS SDS Running Buffer (20X)	**Invitrogen**
NuPAGE® Antioxidant	**Invitrogen**
SeeBlue® Plus2 Prestained Standard	**Invitrogen**
Immobilon™ Western chemiluminescent HRP Substrate	**Millipore**
Novex Mini Cell tank apparatus	**Invitrogen**
Power pack	**PowerEase 500**

Heating block	**Techne Dri-Block DB.2A**
X-Omat Processor	**Kodak**
Scanner, Perfection V500 Photo	**Epson**
Shaker, Vibramax 100	**Heidolph Instruments**

2.2 General Solutions

PBS

1 x PBS tablet dissolved in 200ml H_2O

Permeabilising buffer

100ml PBS

10.3g sucrose

0.292g NaCL

0.06g $MgCl_2$ (hexahydrae)

0.476g Hepes

pH adjusted to 7.2, followed by the addition of 0.5ml Triton X

Fixative

90ml PBS

10ml (38%) formaldehyde

2g sucrose

PBS/BSA

100ml PBS

1g BSA

PBS/Tween

100ml PBS

0.5ml Tween 20

RIPA buffer

45ml H_2O

150mM NaCl

50mM TRIZMA® base

0.5ml Triton 1% (t-Octyl phenoxy polyethoxy ethanol)

0.5g Sodium deoxycholate 1%

0.05g SDS 1% (Sodium Dodecyl Sulphate)

Make up to 50ml with H_2O

Protein Extraction Buffer (PEB)

1ml RIPA buffer

100µl Protease inhibitor (10X stock)

100µl Phosphatase inhibitor (10X stock)

Sample Loading Buffer

950µl NuPAGE® LDS Sample Buffer (4X)

50µl ß-mercaptoethanol

Running buffer

50ml 20X NuPAGE® MOPS SDS Running Buffer

950ml H_2O

Transfer buffer

50ml 20X NuPAGE® Transfer buffer

100ml methanol

850ml H_2O

1ml NuPAGE® antioxidant

PBS-Tween

5x PBS tablets

1L H_2O

1ml Tween 20

Blocking buffer

30ml PBS-Tween

1.5g Marvel milk

Stripping buffer

25mM Glycine, pH 2.5

Versine

1L H_2O

8g NaCl

0.4g KCl

1g glucose

2.38g Hepes

0.2g EDTA

2ml 0.5% phenol red

Adjusted to pH 7.5 with 5M NaOH

Dispensed into 20ml aliquots and autoclaved

Stored at 4°C

Electron Microscopy fixative (EM fixative)

1.5% gluteraldehyde in 0.1M sodium cacodylate

2.3 Cell Culture

2.3.1 Human Cell Lines

Fibroblasts

- h-TERT-BJ1 cells   **Clontech Laboratories, Inc.**

Breast Cancer

- MCF-7 cells   **Sigma**

Cervical carcinoma

- HeLa cells   **Gifted from Prof Gwyn Gould**
                            (The University of Glasgow)

2.3.2 Media

Bj5-ta, h-TERT and MCF-7 cells were grown in Dulbecco's Modified Eagle Medium (DMEM), supplemented with 17.5% Medium 199, 10% FBS, 0.5% 100mM sodium pyruvate, and 1% penicillin streptomycin.

HeLa cells were grown in Dulbecco's Modified Eagle Medium (DMEM), supplemented with 10% FBS and 2mM glutamine.

Cells were grown in T75 flasks in complete medium and passaged by trypsinization when confluent. Cells were cultured at 37°C with 5% CO_2.

2.4 General Methods

2.4.1 NP Characterisation

A 2μl aliquot of each NP sample (0.1mg/ml in MilliQ H_2O) was dried onto a carbon-coated grid and viewed under the TEM at 120kV, at 40,000x magnification. In addition, NP size and charge were characterised by dynamic light scattering (DLS) and zeta potential respectively on a Malvern Zetasizer following manufacturers guidelines.

2.4.2 Toxicity Testing (MTT Assay)

MTT (3-(4,5-Dimethylthiazol-2-yl)-2,5-diphenyltetrazolium bromide) is a yellow tetrazole. The MTT assay is a colorimetric assay for measuring the activity of enzymes that reduce MTT to formazan dyes, producing a purple colour. The strength of this enzymatic activity and resulting purple colour can be used as an indication of cellular viability, and used to check for any cytotoxicity caused by a test substance, such as NPs. Cells were seeded at 1 x 10^4 cells per well in a 96 well plate and allowed to adhere overnight. AuNP treatments were added (75μl at various test concentrations) and incubated with the cells for 24, 48 or 72 hours (control cells were incubated with media instead). After treatment incubation, cells were washed with warmed PBS; 100μl MTT solution was added per well (0.5mg/ml MTT powder in PBS) and cells were incubated for 1.5 h at 37°C. MTT solution was removed, and replaced with 100μl DMSO. Cells were left for 10 min at room temperature and then the absorbance (Abs) was read at 550nm using a plate reader.

MTT data analysis: Percentage viability was calculated using the following equation: (Abs NP-treated cells / Abs control cells) x 100 = % viability) [n=3]

2.4.3 Uptake Analysis

2.4.3.1 Transmission Electron Microscopy (TEM)

Cells were seeded at 1 x 10^5 cells per well on Thermanox coverslips in a 24 well plate and allowed to adhere overnight. NP treatments were added to coverslips/gels (500µl at 0.2mg/ml) and incubated for 1, 18, 24 or 48 hours (control cells were incubated with media instead).

TEM processing of 2D/3D cell cultures
Coverslips/gels were covered in 1ml EM fixative and left at 4°C for 30 min, then post fixed in 1% osmium tetroxide in phosphate buffer for 1 h, followed by 0.5% uranyl acetate for 1 h and then dehydrated through a series of alcohol increments (30 – 100%) and left in propylene oxide Epon 812 resin mix (1:1) overnight. Samples were put into pure resin and kept in an oven for 24 h to cure. Blocks were then cut into ultrathin sections, stained with 2% methanolic uranyl acetate and Reynolds lead citrate, and viewed under the TEM at 120kV.

2.4.3.2 Inductively Coupled Plasma Mass Spectrometry (ICP-MS)

- **Background**

ICP-MS, also known as element analysis, is a branch of mass spectrometry that can measure and quantify trace levels of a specified element. It is a popular choice commonly used to analyse the levels of NP cellular uptake; its main advantage being that it is highly quantitative compared to microscopy. The most commonly published method for ICP-MS analysis of NP cellular uptake is to measure the NP-element level in the cells after they have been incubated with the NP treatment. This involves removing the cell monolayer from the NP treatment, degrading all cellular organic matter with a strong acid and measuring the remaining amount of NP-element present in each sample. It follows that if more NPs have been taken up into the cell monolayer, then more NP-element will be present in the end sample.

A modified version of this method was used in this PhD to analyse the levels of;

1) mNP (iron) uptake into 3D gels (results presented in Figure 3-8)

2) mNP (iron) uptake into 2D cell monolayers (results presented in Figure 3-9)

3) AuNP (gold) uptake into 2D cell monolayers (results presented in Figure 4-11B)

To facilitate this work, a collaboration was set up with the chemistry department at the University of the West of Scotland (UWS) in Paisley. It was realised that acidic degradation of 3D collagen gels could not be performed as effectively as acidic degradation of 2D cell monolayers. Therefore, the original published method described above had to be modified; particularly since the introduction of any organic matter resulting from partially-degraded gel debris to the mass spec may prove detrimental.

- **Modified ICP-MS Method**

An alternative method was therefore introduced and applied to both 2D and 3D cell cultures (in the following description, 'cell culture' is used to refer to both 2D cell monolayers and 3D cell cultures).

The level of NP-element found in the spent media after incubation with the cell culture was analysed by ICP-MS. In addition, the amount of NP-element found in the neat NP-treatment (incubated without the cell culture) was also measured. These values were used in the following equation to calculate the amount of NP-element uptake into the cell culture;

> **Element uptake = (element level after incubated *without* cell culture) -**
> **(element level after incubated *with* cell culture)**

- **Cell Culture Procedures**

2D Cell Monolayer

Cells were seeded at 1×10^4 in a 96 well plate and allowed to adhere overnight. Media was replaced with NP treatments (75μl at 0.1mg/ml in DMEM). In an identical manner, each NP treatment was also incubated without cells, for

comparison (graphed as 0 hour time point). Incubation was performed for 1 or 18 hours.

3D Gel Culture

Gel media was replaced with NP treatments (75μl at 0.1mg/ml in DMEM). In an identical manner, each NP sample was also incubated without gels, for comparison (graphed as 0 hour time point). Incubation was performed for 1 or 18 hours.

- **ICP-MS Sample Processing**

After incubation, the treatment media from each sample was removed and added to 1ml of H_2O, together with 100μl H_2O that had been use to wash the cells and wells. Samples were treated with 1ml of 70% nitric acid and then heated in a water bath at 70°C overnight. After heating, samples were cooled and then diluted to 50ml with H_2O (MilliQ H_2O used throughout). Samples were analysed using ICP-MS at the UWS.

3 Delivery of Iron mNPs to Cells in 3D

3.1 Introduction

Disease treatments, such as chemotherapy, currently lack specificity (Parveen and Sahoo, 2008; Sawant and Torchilin, 2010), thus cytotoxicity is a common problem as the drugs administered attack both healthy and diseased cells alike. It is hoped that NPs can be used to solve this problem by carrying and delivering drugs specifically into diseased cells, thereby preventing the attack of healthy cells and improving drug efficacy (Ahmad *et al.*, 2010; Berry and Curtis, 2003). In addition, it is anticipated that NP-mediated delivery of nucleic acids will enable the long-awaited clinical use of gene therapy. Two of the biggest problems currently facing NP-mediated drug delivery are the site-specific targeting and subsequent cellular uptake of NPs within the body (e.g. into cancerous cells within a tumour).

One favourable method to improve NP targeting is to distally control their movement within the body through the application of an external magnetic field (MF) (Widder *et al.*, 1978b). Magnetic nanoparticles (mNPs), such as those composed of iron oxide, are ideal for use in this targeting strategy since they display good biocompatibility (Jain *et al.*, 2008), strong magnetism (Corchero and Villaverde, 2009), useful imaging properties (such as MRI) (Wu *et al.*, 2010), ease of functionalisation and have been extensively researched *in vitro* (Dobson, 2006a). The effectiveness of mNP-mediated magnetic targeting has already been exemplified *in vitro* by its widescale use as a research tool for gene transfection, this popular technique being coined 'magnetofection' (Plank *et al.*, 2003; Mah *et al.*, 2000; Pickard and Chari, 2010). In light of the efficiency of mNP-targeting already seen *in vitro* it is hoped that a MF can be used in the same way *in vivo* to successfully target mNPs to the site of disease within a human body.

Once at the site of disease, NPs face the second problem of cellular uptake; an essential feat required for delivery of their therapeutic payload. NP functionalisation with cell penetrating peptides (CPPs) is a promising solution to this hurdle (Berry, 2008). CPPs, such as Tat and penetratin, are short, highly basic, peptide sequences (<20 amino acids), able to promote conjugated cargo transport across the plasma membrane (Schwarze and Dowdy, 2000; Derossi *et*

al., 1994). Their ability to promote cellular uptake of NPs was first reported in 1999 when Josephson *et al* demonstrated a 100-fold increase in Tat-functionalised mNP uptake as compared to plain NPs (Josephson *et al.*, 1999). Since then, increased cellular uptake of NPs functionalised with CPPs has been repeated in numerous *in vitro* studies (Smith *et al.*; De La Fuente and Berry, 2005; Berry *et al.*, 2009a). However, despite such encouraging findings, CPPs are not receptor-dependent and thus, not cell-specific (Deshayes *et al.*, 2005). Therefore, to enable site-specific drug delivery they will need to be used in conjunction with a targeting strategy, such as a MF.

This chapter has investigated the combined use of a 280mT MF with a CPP (penetratin) in order to simultaneously improve both targeting and uptake of mNPs to human fibroblasts in 3D. Previous theoretical studies have calculated that in order to facilitate *in vivo* magnetic targeting of mNPs, the magnetic flux density (field strength) at the target site must be in the order of 200-700mT in order to efficiently capture particles flowing in the blood stream (Voltairas *et al.*, 2002; Pankhurst *et al.*, 2003; Mykhaylyk *et al.*, 2008; Dobson, 2006a). This suggests that the 280mT MF used in this study is of a suitable strength to induce movement of mNPs through a 3D tissue. The majority of magnetofection studies described in the literature have also used MF strengths within this recommended range of 200-700mT. For example Alexiou *et al* used a 400mT MF to pull mNPs into HeLa cells (Alexiou *et al.*, 2005), Lamkowsky *et al* used a 367mT MF to pull mNPs into astrocytes ((Lamkowsky *et al.*, 2012), Ang *et al* used a 130mT MF to transfect COS-7 cells (Ang *et al.*, 2011b), del Pino *et al* used a 130-240mT MF to deliver siRNA to HeLa and H441 epithelial cells (Del Pino *et al.*, 2010) and Darton *et al* used a 500mT MF to capture mNPs in flow (Darton *et al.*, 2008).

In comparison, the numerous studies into magnetic delivery of mNPs to 2D cell monolayers performed by Christian Plank's group have used a stronger MF of 1080-1150mT (Scherer *et al.*, 2002; Plank *et al.*, 2003; Gersting *et al.*, 2004), which is similar to the 1-1.2T magnetic field produced by magnetic plates from Oz Biosciences, which have been used in numerous 2D magnetofection studies (Buerli *et al.*, 2007; Mykhaylyk *et al.*, 2007).

It would appear that although some groups are using higher MF strengths of around 1T for 2D magnetofection (being comparable to the high MF strength of 1.5T required for conventional MRI scanners), lower strength MFs within the recommended range of 200-700mT are perfectly sufficient for magnetic targeting of mNPs. Evidence for this statement is that upon comparison of MF strengths of up to 250mT, Ang *et al* found that 130mT was an optimal MF strength to achieve maximum transfection efficiency in 2D *in vitro* cell cultures (Ang *et al.*, 2011a). In addition, an important *in vivo* study by Kumar *et al* found that a relatively weak MF of only 2.5mT (~460x weaker than that used in Plank's 2D studies) was sufficient to target mNPs in the heart and kidneys of rats after intravenous injection into the tail (Kumar *et al.*, 2010), bringing into question the need for higher-strength MFs to achieve *in vivo* magnetic targeting, and highlighting the useful information that can be gained from testing delivery strategies *in vivo*.

The novelty of the work presented in this chapter lies in the use of a well established 3D tissue-equivalent model whereby cells are cultured within a type-1 collagen gel matrix (Bell *et al.*, 1979). The use of this 3D model provides a cell culture environment that is more comparable to *in vivo* tissue than are traditional 2D monolayer cultures. This is important, since research in 2D monolayer cell cultures may not reliably predict later-stage clinical responses to therapeutic NPs (Zhang *et al.*, 2010). This is because in the latter scenario cells are surrounded by and interact with the extracellular matrix (ECM), which can produce phenotypic differences - altering behaviour to that observed in monolayer cell culture. Therefore, 2D testing of NP-delivery systems is ultimately of limited use as NP behaviour may be very different once introduced into a living system. The 3D study reported in this chapter therefore provides a more accurate prediction of how a MF and a CPP (in this case penetratin) could be used to deliver drug- loaded mNPs to diseased cells inside the human body.

Results demonstrated that while a MF increased the rate and depth of mNP uptake into the gel, penetratin encouraged cell-NP association and subsequent cellular uptake. Thus a combination of both techniques would be recommended for therapeutic drug delivery *in vivo*. This study represents an important

stepping-stone in the journey from traditional 2D research towards the development of a NP-based drug delivery system for clinical use.

3.2 Aims

The aim of this study was to investigate if an external MF and/or penetratin can be used to improve mNP-delivery to cells growing in a 3D environment, as they have previously been demonstrated to do in 2D monolayer cell culture. As such, this study provides a more realistic assessment of how these techniques might perform in future clinical settings.

3.3 Methods

3.3.1 mNP Design and Synthesis

The mNPs used in this project were commercially sourced in two different sizes; 100 and 200nm. The design of these commercial mNPs involved a magnetic iron oxide core encased by two outer molecular shells containing green-lipophilic fluorescent dye and a polysaccharide matrix. After purchase from Chemicell, aliquots of 100 and 200nm mNPs were sent to grant partners in Spain, who further functionalised them with the CPP penetratin. This provided a total of four mNP samples for use in this project; 100nm plain, 100nm penetratin, 200nm plain and 200nm penetratin (Figure 3-1).
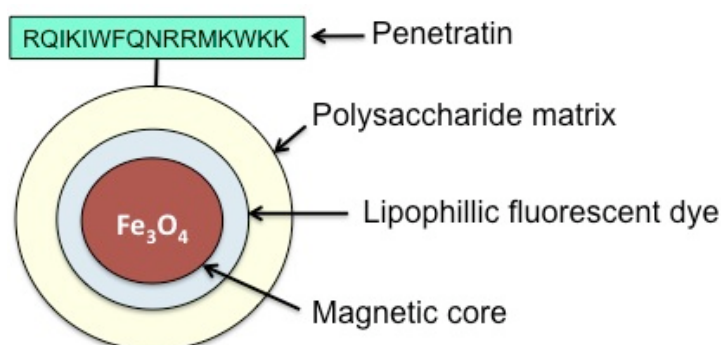
Figure 3-1 Schematic outline of the mNP design
This figure demonstrates the main design features of the mNPs used in this project. As bought from Chemicell, the mNPs have a magnetic iron oxide core surrounded by a fluorescent dye and a polysaccharide matrix. Grant partners attached the CPP penetratin. This mNP design was bought in two sizes; 100 and 200nm, and each was functionalised with penetratin. Therefore this chapter involves a total of four mNP samples; 100nm plain, 100nm penetratin, 200nm plain and 200nm penetratin.

3.3.1.1 mNP Functionalisation with Penetratin (provided by grant partners)

Iron oxide magnetic green-fluorescence nanoparticles (100 and 200nm, nano-screenMAG/G-PEA) were bought from Chemicell GmbH (article no. 4417). The amine groups of each mNP sample were activated with sulfosuccinimidyl 4-[N-maleimidomethyl]cyclohexane-1-carboxylate (sulfo-SMCC) for further functionalisation with the peptide penetratin. The amount of penetratin added aimed to derivatise 1000 of the activated amino groups on the 100nm mNPs, and 7800 on the 200nm mNPs. This difference was to allow for the difference in surface area between the two sizes of mNPs. Therefore, supposing that the sulfo-SMCC activation and the peptide coupling worked 100%, the mNP to penetratin molar ratio is [1:1000] for the 100nm size, and [1:7800] for the 200nm size. Both sizes were prepared to a final concentration of 1mg/ml of mNPs in H_2O.

3.3.1.2 Reaction Details (provided by grant partners)

Ice cold buffer was prepared (100mM 2-(N-morpholino)ethanesulfonic acid (MES), 150mM NaCl, pH 7.2) containing 500µg of sulfo-SMCC (article no. 22322 from Pierce)). 335µl from a 30mg/ml stock solution of 100nm mNPs was added to 165µl buffer and 290µl from a 35mg/ml stock solution of 200nm mNPs was added to 210µl of buffer, to permit functionalisation of the 100nm and 200nm mNPs respectively. The two reaction mixtures were incubated for 30 minutes at room temperature and then 15µl from a 5mg/ml solution of activated Penetratin 1 (cat. no. PENA0500 from MP Biomedicals) was added to each. The reaction mixtures were incubated overnight at 4° C. The functionalised nanoparticles were washed by magnetic precipitation with the previously used buffer to remove excess of sulfo-SMCC and peptide. Their final volume was adjusted to 1ml (Table 3-1).

mNP size	mNP concentration		~Molar ratio	Penetratin added	~Molar ratio
(nm)	(mg/ml)	(mM)	(mNP:sulfoSMCC)	(mM)	(mNP:added penetratin)
100	10	30×10^{-3}	$[1.38 \times 10^{3}]$	29	$[1:1 \times 10^{3}]$
200	10	3.7×10^{-3}	$[1.310 \times 10^{3}]$	29	$[1:7.8 \times 10^{3}]$

Table 3-1 Chemical description of mNPs after functionalisation with penetratin
The concentration of mNPs in each 1ml sample is displayed in both mg and molarity. The molar ratio of mNPs to sulfo-SMCC used for amine activation is shown. The concentration of penetratin in each 1ml sample and the molar ratio of mNPs to penetratin is also shown.

3.3.2 MagnetoFACTOR Plate

A MagnetoFACTOR plate was purchased from Chemicell for use with the mNPs. The plate is designed to be positioned underneath a 96-well cell culture plate, and exerts a 280mT strength magnetic field through the plate, in order to pull nanoparticles through any cell culture systems being grown inside the plate. In this project, gels were synthesised in 24 well plates, so that when fully contracted, they were small enough to fit inside the wells of a 96-well plate, which could then be placed on top of the MagnetoFACTOR plate, as shown in Figure 3-2. N.B [Calculations performed by Furlani and Xue confirm that the MF used can cover the whole thickness of 3D gels (Furlani and Xue, 2012).]
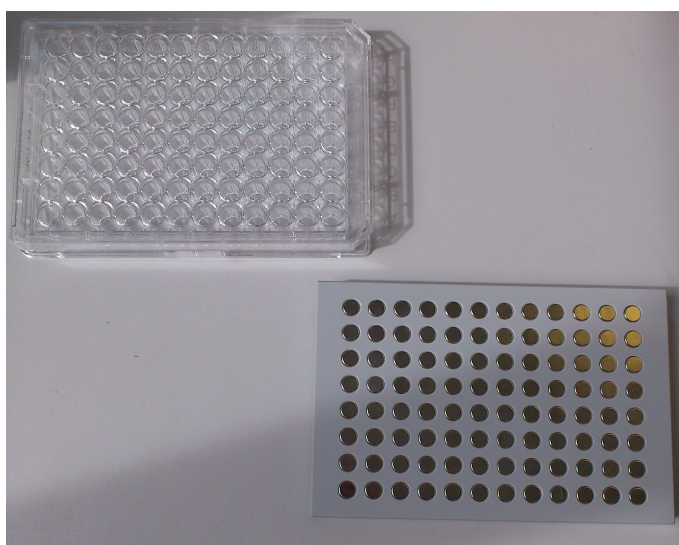
Figure 3-2 MagnetoFACTOR plate
This photograph shows the MagnetoFACTOR plate purchased from Chemicell (bottom right) that was placed underneath 96-well cell culture plates (top left) in order to exert a 280mT magnetic field through 3D collagen gels placed inside wells within the 96-well plate. This acted to pull mNPs through the gel, towards the underlying magnets.

3.3.3 Cell Seeded Collagen Gel Synthesis

Gels were made in batches of 6 by mixing (on ice) 0.5ml FBS, 0.5ml 10x DMEM, 1 x 10^6 human fibroblast cells (h-TERT BJ-1) suspended in 0.5ml complete medium, 2.5ml Type 1 collagen (2mg/ml) and 3.5ml 0.1M NaOH (to neutralise and solidify collagen). Gel mixture was vortexed, pipetted into a 24 well plate (1ml per well) and incubated at 37°C overnight to solidify. A needle was run around the edge of each solid gel to detach it from the plastic. Fresh media was added and changed daily. Following diameter measurements, gels were used in experiments four days after detachment to allow full gel contraction. The diameter measurements recorded for a typical gel are presented in Figure 3-3.
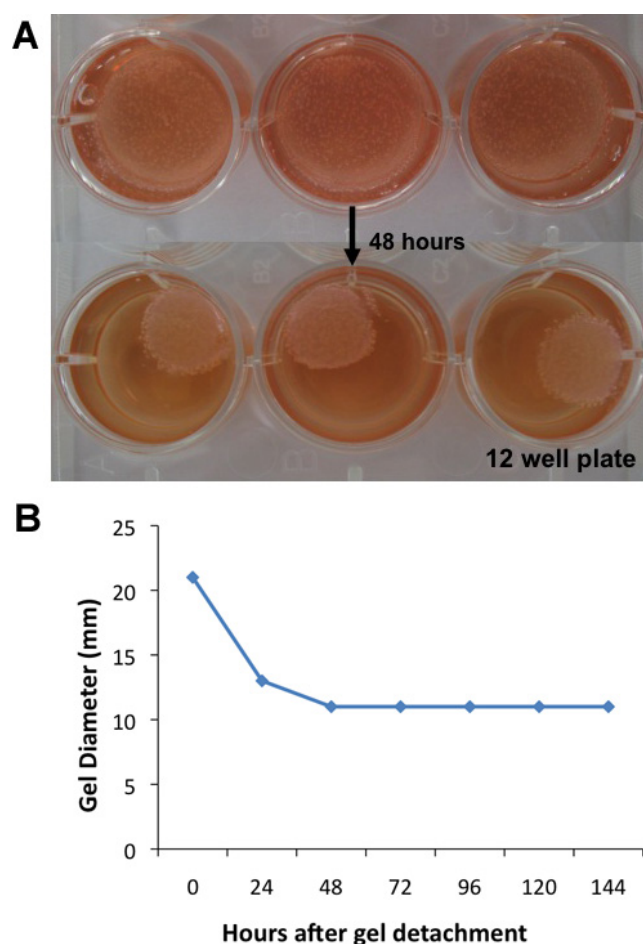
Figure 3-3 Gel contraction
Photographs of 3 gels made within a 12-well cell culture plate are shown in A (each well has a diameter of 22mm). The top three images were taken immediately after detachment of gels from plastic using a needle, and the bottom three images were taken 48 hours later, when the gels had contracted to roughly half their original size. Diameter measurements of a typical gel were recorded using a ruler every 24 hours for a 144 hour period, and are presented graphically in B. [N.B. For experiments gels were made to a smaller size within 24 well plates in order to fit on the magnetoFACTOR plate. The same pattern of contraction was displayed, with gels reducing to half their original diameter after 48 hours.]

3.3.4 Gel Characterisation

3.3.4.1 Rheology

Rheology was used to measure the elastic modulus (G′) and viscous modulus (G″) of the gels in order to verify their mechanical properties and gauge their elasticity/stiffness. This was performed to assess if the composition of the gel was suitably comparable to the stiffness of natural human tissue in order to be a reliable tissue-equivalent model. Dynamic frequency sweep experiments were carried out on a strain-controlled rheometer using a parallel-plate geometry (20mm diameter). The experiments were performed at 25°C and this temperature was controlled throughout the experiment using an integrated electrical heater. Extra precautions were taken to minimize solvent evaporation and to keep the sample hydrated by using a solvent trap and by saturating the internal atmosphere with H_2O. To ensure the measurements were made in the linear viscoelastic region, an amplitude sweep was performed and the results showed no variation in elastic modulus (G′) and viscous modulus (G″) up to a strain of 0.01%. The dynamic modulus of the gel was measured as a frequency function where the frequency sweeps were carried out between 1 and 40Hz. Measurements were repeated at least three times to ensure reproducibility. Gels were not fixed before use.

3.3.4.2 Atomic Force Microscopy (AFM)

AFM was used to measure the Young's modulus of the gels in order to compare their elasticity/stiffness to that of human tissue. Analysis was carried out with a NanoWizard II Bio AFM mounted on a Zeiss Observer A1 inverted optical microscope. The complete set-up was acoustically isolated in order to reduce the interference of ambient noise during the measurements. The probes used for the indentations were prepared in-house by attaching a 4.8μm silica microsphere to a tipless silicon nitride cantilever using a UV curable glue. Before any measurements were recorded the spring constant of the modified cantilever was determined using the thermal calibration method according to the AFM user manual. The value was 0.121 N/m. Force-indentation curves were carried out at 10μm/sec with a 10μm Z-ramp until a maximum force of 5nN was reached.

Three positions spread evenly across the surface of the gel were selected for indentation measurements. Gels were not fixed before use.

3.3.4.3 Scanning Electron Microscopy (SEM)

SEM was used to image the gel surface in order to investigate cellular morphology and the structure of the collagen fibres and pores. Gels were fixed in 1.5% gluteraldehyde in 0.1M sodium cacodylate at 4°C for 1.5 hours then postfixed in 1% osmium tetroxide for 1 hour. Samples were subsequently stained with 0.5% uranyl acetate and dehydrated through a series of alcohol increments (30%, 50%, 70%, 90%, 100%, 100% (dry)) and hexamethyl-disilazane. After dehydration gels were then air dried and viewed on a Jeol 6400 SEM at an accelerating voltage of 6kV, at 1000 or 3000x magnification.

3.3.4.4 Histology

Histology was used to obtain a cross-sectional view of the gels, thus allowing observation of both collagen and cell density and dispersal in the gel structure. Gels were fixed in 4% formaldehyde/PBS with 1% sucrose at 37°C for 15 min, submerged in 1ml permeabilisation buffer at 4°C for 15 min and embedded in paraffin wax. Sections of 4μm thickness were cut from the gel centre onto polysine coated slides and baked at 60°C overnight. Sections were then de-waxed in xylene for 5 min and rehydrated through graded alcohols (100%, 70%) before rinsing with H_2O for 5mins. After rinsing, sections were stained with Haematoxylin & Eosin (H&E) to display general structures present, or Martius Scarlet Blue (MSB) to display fibrin/connective tissue. After staining, sections were dehydrated through graded alcohols (70%, 100%), placed in xylene for 1 min, mounted and imaged on a Zeiss Axiovert 25 light microscope at 10x magnification. Histology staining was performed at The Beatson West of Scotland Cancer Centre.

3.3.4.5 Cell Viability

Cell viability in the 3D gel model was assessed after 96 hours using a live/dead staining kit. Gels were incubated at 37°C for 1 hour in 600μl of Calcein AM and

ethidium homodimer (1μl/ml in DMEM). Images were taken on a Leica Leitz DMRB fluorescence microscope at 10x magnification.

3.3.4.6 Cell Cytoskeleton F-actin Immunofluorescence

Immunofluorescent staining was performed to visualise cellular F-actin in order to determine cell structure within the gel. Gels were fixed as per section 3.3.4.4 and then incubated with rhodamine phalloidin (1:50 in PBS/BSA) at 37°C for 1 hour. Gels were rinsed twice with PBS between each step. Images were taken on a Leica Leitz DMRB fluorescence microscope at 20x magnification.

3.3.5 Uptake Analysis

For all uptake experiments, contracted gels were transferred to a 96-well plate and incubated with 75μl of the mNP solution (0.1mg/ml in DMEM). Control gels were incubated with 75μl of DMEM. A static MF was applied by sitting the 96-well plates on top of a MagnetoFACTOR-96 magnetic plate, which exposed the wells to a 280mT magnetic field. Gel-mNP incubation was performed in this manner at 37°C for the time periods indicated in each experiment.

3.3.5.1 Histology

To identify mNPs in the cell seeded gels, gel-mNP incubation was performed with all four mNP species (100nm plain/penetratin, 200nm plain/penetratin) +/- a MF, for 18 hours and, following washing in PBS, processed for histology as in 3.3.4.4. Sections were stained with Perls Prussian blue (stains iron) to visualise the mNPs and imaged on a Zeiss Axiovert 25 light microscope at 10 and 40x magnification.

3.3.5.2 Fluorescence Microscopy

To assess any possible surface localisation of 100nm mNPs, gels were incubated with 100nm plain/penetratin mNPs, +/- a MF for 18 hours. Gels were then washed twice in PBS and the gel surface was imaged on a Zeiss Axiophot fluorescence microscope at 10x magnification.

3.3.5.3 Confocal Microscopy

To assess the depth of 100nm penetratin mNP uptake, gels were incubated with 100nm penetratin mNPs, +/- a MF, for 1 or 22 hours. After incubation, gels were washed twice in PBS and fixed in 4% formaldehyde/PBS with 1% sucrose for 25mins. A Zeiss LSM 510 META confocal microscope (at 10x magnification) was then used to produce a z-stack of each gel composed of sequential images taken 1μm apart. Each compressed z-stack was analysed from the first image downwards through the gel and the depth of mNP penetration was recorded. These distances were then averaged (n=3) and used for statistical analysis and graphical representation (Figure 3-11).

3.3.5.4 Transmission Electron Microscopy (TEM)

To visualise the cellular interaction of 100nm penetratin mNPs, gels were incubated with 100nm penetratin mNPs, +/- a MF for 18 hours. Gels were sectioned into quarters (to a size which permitted viewing under the microscope) and processed as per section 2.4.3.1.

3.3.5.5 Statistics

Statistical analysis was performed in SPSS. The ICP-MS data for each size of mNP (100 or 200nm) for each time point (1 or 18 hours) was analysed by 1-way ANOVA with Dunnett's test. The confocal data was analysed by 1-way ANOVA with Tukey's test. For the rheology, ICP-MS and confocal data, n=3. In all figures * = $p < 0.05$, ** = $p < 0.01$ and *** = $p < 0.001$.

3.4 Results

3.4.1 NP Characterisation

TEM allowed visualisation of the four mNP species (Figure 3-4). Whilst the sizes of the mNPs are described as 100 and 200nm by Chemicell, in TEM both species appeared much smaller as only the electron- dense core is visible. Since the aggregation seen here could have been caused by the TEM processing, additional characterisation was performed using a Malvern Zetasizer. Analysis of particle size by dynamic light scattering (DLS) confirmed that the 100nm species were not aggregated, but that the 200nm species were slightly aggregated into groups of 5-10 particles. This was also reflected in the zeta potential values, as the 200nm mNPs had a lower zeta potential than the 100nm mNPs, indicating that aggregation was more likely to occur in these samples due to less steric repulsion between particles. In addition, an increase in particle negativity as measured by zeta potential confirmed the successful attachment of penetratin (Table 3-2).
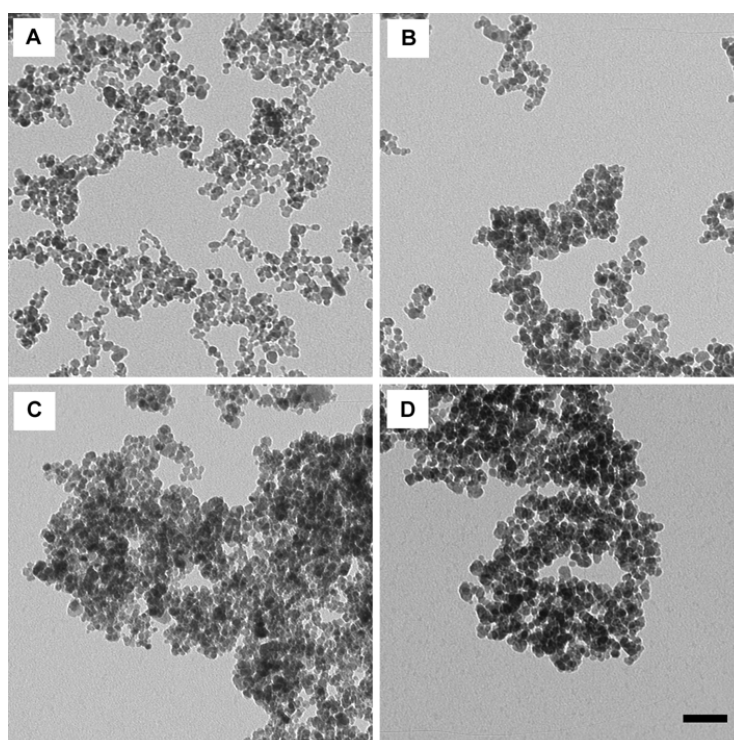
Figure 3-4 TEM images of the four mNP species
Images represent plain 100nm mNPs (A), 100nm with penetratin (B), plain 200nm mNPs (C) and 200nm with penetratin (D). Please note that the polysaccharide matrix, the fluorescent dye and the penetratin peptide (16 amino acids) surrounding the mNPs cannot be seen by TEM. Hence this figure shows only the electron-dense iron core of each mNP [scale bar = 50nm].

mNP sample	Size (nm)	Zeta potential (mV)
100nm plain	183.2 $\pm$ 0.7	-27.3 $\pm$ 0.6
100nm penetratin	205.5 $\pm$ 8.1	-31.8 $\pm$ 0.8
200nm plain	1902 $\pm$ 334.5	-8.6 $\pm$ 0.2
200nm penetratin	2006.7 $\pm$ 403	-12.1 $\pm$ 0.2

Table 3-2 Zetasizer analysis of mNPs
Dynamic light scattering (DLS) measured the hydrodynamic diameter of each of the four mNPs. These size measurements are larger than those advertised by Chemicell (100nm and 200nm), however taken together with the TEM images (Figure 3-4) it is clear that this difference is not due to larger individual particle size but rather due to slight particle aggregation. Please note that the non-aggregated 100nm samples were the main focus of this chapter. Furthermore it is noted that (i) the attachment of penetratin does not significantly increase particle size, and (ii) the zeta potential increases in negativity with the attachment of penetratin, as expected, and confirms peptide attachment.

3.4.2 Gel Characterisation

3.4.2.1 Atomic Force Microscopy (AFM) & Rheology

The Young's modulus (stiffness) of the gel (fully contracted) was found to be 2kPa $\pm$ 1.7 (mean $\pm$ SD) as measured by AFM, being comparable to the Young's modulus of human fibroblast cells, which is reported as 2- 60kPa as measured by AFM (Alonso and Goldmann, 2003).

Rheology is a method of measuring a material's elasticity (termed it's elastic modulus) through the application of force. In this case, the elastic modulus of the gel was found to be between 1-10kPa (Figure 3-5) as measured by rheology, being comparable to the elastic modulus of human adipose tissue as tested by rheology (3-6kPa) (Discher *et al.*, 2009). The AFM and rheology results presented here both demonstrate that the gels have a consistency similar to human tissue, highlighting the suitability of this cell culture model for use in realistic 3D studies.
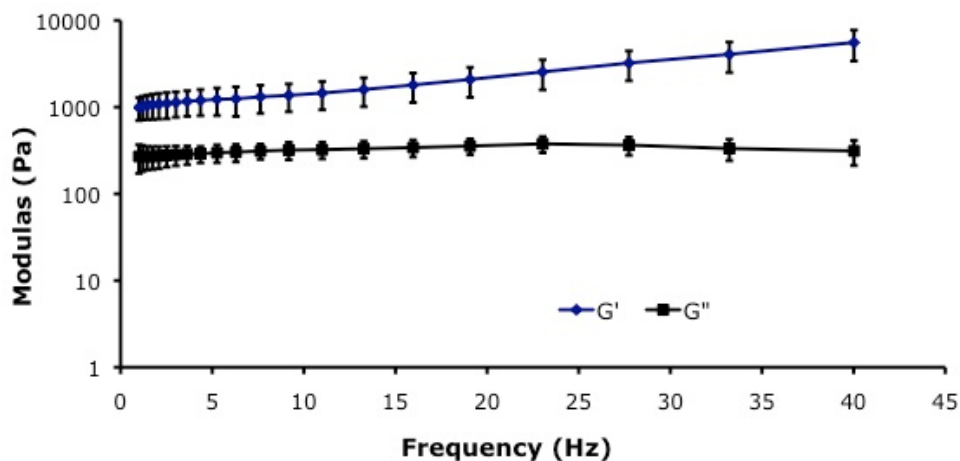
Figure 3-5 Gel stiffness
The elastic modulus (G') and the viscous modulus (G'') of the gel as measured by rheology indicated that G' lies between 1 and 10kPa - a stiffness in line with human tissue (error bars are SD, n=3).

3.4.2.2 Microscopy Characterisation

Gels were further analysed to determine cell distribution and viability in the 3D construct (Figure 3-6). SEM images showed cells growing in a confluent, parallel sheet over the top surface of the gel (Figure 3-6A) with collagen fibres visible between the cells (Figure 3-6B). These fibres appeared as a dense, random network with pores of less than 5μm in diameter with the cellular extensions interacting and probing the collagen fibrous network. Histology cross-sections showed cells distributed uniformly throughout the gel (Figure 3-6C and D). The surface layer of cells, as was noted in the SEM, was again observable here, running along the top edge of the section. The MSB stain indicated that the collagen was fibrous in appearance and homogeneous throughout the gel (Figure 3-6D). The gel thus structurally presented as a dense, tissue-equivalent model.

Cell viability staining demonstrated viable cells both in the centre and at the edge of the gel after 96 hours of culture (Figure 3-6E and F respectively). No dead cells were observed. A higher density of cells was visible at the gel periphery due to radial gel contraction condensing this area. Cellular F-actin immunofluorescence indicated a dense concentration of cells growing in a parallel fashion on the gel surface (Figure 3-6G), in agreement with SEM and histological analysis. Cells at the edge of the gel were observed growing in line with the contour of the gel (Figure 3-6H).
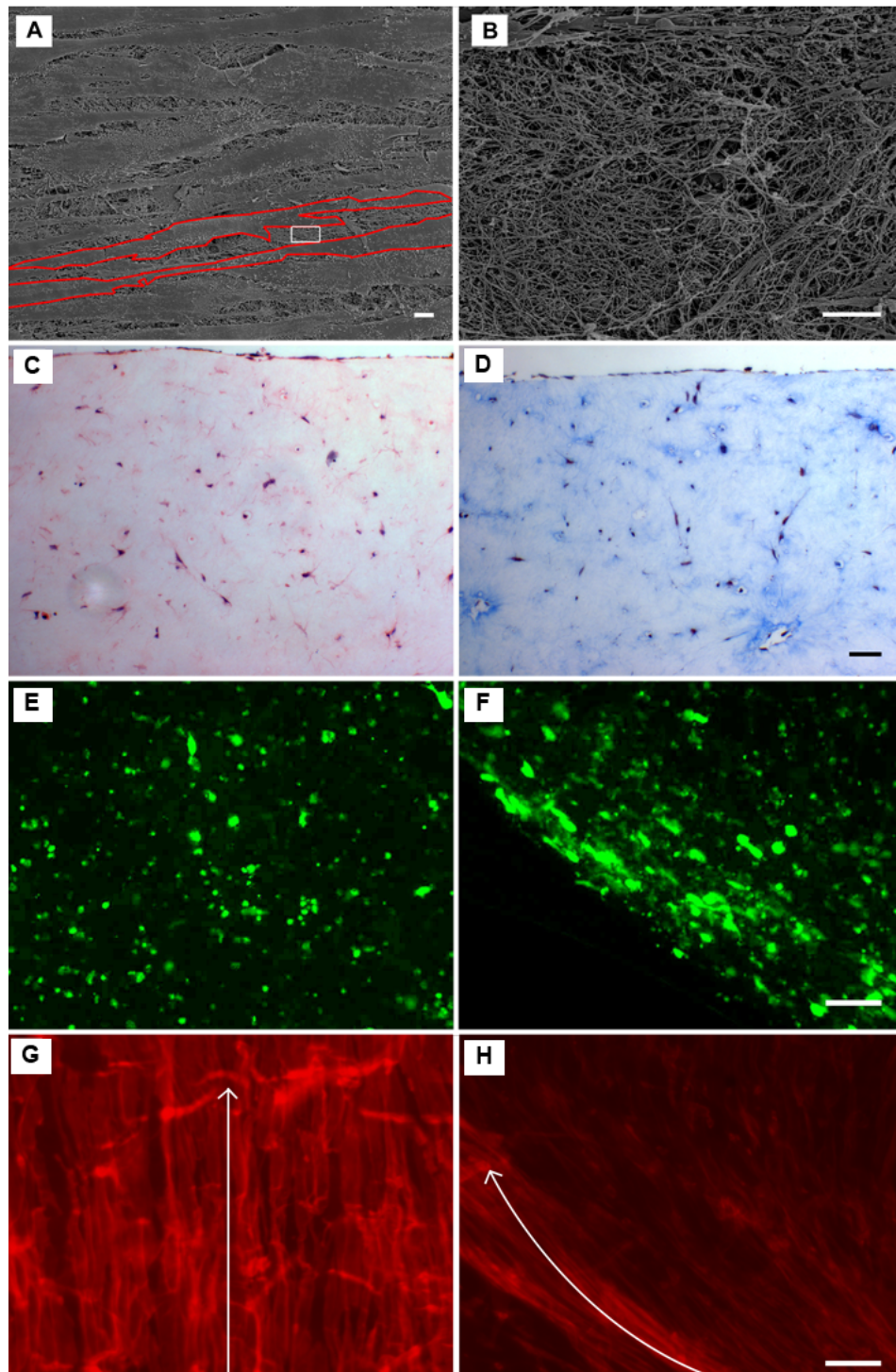
Figure 3-6 Microscopy gel characterisation
SEM images of gel surface structure (A and B, scale bars 5μm) indicated cells growing over
the gel surface (A, 1000x magnification) with a magnified area between the cells showing
the collagen fibre network in the gel, typically with pores less then 5μm (B, 3000x
magnification). Gel histology cross-sections (C and D, scale bar 50μm) demonstrated
uniform cell and collagen distribution throughout the gel. H&E depicts cells as red (C), MSB
depicts collagen as blue (D). Viability staining (E and F, scale bar 100μm) showed viable
cells at both the gel centre (E) and the gel edge (F). Cellular F-actin immunofluorescence (G
and H, scale bar 50μm) indicated cells at the gel centre growing in a parallel direction (G,
white arrow denotes cell orientation), and cells at the gel edge growing in line with the
contour of the gel (H, white arrow denotes cell orientation). This figure demonstrated that
the gel is a good tissue-equivalent model.

3.4.3 Uptake Analysis

3.4.3.1 Histology

An initial qualitative assessment of mNP-gel interaction was obtained by staining histology cross-sections of the gel (1cm length x 0.5cm width, cut to a thickness of 4µm) with Perls Prussian blue to visualise the iron mNPs. All four mNP species (100nm plain/penetratin, 200nm plain/penetratin) were investigated + MF for 18 hours. Results demonstrated that all four mNP species could become associated with the gel, being seen as dark blue/black clusters (Figure 3-7). Since individual mNPs are not visible at this low magnification, assessment of total uptake level was not possible. However, this figure does clearly show that groups of mNPs were abundant on the gel surface (upwards pointing arrows). These surface particles may either be particles interacting with cells on the top layer of the gel, or perhaps larger aggregates that have remained attached to the gel surface, being too large to fit between the collagen fibres. In addition, clusters of both 100nm plain and 100nm penetratin mNPs were noted inside the gel (downwards pointing arrows) demonstrating successful gel penetration. Following this initial proof of gel-mNP association, further quantitative techniques were employed to assess the effect of a MF and penetratin on gel-mNP uptake.
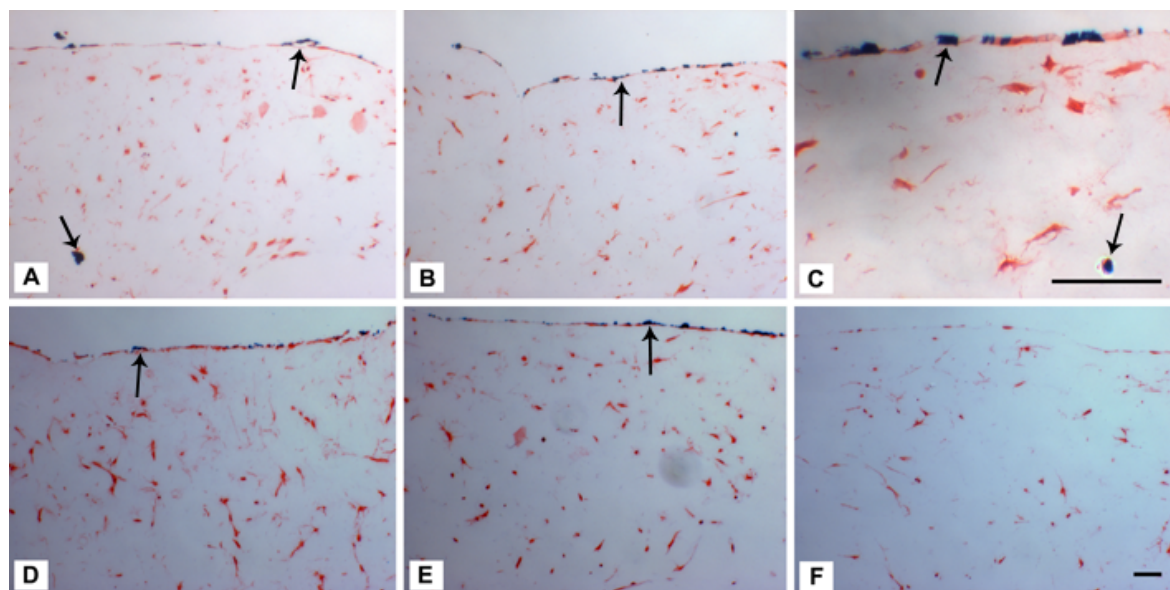
Figure 3-7 Histology sections of gels stained with Perls Prussian blue to visualise iron mNPs after incubation in a magnetic field for 18 hours
Images refer to 100nm mNPs (A-C), 200nm mNPs (D-E) and control sample (F, no mNPs). Plain mNPs are shown in A and D whilst penetratin functionalised mNPs are shown in B and E. Figure 4C refers to penetratin functionalised 100nm mNPs at a higher magnification. This figure demonstrated that mNPs became associated with the gel surface (upwards pointing arrows) and were also seen within the gel itself (downwards pointing arrows) [scale bars 50μm].

3.4.3.2 Inductively Coupled Plasma Mass Spectrometry (ICP-MS)

The amount of gel-mNP uptake was quantified by ICP-MS analysis of iron after each of the four mNP species (100nm plain/penetratin, 200nm plain/penetratin) had been incubated with the gel, +/- a MF, for either 1 or 18 hours (Figure 3-8). The term 'uptake' is used to describe any mNP association with the gel that was not removed by washing (penetratin NPs, being positively charged, naturally repel positively charged collagen, thus no cross association was assumed). Results demonstrated that after 1 hour, uptake of 100nm mNPs was dramatically increased on average 103% by a MF ($p<0.01$), and 162% by penetratin ($p<0.001$). Similarly, uptake of 200nm mNPs was increased on average 103% by a MF (no significance), and 243% by penetratin ($p<0.01$) Figure 3-8B. Interestingly, at 18 hours, uptake levels were comparable, irrespective of a MF or penetratin (with the exception of 200nm penetratin without MF). Combining both a MF and penetratin simultaneously had a slightly attenuating effect on uptake of 100nm mNPs after 1 hour. After 18 hours, no significant attenuating effect was seen for either size. It is apparent from these results that the application of a MF and the

presence of penetratin both increased the speed of gel mNP-uptake, with penetratin being the fastest. It was interesting to compare the effect of a MF between plain and penetratin mNPs. To do this plain mNPs without a MF was considered the base rate of standard, "unaided" mNP-gel uptake. This comparison showed that a MF was required to increase plain mNP uptake, whereas when penetratin was attached, this requirement no longer existed - penetratin mNPs were able to reach the maximal level of uptake after 1 hour without a MF. There was little to no difference between the uptake levels induced by a MF and by penetratin. A MF had no additional effect on the level of penetratin mNP-gel uptake.

In a side-experiment, ICP-MS was also used to quantify the level of uptake of the same four mNP species into h-TERT cells grown in 2D monolayer cell culture (Figure 3-9). This provided a useful comparison to the data obtained for the 3D gel system presented in Figure 3-8. Interestingly, the results showed that the pattern of uptake in the 3D system followed a similar trend to the pattern of uptake in the 2D system. The main conclusion that can be drawn from this finding is that the uptake observed in 3D was definitely cell-dependant, rather than simply diffusion into the gel.

N.B [Since results were similar for both sizes of mNPs, and a smaller size is deemed optimal for dense tissue penetration, only the 100nm mNPs were used in all further investigations.]
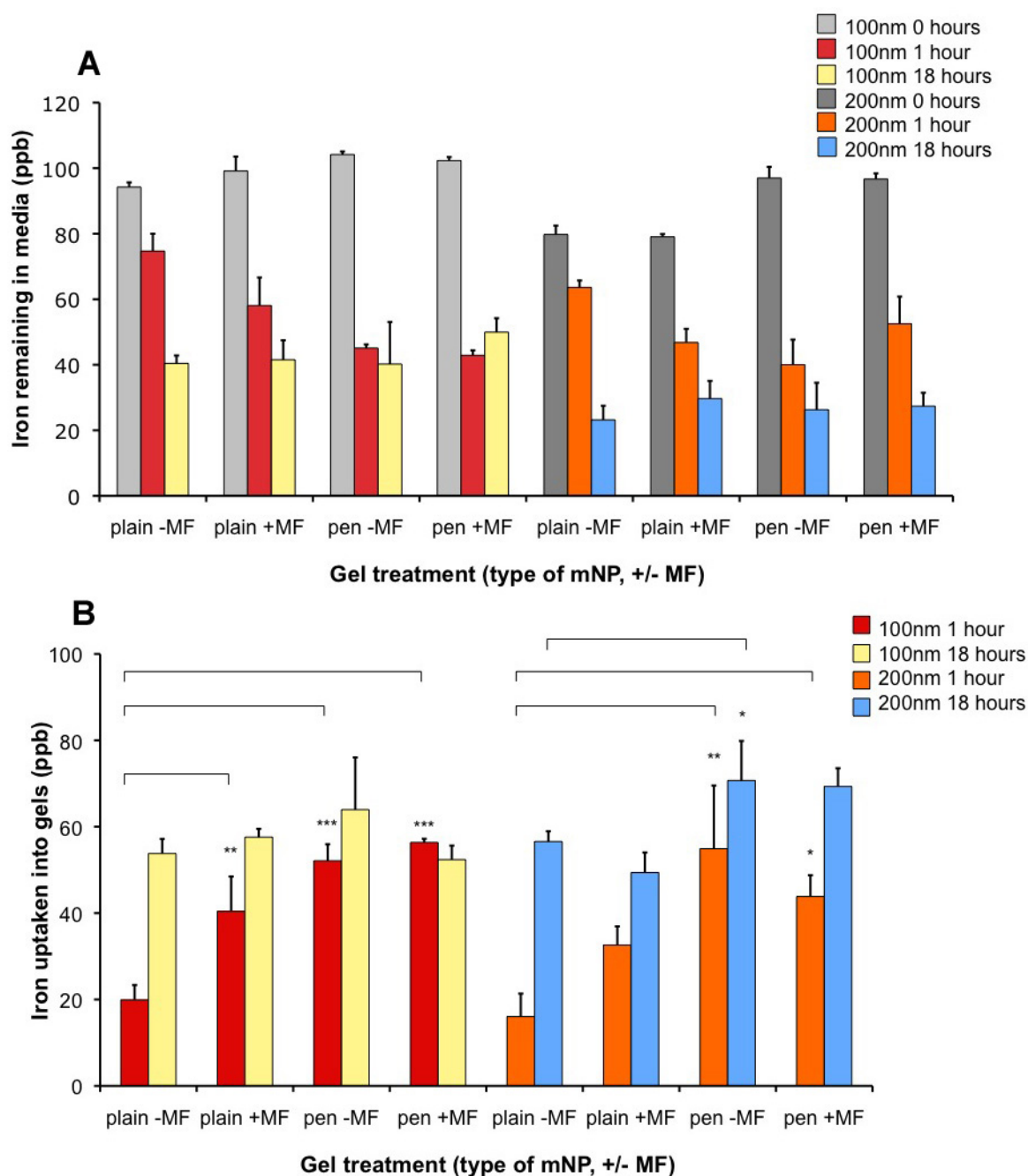
Figure 3-8 Iron uptake into 3D cell cultures as assessed by ICP-MS
Graph A is the raw ICP-MS data showing the levels of iron that remained in the culture media after incubation. Graph B is the converted data showing the levels of iron uptake into the 3D collagen gels after incubation. 100nm mNPs are represented in the left hand side of these graphs by red (1 hour) and yellow (18 hours) bars. 200nm mNPs are represented in the right hand side of these graphs by orange (1 hour) and blue (18 hours) bars. The x-axis refers to plain or penetratin functionalised mNPs samples (indicated by plain or pen respectively) treated without or with a magnetic field (indicated by -MF or +MF respectively). This figure shows that a MF and penetratin both increased the speed of mNP uptake into 3D cell cultures. (* = p<0.05, ** = p<0.01 and *** = p<0.001 as analysed by one-way ANOVA with Dunnett's test in SPSS. Error bars are SD, n=3.)
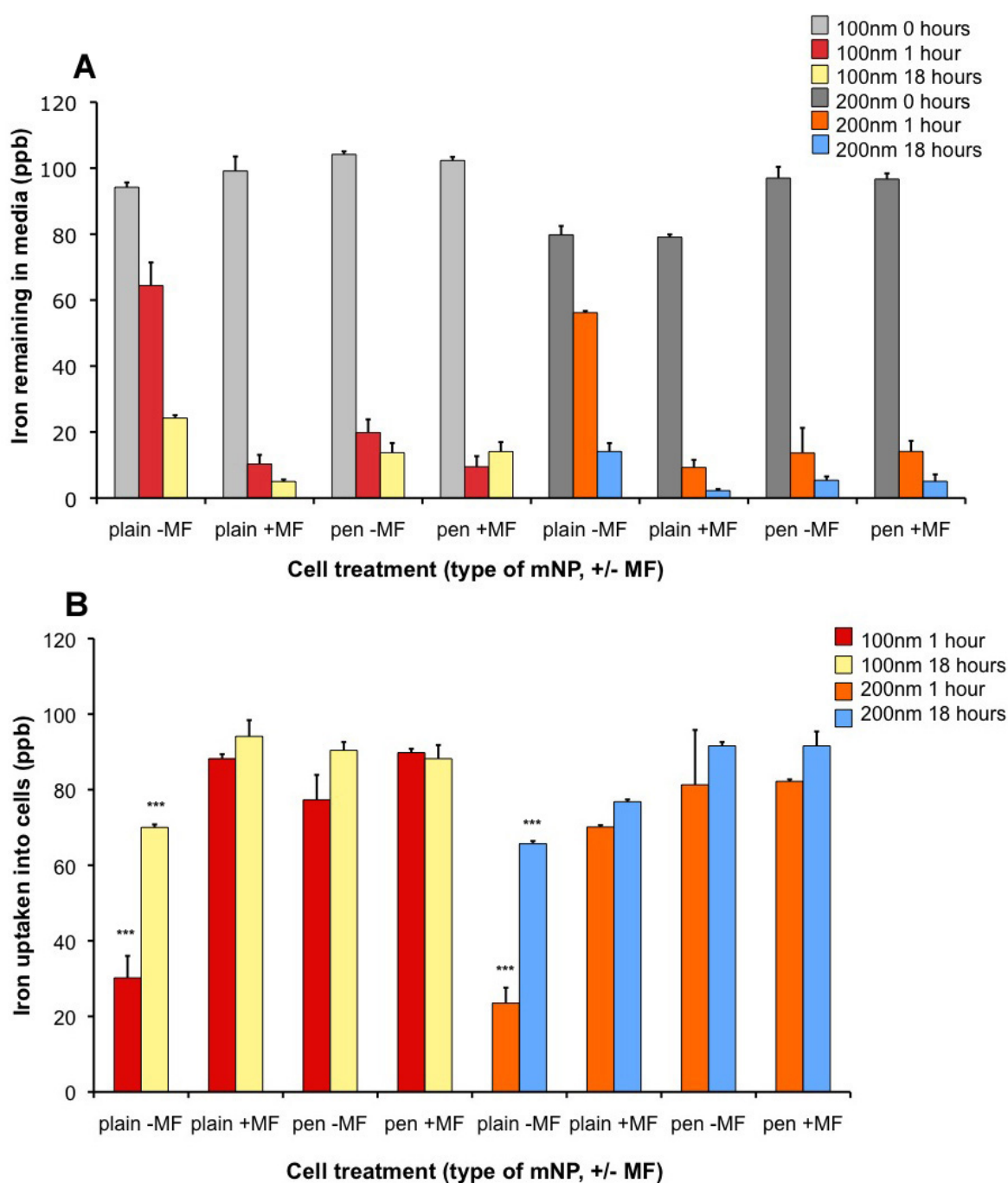
Figure 3-9 Iron uptake into 2D cell cultures as assessed by ICP-MS
Graph A is the raw ICP-MS data showing the levels of iron that remained in the culture media after incubation. Graph B is the converted data showing the levels of iron uptake into the 2D monolayer cell cultures after incubation. 100nm mNPs are represented in the left hand side of these graphs by red (1 hour) and yellow (18 hours) bars. 200nm mNPs are represented in the right hand side of these graphs by orange (1 hour) and blue (18 hours) bars. The x-axis refers to plain or penetratin functionalised mNPs samples (indicated by plain or pen respectively) treated without or with a magnetic field (indicated by -MF or +MF respectively). This figure shows that a MF and penetratin both increased the speed of mNP uptake into 2D cell cultures. (The four bars denoted with *** were found to have p<0.001 compared to all three other bars within that colour group (red, yellow, orange or blue), as analysed by one-way ANOVA with Dunnett's test in SPSS. Error bars are SD n=3.)

3.4.3.3 Fluorescence Microscopy

In order to visualise the possible interaction of 100nm mNPs with the surface layer of the gel, gels were imaged on a fluorescence microscope after 18 hours of incubation with plain or penetratin 100nm mNPs, +/- a MF. Results indicated that a high number of both plain and penetratin mNPs became associated with the surface of the gel in all conditions (Figure 3-10), an observation confirmed by analysis using Image J. From these images it is suggested that without a MF there were more penetratin mNPs on the surface of the gel (Figure 3-10E) than there were plain mNPs (Figure 3-10C). This reflected the ability of penetratin to enable the mNPs to become cell-associated on the surface of the gel. While this technique was useful to visualise mNP interaction on the gel surface, the depth of gel uptake of 100nm penetratin mNPs was subsequently assessed using confocal microscopy (Figure 3-11).
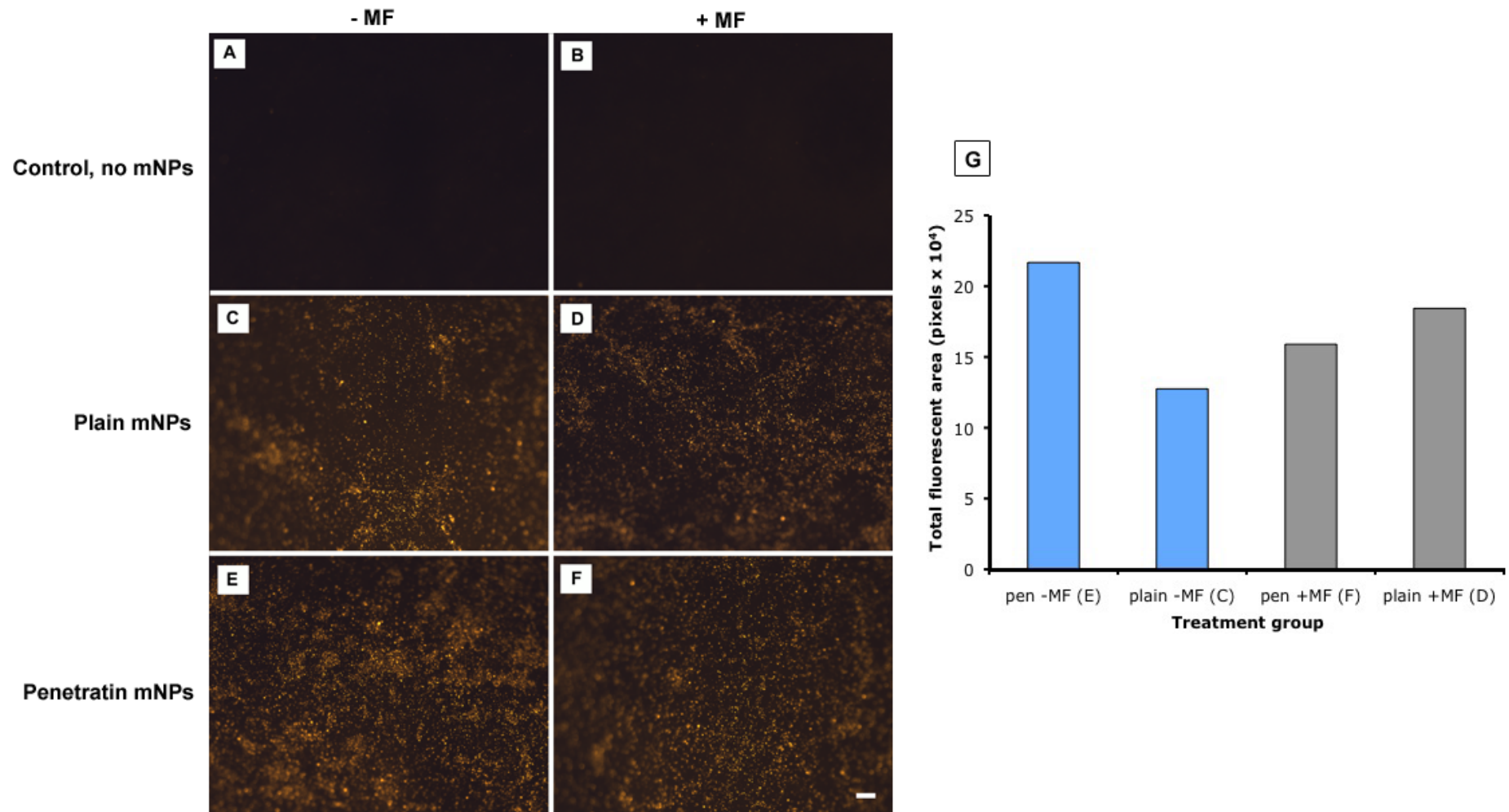
Figure 3-10 Gel surface localisation of 100nm mNPs after 18 hour incubation
Control gels had no mNPs present (A, B). Plain mNPs (C, D) and penetratin mNPs (E, F) were both clearly evident on the gel surface after incubation. A, C, and E were incubated without a magnetic field (-MF), whereas B, D, and F were incubated with a magnetic field (+MF). The fluorescence signal in images C-F was quantified *via* Image J and expressed graphically (G) [scale bar = 50μm].

3.4.3.4 Confocal Microscopy

To assess the depth of 100nm penetratin mNP uptake, gels (with a total depth of 3mm) were imaged on a confocal microscope, +/- a MF, after 1 and 22 hours incubation. This allowed visualisation of the fluorescent mNPs within the gel through the z-axis, and consequent measurement of the depth to which they had penetrated +/- a MF (Figure 3-11). The Z-stacks showed that 1 hour incubation +/-MF, and also 22 hour incubation -MF resulted in a shallow penetration depth with no significant difference between groups. Thus, 100nm penetratin mNPs were only able to penetrate the gel to a very minimal depth, which was not increased with longer incubation. However, when a MF was applied, after a 22 hour incubation mNP uptake distance was increased on average by 503% (p<0.01), to a depth of 728μm, at a rate of 33μm h$_{-1}$. This experiment demonstrated that penetratin alone did not facilitate mNP movement in 3D, but if aided by a MF and incubated for enough time, functionalised mNPs can be pulled to a considerable depth within the gel. These results are in agreement with the findings of fluorescence microscopy, which indicated that there was a higher density of penetratin mNPs evident on the gel surface without a MF (Figure 3-10E) as compared to with a MF (Figure 3-10F). N.B [The accuracy of confocal microscopy depended on the starting plane height of each gel, which inevitably varied very slightly between each individual gel. This could explain the insignificant variation in results between 1 and 22 hours, without a MF.]
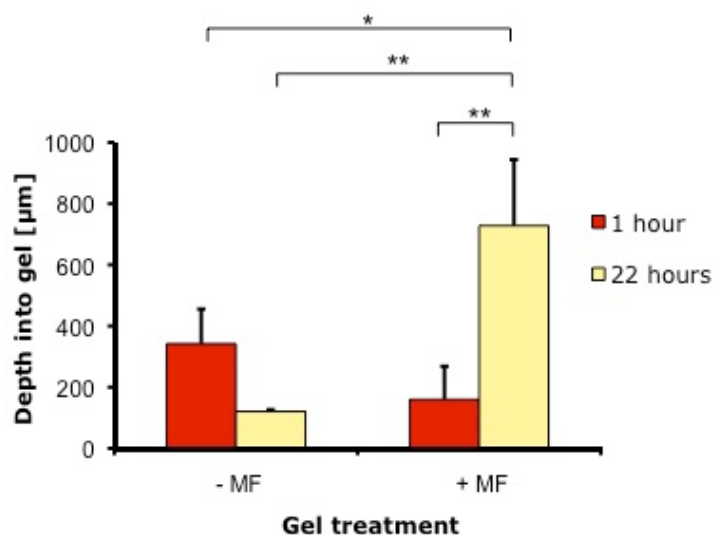
Figure 3-11 Gel uptake depth of 100nm penetratin mNPs
This figure shows the uptake depth of 100nm penetratin-functionalised mNPs into 3D collagen gels as assessed by confocal microscopy. On the x-axis, samples treated without or with a magnetic field (MF) are indicated by – MF or + MF respectively. Red or yellow bars refer to 1 or 22 hours of incubation respectively. This figure indicates that after 22 hours a MF significantly increased the depth of gel-uptake of 100nm penetratin mNPs. (* p<0.05, ** p<0.01 as analysed by one-way ANOVA with Tukey's test in SPSS. Error bars are SD, n=3.)

3.4.3.5 Transmission Electron Microscopy (TEM)

Confocal microscopy results demonstrated that a MF was able to pull mNPs into the gel. However it was also important to identify if these functionalised mNPs were being taken up by cells at this depth; a requirement for *in vivo* drug delivery. To answer this question, TEM was used to image gels after incubation with 100nm penetratin mNPs for 18 hours, +/- a MF (Figure 3-12). TEM results showed that 100nm penetratin mNPs localised within cells at a gel depth of around 500μm, when treated with a MF (Figure 3-12C and D). For comparison, images were taken of 100nm penetratin mNPs inside cells grown in 2D monolayer cell culture (Figure 3-12 A and B). This experiment supported the confocal results, demonstrating that a MF was able to pull functionalised mNPs through the gel structure, where cells growing within it can internalise them. This cellular uptake is most likely aided by penetratin attachment, since the mNPs observed were not located in cellular vesicles, resulting from the fact that CPPs are reported to facilitate direct translocation across the plasma membrane, thereby avoiding the endo-lysosomal pathway (Jarver and Langel, 2006).
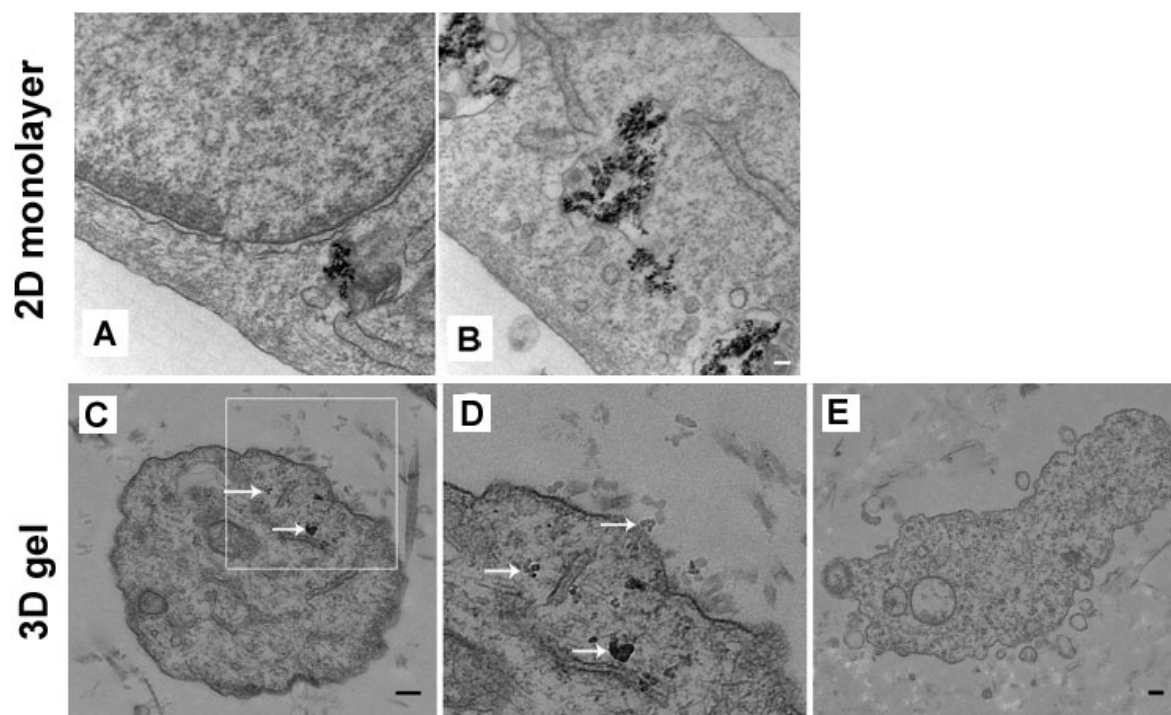
Figure 3-12 Uptake of 100nm penetratin mNPs into cells grown in 2D and 3D
A and B show mNPs inside a cell grown in 2D monolayer in the presence of a magnetic field
(MF). C and D show mNPs (indicated by white arrows) inside a cell grown in a 3D collagen
gel in the presence of a MF at a depth of around 500μm into the gel. D is a magnified section
of C. E is a control gel (no mNPs). This figure demonstrates that the combination of a CPP
with a MF can facilitate the delivery of mNPs to cells growing in 3D [scale bars = 200nm].

3.5 Summary

This study has utilised fibroblast-seeded collagen gels to investigate whether a MF and NP- functionalisation with the CPP penetratin could be used to enhance the delivery of mNPs to cells grown in 3D, in order to assess the potential of these techniques for *in vivo* drug delivery. Gel-mNP uptake analysis showed that on average a MF doubled the speed of gel-mNP uptake, and caused a 5-fold increase in the depth of gel-mNP uptake, occurring at a rate of $33\mu m\ h^{-1}$. Penetratin, however, more than doubled the speed of 100nm gel uptake, more than tripled the speed of 200nm mNP gel uptake, increased the localisation of mNPs to cells on the gel surface, but had no effect on the depth of gel-mNP uptake.

3.6 Discussion

3.6.1 Characterisation of the 3D Model

The characterisation results suggested that the 3D cell-seeded collagen gels used in this project were a realistic tissue-equivalent model suitable for the assessment of NP delivery. The gels were shown to have an elasticity similar to that of human tissue, and to contain viable cells that were well dispersed throughout the collagen matrix. Previous 3D models that have been used to test NP delivery include acellular gels and multicellular spheroids. These 3D systems are not ideal and it is believed that collagen gels overcome some of the disadvantages associated with these types of earlier models.

Acellular Gels

The use of acellular gels was demonstrated by Kim *et al*, who used acellular 2% agarose gels with pore sizes of 100nm to assess the therapeutic potential of drug-loaded worm micelles composed of polylactic acid (PLA) and amphiphiles. This agarose gel model was used to measure the 3D permeation abilities of the fluorescently tagged worm micelles, and demonstrated that their elongated shape provided a physical advantage to deliver drugs deep into tissue (Kim *et al.*, 2005). A second example of the use of acellular gels is a study by Valentine *et al*, who used 3D biopolymer networks composed of fibrin or actin to assess

the effect of different microsphere surface modifications on particle mobility. Results showed that the attachment of PEG reduced protein adsorbtion, and thereby increased particle movement within the 3D biopolymer network, as would be a desirable attribute to achieve targeted drug delivery *in vivo* (Valentine *et al.*, 2004).

The main advantage of using acellular gels is that they mimic some of the types of extracellular hindrances to NP delivery that exist *in vivo*, which are not present in 2D monolayer cell culture, including small pore size and the ECM. However, their main shortcoming is an inability to accurately predict cell responses to NPs. In comparison to my work, although acellular gels do represent a step forward from 2D monolayer cell culture, cell-seeded collagen gels are a better choice since they are more comparable to natural tissue due to the inclusion of cells. Results presented in this chapter have demonstrated that cells were evenly distributed throughout the collagen gel, and remained viable at both the gel centre and edge, indicating that this 3D model suitably mimics the *in vivo* cellular environment and therefore acts as a good tissue-equivalent model for testing NP delivery.

Multicellular Spheroids

Multicellular spheroid growth can be initiated by growing cell cultures in a spinner flask or on agar-coated culture plates (Nederman and Twentyman, 1984) Their use was demonstrated by Goodman *et al* who used SiHa cervical carcinoma cell spheroids as a 3D tumour model to investigate the penetration of carboxylated polystyrene NPs. This study reported that NPs functionalised with ECM degrading enzymes such as collagenase, displayed a 4-fold increase in penetration into the spheroid (Goodman *et al.*, 2007).

Multicellular spheroids are considered to be a good 3D tumour model due to the fact that they mimic properties of avascular regions of solid tumours, including regions of proliferation, quiescence and a necrotic core (Waleh *et al.*, 1994). However, their main disadvantage is a lack of ECM proteins and outside forces such as mechanical stress (Goodman *et al.*, 2008). In comparison to my work, the main difference between the two models is cell density; in multicellular spheroids the cells are arranged in very dense, compact clusters, whereas in the

collagen gels the cells are more spread out and interspersed with the collagen matrix, which provides them with a more realistic ECM. Most likely, the cell density of real tissue is somewhere in-between these two models, although the spheroids may be more representative of the high density environment within a tumour since a necrotic core was not visualised within the collagen gels, where cells remained viable throughout. (This core viability was most likely due to the fact that matrix pore sizes of 5μm allowed for free diffusion of nutrients to the centre of the gel.) In addition to the benefits of high cellular viability and the provision of an ECM, cells grown within collagen gels aligned in a striated fashion, indicative of inherent cell-mediated gel tensile forces (Eastwood *et al.*, 1998), which do not exist to such an extent in multicellular spheroids. Therefore, although multicellular spheroids are a more realistic 3D model than acellular gels, collagen gels are deemed to be a better choice since they provide a suitable ECM matrix and tensile forces, such as the cells would experience in natural *in vivo* tissue.

3.6.2 ICP-MS

The trends observed with the ICP-MS data were the same for both 100 and 200nm mNPs. The only notable difference was that penetratin (-MF) resulted in a greater increase in the gel uptake of 200nm mNPs compared with the 100nm mNPs. This difference could be an artefact because since the 200nm mNPs have a larger hydrodynamic diameter they contain more iron (i.e. the volume ratio of 100nm:200nm mNPs is 1:8.2). This means that even though the level of iron uptake was different the number of particles taken up may actually be the same However, it is likely that the difference in penetratin-induced uptake was caused by the 200nm mNPs carrying more penetratin molecules per particle than the 100nm mNPs (Table 3-1), resulting in increased cell uptake. As smaller NPs were considered to be better drug delivery candidates (due to cell accessibility in the tight collagen matrix and their larger surface area to volume ratio) the 100nm mNPs were used in all further investigations.

It is useful to clarify that 'increased speed of uptake', refers to the fact that the level of gel-mNP uptake that occurred under the influence of a MF/penetratin, was higher than that of the control mNPs (no MF/penetratin) after 1 hour, but became equal to that of the control mNPs after 18hours.

We know that the mNP sample added did not expire, thereby preventing any further uptake, as the level of uptake reached after 18 hours always remained lower than the total level of sample that the gels were challenged with (Figure 3-8A). Therefore it seems more likely that, for some reason, the gels have a maximum threshold level of gel-mNP uptake, which was reached much faster than normal under the influence of a MF/penetratin, but once reached it could not be increased any further. This uptake threshold was evident in both the 2D and 3D data, suggesting that the effect is cell- rather than gel-dependent, and is most likely due to cell uptake saturation. The idea that cells have a natural threshold level for NP uptake is supported by numerous publications reporting a NP 'uptake plateau' after a certain length of time. For example, in a 2D magnetofection study, Plank *et al* showed that a MF increased the amount of mNP uptake after 10mins, but did not increase the amount of uptake achieved after 4 hours, suggesting that the cells reached their threshold level of mNP uptake which could not be bypassed once it had been reached (Plank *et al*., 2003). In addition, Harush-Frenkel *et al* used fluorescence-activated cell sorting (FACs) analysis to quantify the uptake of PLA fluorescent NPs into HeLa cells, and found that NP uptake plateaued within 45-60mins. The authors postulated that this indicated possible NP recycling and or binding saturation, which might have resulted in an inability to internalise additional NPs (Harush-Frenkel *et al*., 2007). Similarly, Zaki *et al* used fluorimetry to quantify the uptake of hyaluronic-acid (HA)-coated chitosan NPs into macrophages, and found that NP uptake plateaued after 6 hours. The authors postulated that this plateau effect indicated that NP-uptake is dependent on receptor-mediated endocytosis, and that this apparent saturation may have been caused by the kinetics of recycling of the HA receptors. This idea is based on the fact that for soluble HA, the receptors are internalised with their ligands and require a significant time to be transported back to the cell surface, during which time the internalisation capacity of the cell is reduced (Zaki *et al*., 2011).

This list of 2D studies reporting NP uptake plateaus supports my ICP-MS data, which suggests that a cellular threshold level of NP uptake exists. However, my work is one of the first to exemplify that this phenomenon also effects NP uptake in 3D, an important aspect to consider for NP delivery *in vivo*.

3.6.3 Effect of the Magnetic Field (MF)

MFs are commonly used to attract mNPs into cells grown in 2D. The confocal data presented in this chapter demonstrated that a MF was also able to pull mNPs into a 3D system; pulling 100nm penetratin mNPs to an average depth of 728μm, at a rate of 33μm h^{-1}. Similar 3D studies by Kuhn *et al* have reported that under the influence of a static MF, 145nm mNPs travelled through a hydrogel at 1.5mm h^{-1} (Kuhn *et al.*, 2006b) and travelled through a collagen-supplemented gel at 90μm h^{-1} when functionalized with the enzyme collagenase (Kuhn *et al.*, 2006a). For both of these studies, the MF strength was 100-500mT, which is comparable to the 280mT used in my experiments on collagen gels. The NP travel-rate of 1.5mm h^{-1} achieved by Kuhn *et al* is much faster than my NP travel-rate of 33μm h^{-1}. However, this difference can be explained by the fact that Kuhn *et al* were using a hydrogel that does not contain the same resistance to NP-travel as that of a gel composed of collagen fibres. Indeed, the hindrance to NP-travel caused by the presence of collagen is exemplified by the fact that Kuhn's rate of NP-travel was significantly reduced to 90μm h^{-1} upon the introduction of collagen into the 3D model. Collagen is one of the main components of the ECM (Di Lullo *et al.*, 2002) and these comparative studies demonstrate that the presence of this protein significantly increases resistance to mNP movement. This highlights the importance of testing NP delivery in a 3D model that realistically represents the *in vivo* barriers to NP delivery posed by the ECM. The results in this chapter demonstrate that a MF caused on average a 5-fold increase in the depth of gel-mNP uptake, and the literature suggests that mNP functionalisation with a proteolytic enzyme such as collagenase could increase this depth even further.

One of the best comparisons to the work presented in this chapter is a recent study by Zhang *et al*, who used a very similar 3D fibroblast seeded collagen gel model to achieve 3D magnetic delivery of 30nm mNPs conjugated to siRNA,

resulting in up to 82% silencing efficiencies (Zhang *et al.*, 2010). As a proof-of-concept, the authors demonstrated that traditional transfection agents (such as Lipofectamine and FuGene), which displayed transfection efficiencies of 90-95% in 2D, did not work at all in 3D due to a lack of permeation into the collagen matrix (exemplifying the uselessness of these transfection agents *in vivo*). The authors found that collagen gel transfection efficiencies could be improved to 5% using 250nm mNPs, and to 64% using 30nm mNPs (in both cases using a 1.2T MF). This highlights the potential of using magnetically guided NPs to overcome the barriers associated with 3D tissue transfection. It also demonstrates the fact that larger mNPs find it more difficult to permeate the tight collagen matrix than smaller mNPs, even under an external MF, which supports my decision to choose 100nm mNPs over 200nm mNPs for optimal delivery in my collagen gel model. Interestingly, the authors also noted that 3D transfection reached a maximum at 3 hours, supporting my previously discussed finding that 3D collagen gels displayed a maximum threshold for mNP-delivery. Interestingly, the authors also demonstrated the effectiveness of using collagen gels to quickly and easily screen shRNA plasmids for toxicity (some of which were shown to cause up to 51% cell death), which I think will be an important aspect of pre-clinical 3D screening if therapeutic gene therapy is to be made widely available.

3.6.4 Effect of the CPP

This chapter confirms previous findings from our lab that the CPP penetratin can increase the uptake of mNPs into fibroblast cells (Dejardin *et al.*, 2011). This penetratin-induced increase in NP cellular uptake has also been reported by Nativo *et al*, who found that penetratin-conjugated gold NPs displayed increased endocytosis in Hela cells after 2 hours as assessed by TEM (Nativo *et al.*, 2008). In addition, Petersen *et al* found that the attachment of penetratin doubled the amount of AuNP uptake in endothelial cells after 2 hours as assessed by laser scanning confocal microscopy (Petersen *et al.*, 2011). Tseng *et al* reported that there was a 1 hour peak of penetratin-induced cellular uptake of liposomes, after which time uptake declined (Tseng *et al.*, 2002). This could relate to the pattern of penetratin-induced uptake reported in this chapter, since ICP-MS showed that maximal mNP uptake was also achieved after a 1 hour incubation.

As described, it is well reported that CPPs increase cellular uptake of associated NPs in 2D cell systems. However, no other studies can be found on the effects of penetratin on NP delivery to cells in 3D, highlighting the novelty of this chapter, which allows for fresh insights to be gained about how this CPP may perform *in vivo*.

ICP-MS results showed that penetratin increased the speed of mNP uptake into the 3D gel. In this 3D model system, a cell layer was observed on the gel surface, most likely due to the initial gel contraction, causing a concentration of cells at the periphery. Penetratin-induced gel-mNP uptake is thus most likely caused by the increased uptake of mNPs into this surface layer of cells. The confocal data confirmed that penetratin mNPs did not move deeply into the gel and away from this surface layer without a MF. This lack of movement is in fact one of the main problems when trying to target functionalised NPs to a diseased tissue *in vivo* (Prijic and Sersa, 2011) (Dobson, 2006b) and is explained by the fact that CPPs cannot independently travel through the collagen gel matrix. Therefore it is imperative that CPPs be used in conjunction with a targeting technique, such as a MF, to enable mNPs to reach and subsequently enter target cells, in order to facilitate drug delivery. While CPPs and magnetic fields have been used in conjunction in a select few 2D studies ((Smith *et al.*, 2010; Song *et al.*, 2010) this is the first use of this combined approach in a 3D model. It was proved successful since TEM images showed that following magnetically induced movement through the gel, the 100nm penetratin mNPs were able to achieve cellular uptake at this increased depth within the gel. Due to the fact that these mNPs were seen free in the cytoplasm, it is possible that they translocated directly across the plasma membrane, facilitated by the attached CPP, thus supporting the hypothesis that CPPs can be used to prevent degradation by the endo-lysosomal pathway (Jarver and Langel, 2006). This work has demonstrated that if used together, a MF and CPPs show huge potential to facilitate targeted drug-delivery *in vivo*.

Although it is hard to directly compare it against additional CPPs, in terms of increasing cell uptake of NPs in 2D and 3D, penetratin appears to be one of the most effective CPPs currently presented in the literature. Interestingly, a recent study by Maniti *et al* investigated the mechanism by which penetratin works to

increase cellular uptake, and concluded that the CPP induces direct translocation across the plasma membrane. The authors also discovered that penetratin induces a second mechanism termed 'physical endocytosis', whereby the creation of endocytotic membrane invaginations is driven by the peptide's self-capacity to induce negative curvature rather than through the use of metabolic energy (Maniti *et al.*, 2012). This leads to speculation that penetratin may hold additional benefits compared to other CPPs, such as Tat, since its unique lack of cellular energy requirement could be considered less disruptive to normal cellular function. This metabolic energy-independent mechanism of action, together with its herein proven ability to increase cellular uptake in 3D, suggest that penetratin is an excellent CPP candidate to be taken further into *in vivo* studies of drug delivery.

3.7 Conclusion

This study has been the first to investigate the combined effects of a MF and a CPP on the delivery of mNPs to cells growing in a 3D environment. This proof-of-concept study has shown that a MF significantly enhanced the movement of mNPs though the tissue-equivalent model, while a CPP facilitated cell uptake at this increased depth. These results suggest that the best strategy for site-specific drug delivery *in vivo* will be to use these techniques together thereby providing both targeting and cellular uptake of drug- loaded mNPs.

4 Cellular Response to AuNPs

4.1 Introduction

Cancer is caused by the incorrect expression of genes that control the cell cycle. One such gene is c-myc, a positive regulator of the cell cycle found to be overexpressed in the majority of cancers (Pelengaris and Khan, 2003; Aulmann *et al.*, 2006; Beroukhim *et al.*, 2010b; Borg *et al.*, 1992; Bourhis *et al.*, 1990; Deming *et al.*, 2000; Kozma *et al.*, 1994). Modern research aims to develop a therapy whereby this incorrect gene expression associated with cancer can be rectified at the molecular level, as a method of disease treatment. One way that incorrect gene expression can be reduced is through RNA interference (RNAi), a natural cellular mechanism discovered by Fire and Mello in 1998 (Fire *et al.*, 1998). This mechanism enables a target gene to be silenced *via* the destruction of its mRNA, by the introduction of a short interfering RNA (siRNA) with complementarity to the target mRNA (Ameres *et al.*, 2007). The siRNA gets incorporated into the enzymatic RISC complex found in the cytoplasm, activating RISC to find and destroy the complementary endogenous target mRNA (Rand *et al.*, 2004), preventing its translation into protein.

Since Tuschl *et al* first demonstrated that artificial siRNA, 21nt in length, can be used to silence mRNA in mammalian cells (Elbashir *et al.*, 2001), RNAi has become a prominent research tool used for gene knockdown studies (Gondi and Rao, 2009; Kurreck, 2009). Currently, the most difficult task in performing RNAi is the cellular uptake of negatively charged siRNA, as it cannot naturally cross the cell membrane (Akhtar *et al.*, 1991; Wittung *et al.*, 1995). For research purposes, the transfection agent Lipofectamine and electroporation are used to promote cellular uptake of siRNA for RNAi. However, due to toxicity issues and lack of specificity, these techniques would be unsuitable to deliver siRNA for RNAi *in vivo*. In addition, naked siRNA suffers from degradation if injected directly into the bloodstream, as it is unprotected from nucleases (Dykxhoorn and Lieberman, 2005). Therefore, in order for RNAi to be used in a clinical setting, a delivery vehicle must be found to enable siRNA entry into diseased cells within the body (Huang *et al.*, 2008; Whitehead *et al.*, 2009). Nanoparticles (NPs) present as a very promising candidate for this delivery task (Juliano *et al.*, 2008). Firstly, because they can have numerous cargos and functional molecules attached to their surface (Song *et al.*, 2005; Derfus *et al.*, 2007; Paciotti *et al.*,

2006), and secondly because they provide the cargo with protection against degradation as it is carried through the body to the target cells requiring RNAi therapy (e.g. to cancer cells within a tumor) (Lee *et al.*, 2009b).

While many different types of NPs are currently under development, gold NPs (AuNPs) are a very popular choice for the development of a therapeutic delivery vehicle (Huang *et al.*, 2007; Sanvicens and Marco, 2008). Reasons for this include its low toxicity (Connor *et al.*, 2005), good optical properties and ease of functionalisation (Lee *et al.*, 2009c; Chen Pc, 2008). Many studies have shown that AuNPs can be internalised by cells, and that this process can be increased by functionalisation with CPPs, such as Tat (Berry, 2008; Braun *et al.*, 2009; Smith *et al.*). Furthermore, AuNPs have proven popular for the delivery of siRNA, although to date the majority of AuNP knockdown studies have used siRNA targeted to reported genes such as luciferase or GFP, instead of an actual gene. The second project of this PhD (as presented in chapters 4 and 5) has aimed to take the next step and use AuNPs to deliver siRNA directed against the c-myc oncogene.

4.1.1 The Nanotruck Project

The Nanotruck project was a European Union funded project with the vision of developing nanoparticle-mediated therapeutic RNAi as a method of cancer treatment. This PhD formed part of the collaborative Nanotruck project aiming to design, develop and test an optimal AuNP species to silence the c-myc oncogene by RNAi, *via* the delivery of complementary siRNA, thus slowing cancerous cell proliferation and growth. The collaborative side of the project involved five separate academic institutes. The AuNP synthesis was carried out by inorganic chemists in Zaragoza, Spain, whereby the particles were designed and functionalised, resulting in a library of different AuNP formulations. The AuNPs were subsequently forwarded to labs in Glasgow, Naples and Munich, for testing/screening with *in vitro* human cell lines, and *in vivo* invertebrate (freshwater polyp *Hydra*) and vertebrate (mouse) models respectively, thus allowing for robust testing of c-myc silencing efficiency.

4.1.1.1 Aims

The aim of the Glasgow lab, and this section of the PhD project, were to test 11 AuNP species synthesised by grant partners (Figure 4-2) in human cell lines in order to develop an optimal AuNP design for the delivery of siRNA to silence the c-myc oncogene by RNAi, as a method of cancer treatment. At the outset, the main screening objectives were investigation of AuNP performance in the following four criteria;

1) potential cell toxicity
2) cellular uptake
3) c-myc knockdown
4) effect on the cell cycle

4.2 Materials and Methods

4.2.1 AuNP Design and Synthesis

The AuNPs were synthesised by the citrate reduction method described by Lee and Meisel (Lee and Meisel, 1982), producing a NP composed of a gold core surrounded by a layer of citrate. These core particles were then functionalised with various different molecular attachments. First, a layer of thiolated-poly(ethylene glycol) (PEG) was attached to the AuNP core, facilitated by direct gold-sulphur bonding between the sulphur atoms in the thiol molecules and Au atoms in the particle core. Two types of PEG molecules were used, ending with either carboxylic acid (COOH) or azide (N3) functional groups. The PEG layer therefore played two main roles; 1) increasing AuNP therapeutic efficiency due to the many previously demonstrated benefits (i.e. to guarantee NP stability & avoid nonspecific interactions), and 2) providing a platform for the attachment of additional molecules that could be conjugated to the COOH/N3 PEG end groups. PEG-COOH was used to attach molecules that contained NH_2 groups (such as amino acids/peptides) *via* the EDC reaction, where COOH and NH_2 are bound together producing a peptide bond with the expulsion of water.
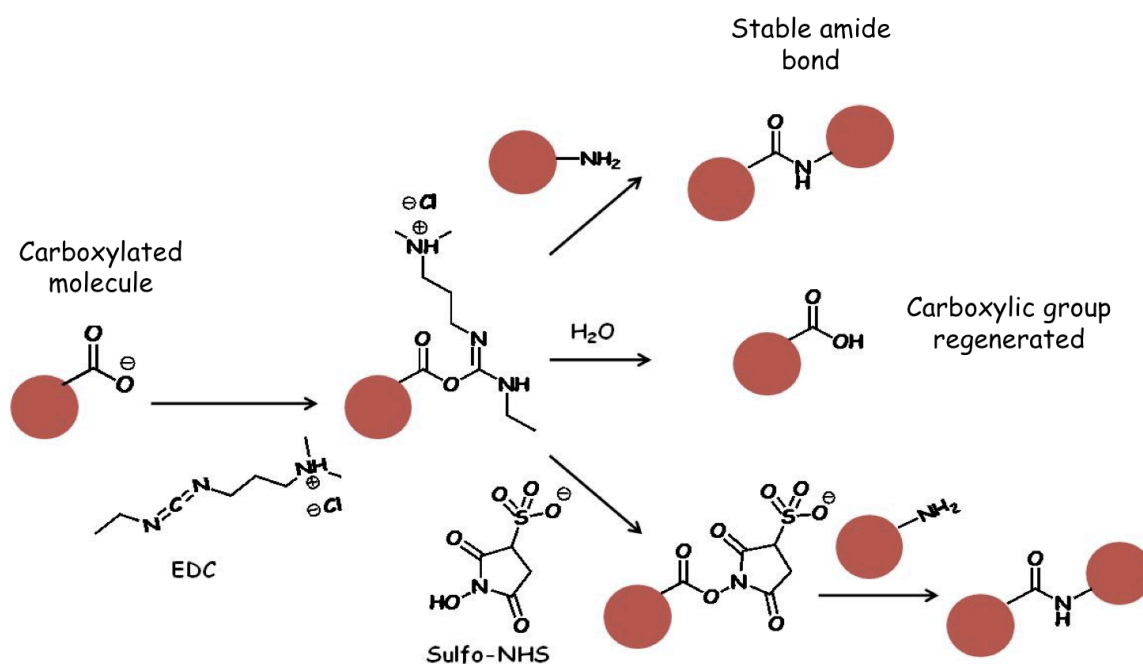
Figure 4-1 The EDC reaction
This figure illustrates the EDC reaction that was used to bind peptides, such as Tat and the R_4N group, to PEG-COOH chains on the AuNPs (image provided by grant partners).

The EDC reaction was used to attach the Tat peptide and the positively charged R_4N group to PEG-COOH on the AuNP. N.B [The R_4N group is a 5 amino acid long peptide composed of 1 asparagine residue (N) and 4 positively charged arginine residues (R). The purpose of the R_4N group was to provide a positive charge in order to ionically bind negatively charged siRNA to the AuNP]. The second type of PEG used, PEG-N3, was intended to be used to attach molecules *via* click chemistry, however synthesis proved difficult.

Two strategies were employed for siRNA attachment to the AuNP 1) the covalent approach, and 2) the ionic approach. The covalent approach involved thiolating the siRNA molecules and using gold-sulphur bonding to bind the siRNA covalently to the gold core of the particles. Alternatively, in the ionic approach, siRNA was attached ionically to the positively charged R_4N group (which was attached to PEG-COOH *via* the EDC reaction). The principles of the ionic approach were based on the fact that the R_4N group is positively charged at all pH values and has a great affinity for the negatively charged siRNA (because of its phosphate backbone). The ionic attachment was performed in DEPC-treated water with a pH around 6.5-7. Great care was taken to perform the ionic attachment at a pH where the siRNA was stable and in water instead of buffer to prevent electrolytes from weakening the bond between nanoparticles and siRNA since electrolytes also form ionic interactions with charged species.

During the process of developing the optimal AuNP species for c-myc RNAi, 11 different AuNP species were created by the chemists for testing/screening. These 11 samples were divided into three main classification groups;

1) **Primary Samples** – This group involved three samples; (i) the initial gold-citrate core produced after citrate reduction (pAu_citrate), (ii) a sample with a layer of PEG-COOH (pAu_COOH) and (iii) a sample with a layer of PEG-N3 (pAu_N3).

2) **Covalent Approach** – This group involved four samples (all of which had a mixed PEG layer including both PEG-COOH and PEG-N3); (i) a sample with no attachments other than PEG (cAu_plain), (ii) a sample with Tat (cAu_Tat), (iii) a sample with thiolated c-myc siRNA covalently bound to the gold core (cAu_siRNA), and (iv) a sample with Tat and thiolated c-myc siRNA covalently bound to the gold core (cAu_Tat, siRNA).

3) **Ionic Approach** – This group involved four samples (all of which had a mixed PEG layer including both PEG-COOH and PEG-N3, and the R_4N group attached to PEG-COOH); (i) a sample with no attachments other than PEG and R_4N (iAu-plain); (ii) a sample with Tat (iAu_Tat), (iii) a sample with c-myc siRNA ionically bound to the R_4N group (iAu_siRNA), and (iv) a sample with Tat and c-myc siRNA ionically bound to the R_4N group (iAu_Tat, siRNA) (see Figure 4-2).

Primary Samples   Covalent Approach   Ionic Approach

Sample Number	Sample Group	Sample Acronym	siRNA (strands/NP)
1	primary	pAu_citrate	-
2	primary	pAu_COOH	-
3	primary	pAu_N3	-
4	covalent	cAu_plain	-
5	covalent	cAu_Tat	-
6	covalent	cAu_siRNA	41
7	covalent	cAu_Tat, siRNA	48
8	ionic	iAu_plain	-
9	ionic	iAu_Tat	-
10	ionic	iAu_siRNA	79
11	ionic	iAu_Tat, siRNA	78
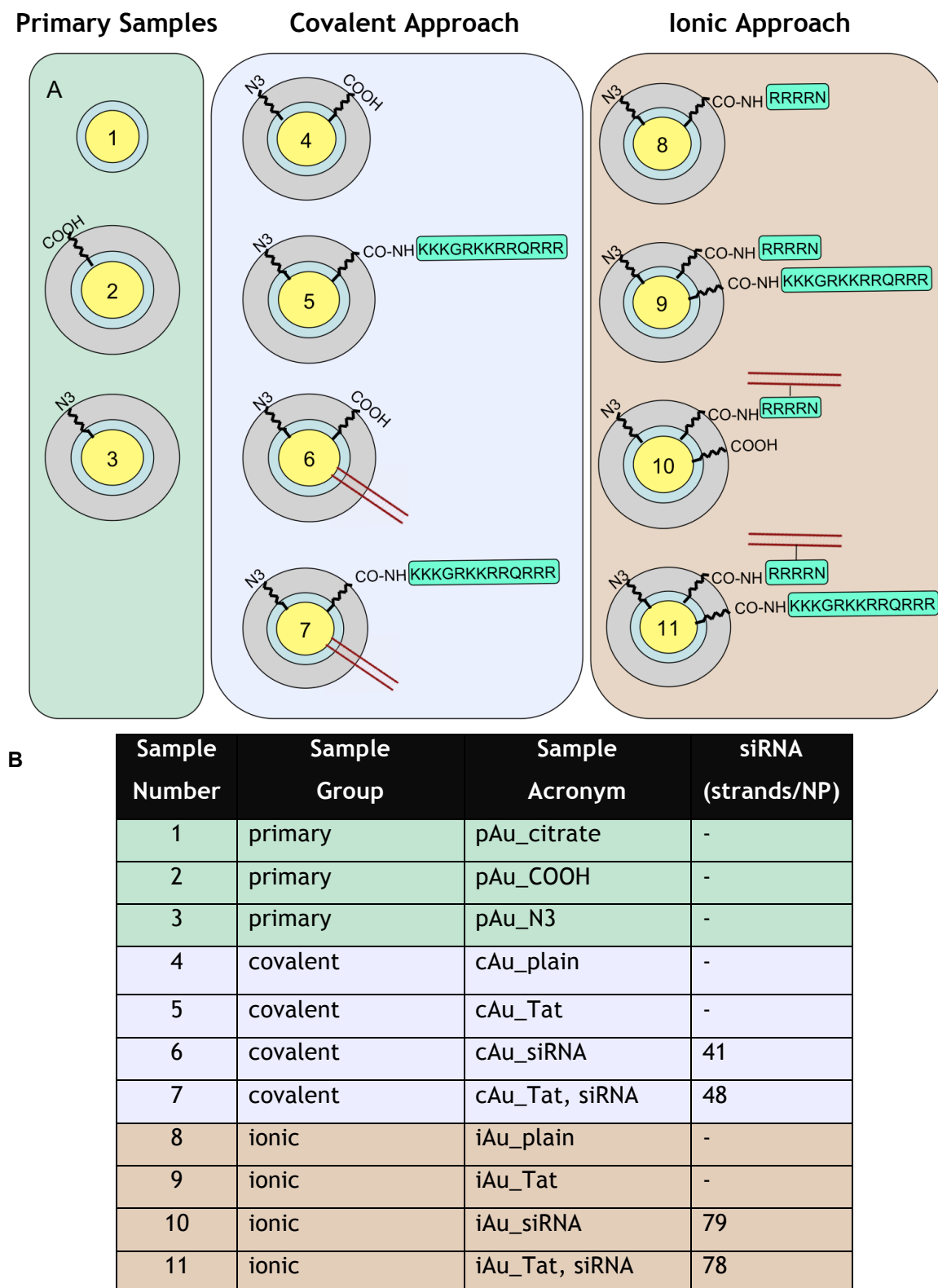
Figure 4-2 Description of the 11 different AuNPs employed in this chapter
Schematic representations of each sample (A) with a corresponding descriptive table (B). The 11 AuNP samples were divided into three classification groups; primary (green), covalent (violet) and ionic (orange). The various molecular attachments on each AuNP species have been displayed in a simplified manner. Yellow is the gold core, grey is the PEG layer, the red ladder is siRNA (complementary to c-myc mRNA), and turquoise boxes are peptides (showing the 1-letter code of each amino acid present). The 16-amino acid peptide is the cell penetrating peptide (CPP) Tat. The shorter, 4-amino acid peptide is the positively charged R_4N group used to ionically attach siRNA to the particle in the ionic samples (schematics not drawn to scale).

4.2.1.1 Experimental Details of AuNP Synthesis (provided by grant partners)

Synthesis of PEG Heterofunctional Surfaces. A mixture of 0.5 mg/ml of the citrate AuNP, 0.028 % SDS and 0.03 mg/ml SH-EG(7)-CH2-COOH (Iris-Biotech) and 0.015 mg/ml SH-CH2-CH2-CONH-EG(6)-CH2-N3 for NP-ionic and 0.015 mg/ml SH-EG(7)-CH2-COOH (Iris-Biotech) and 0.015 mg/ml SH-CH2-CH2-CONH-EG(6)-CH2-N3 for NP-covalent were prepared. NaOH was further added to a final concentration of 25 mM and the mixture was incubated for 16 hours at room temperature. The excess of PEG chains was removed by centrifugation at 14000 rpm for 30 minutes at 4°C and the supernatant was discarded. This washing process was repeated three times and the pellet with AuNPs was dissolved in pure water.

AuNP Functionalisation with Tat Peptides and Quaternary Ammonium Groups by EDC/NHS Coupling Reactions. 1 mg/ml NP-ionic/covalent were incubated in 1.25 mg/ml sulfo-NHS and in 25 mM MES (2-(N-morpholino)ethanesulfonic acid) buffer pH 6.1. For NP-ionic, 6.6 mg/ml of quaternary ammonium groups (R4N+) were added to the mixture, EDC (1-Ethyl-3-(3-dimethylaminopropyl)-carbodiimide) was added at a final concentration of 150 µg/ml and the mixture incubated for 20 min. Tat peptide was added at a final concentration of 0.8 µg/ml and the mixture incubated at room temperature for 16 hours. For NP-covalent EDC was added at a final concentration of 150 µg/ml, the Tat was added at a final concentration of 0.8 µg/ml and the mixture incubated at room temperature for 16 hours. After this period of time, the PEGylated AuNPs were centrifuged at 14000 rpm for 30 minutes at 4°C to remove the excess of the Tat peptide and the supernatants were recovered and tested for protein concentration by the Bradford assay.

AuNP Functionalisation with siRNA. For NP-ionic the unmodified siRNAs, at a constant concentration of 5 nmol/ml, were incubated with RNase-free solution of the NP-ion@R4N+@TAT (0.5 mg/ml) during 16 hours at 4°C. For NP-covalent, the purified SH-siRNAs, at a constant concentration of 5 nmol/ml, were incubated with RNase-free solution of the NP-cov@Tat (0.5 mg/ml) containing 0.028 % SDS. Subsequently, the salt concentration was increased to 0.1M NaCl

with brief ultrasonication following each addition to increase the coverage of oligonucleotides on the nanoparticle surface. After functionalisation during 16 hours at 4ºC, the particles were purified by centrifugation at (13000 rpm, 20 mins) at 4˚C, and re-suspended in DEPC-water. This process was repeated 3 times. The number of siRNA per gold nanoparticle was determined by using a nucleic acid intercalculator – GelRed. Briefly, the supernatants were incubated with GelRed 100× and TBE 0.5× and fluorescence was measured using a fluorometer Perkin Elmer LS55 with emission at 602 nm and compared to a standard curve.

4.3 Results

4.3.1 AuNP Characterisation

4.3.1.1 TEM

TEM was used to visualise each of the 11 AuNP species to provide information regarding their physical size and morphology. Images demonstrated that all 11 samples maintain a uniform particle size of ~20nm and a circular morphology. However, the TEM also indicated that a considerable variation in aggregation state existed between samples (as summarised in Table 4-1). Representative TEM images of the primary samples are shown in Figure 4-3 and the covalent and ionic samples are shown in Figure 4-4.

AuNP Aggregation state		
Low	Medium	High
pAu_citrate	pAu_COOH	pAu_N3
cAu_siRNA	iAu_plain	cAu_plain
cAu_Tat, siRNA	iAu_Tat	cAu_Tat
iAu_siRNA		
iAu_Tat, siRNA		

Table 4-1 Summary of AuNP aggregation state as assessed by TEM
Each of the 11 AuNP species was categorised as having low, medium or high levels of particle aggregation. Samples with 'low aggregation' contained free particles in single form that were not attached to any neighbouring particles. Samples with 'medium aggregation' contained particles that were slightly associated with each other, with some space remaining between each particle. Samples with 'high aggregation' contained particles that were clumped together into dense groups, with no space remaining between each particle. (This table has been colour-coordinated with Figure 4-2, where primary samples are displayed in green, covalent samples in violet and ionic samples in orange.)
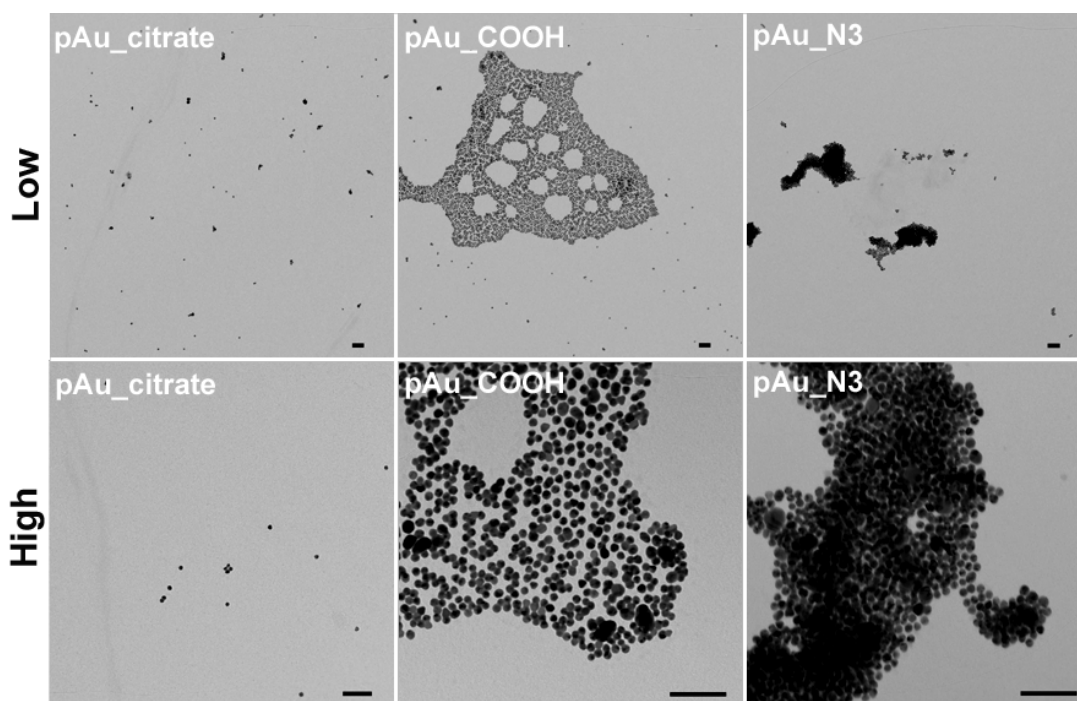
Figure 4-3 TEM images of the three primary AuNP samples
TEM images show the three primary AuNP samples at both high and low magnification (as indicated by the left hand side labels). Particles appeared uniform in size (~20nm) and circular in shape. Images show that a difference in aggregation state existed between samples. pAu_citrate appeared as single particles, pAu_COOH was slightly aggregated, and pAu_N3 was highly aggregated into dense clumps [scale bars = 100nm].
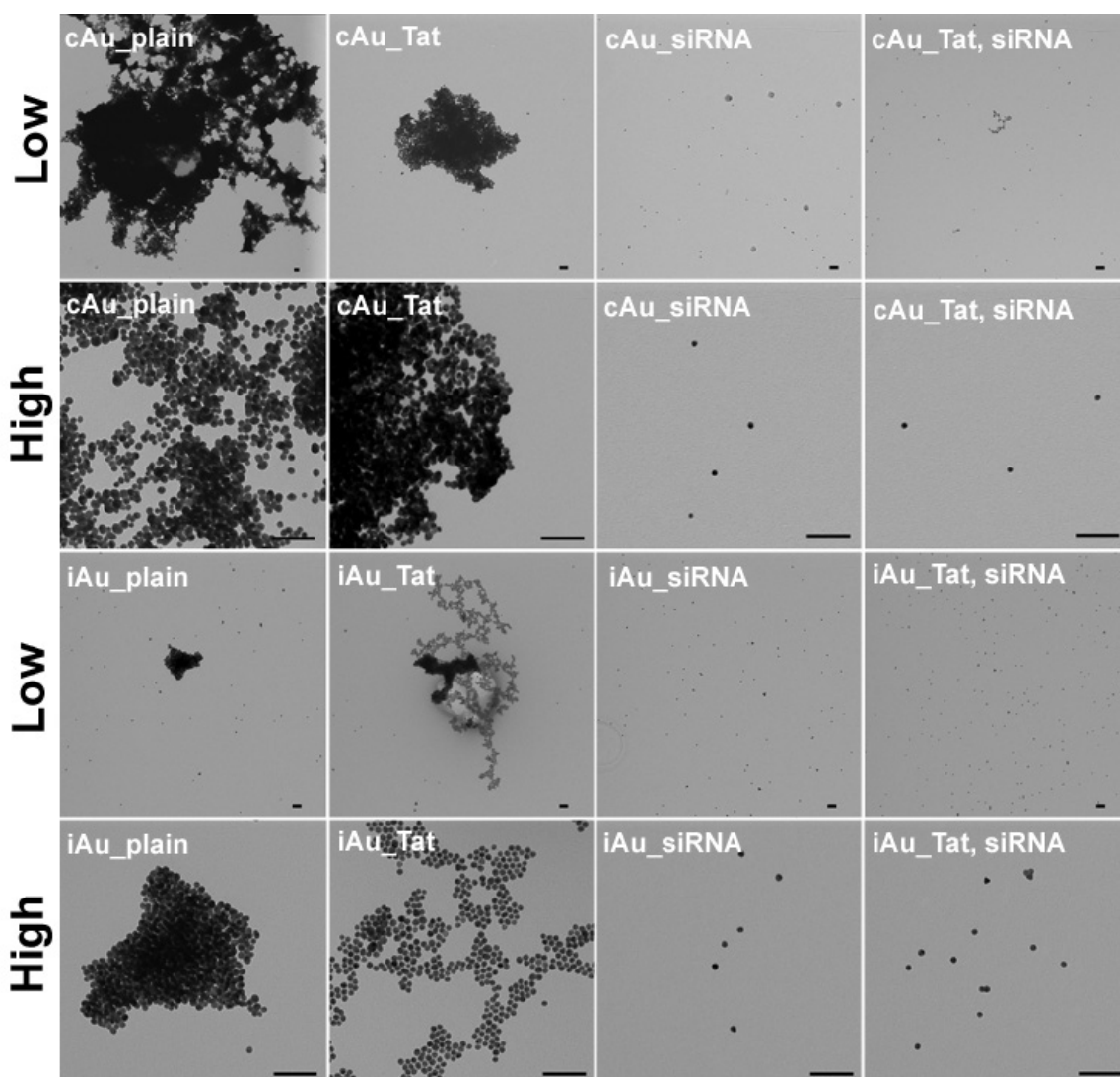
Figure 4-4 TEM images of the eight covalent and ionic AuNP samples
TEM images show the eight AuNP species at both high and low magnification (as indicated by the left hand side labels). Particles appeared uniform in size (~20nm) and circular in shape. Images show that a difference in aggregation state existed between samples. Those with siRNA attached appeared as single particles, whereas those without siRNA attached appear to be clumped together into aggregates [scale bars = 100nm].

4.3.1.2 Zetasizer Analysis

A Malvern Zetasizer was used to measure particle size by dynamic light scattering (DLS), and particle zeta potential, which gives an indication of sample charge and corresponding colloidal stability. DLS results showed that the size of cAu_plain, and all four of the ionic samples measured at the predicted diameter of ~20nm, as was observed by TEM. The remaining three covalent samples measured slightly higher, with reported sizes of up to ~80nm. The zeta potential results measured all samples to have charges between -20 and -55mV.
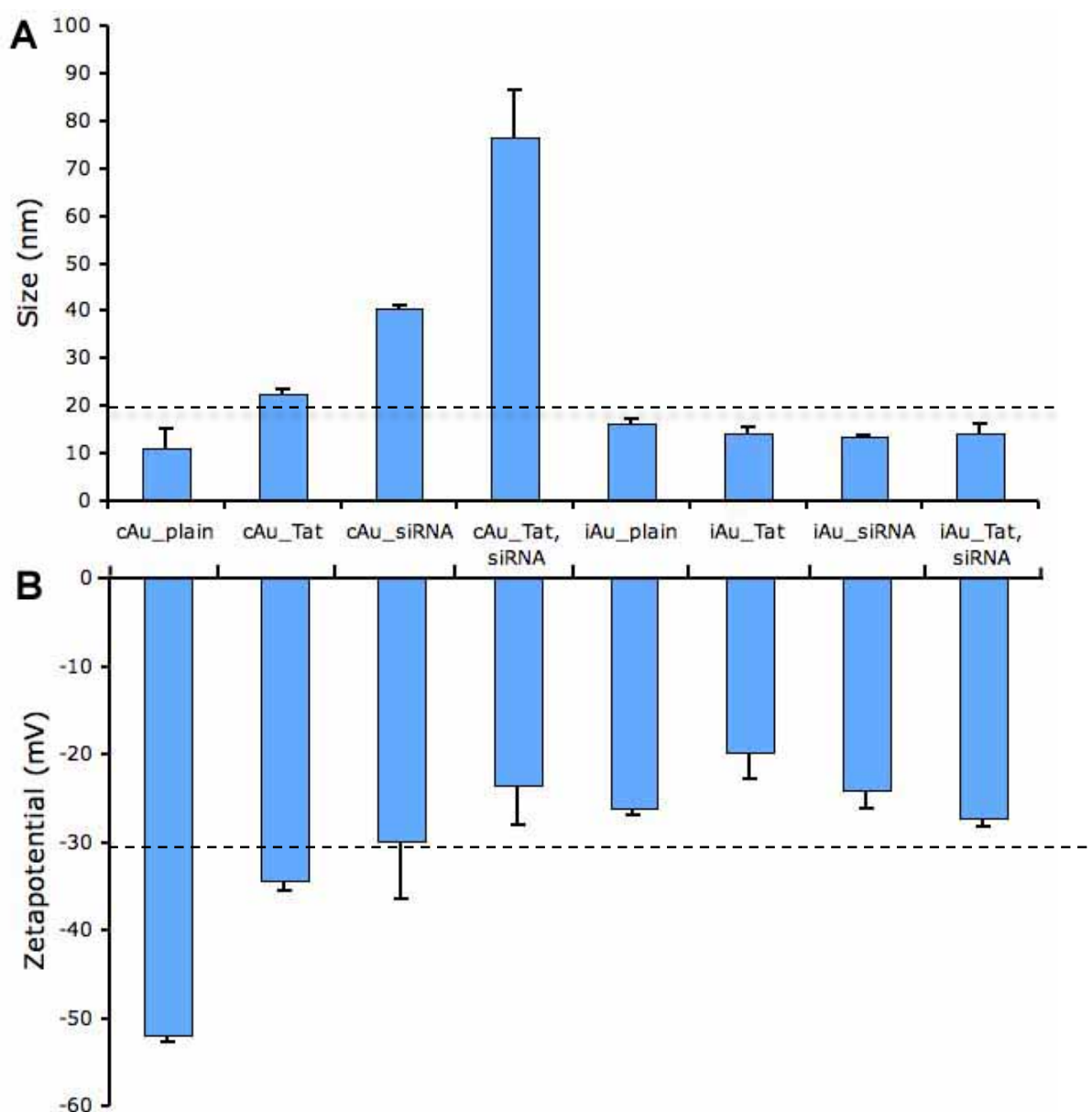
Figure 4-5 Zetasizer analysis of the eight covalent and ionic AuNP samples
The AuNP species in the covalent and ionic groups were analysed using dynamic light scattering (DLS) to measure particle size (A). A dotted line has been drawn at 20nm, which is assumed to be the true diameter of the AuNPs (as advised by the NP synthesis chemists and observed in TEM). In addition, zeta potential analysis was used to measure particle

charge (B). A dotted line has been drawn at -30mV since this is the minimal negative charge that indicates NP stability (as recommended in the Malvern Zetasizer manufacturers guidelines). (Error bars are SD, n=3.)

4.3.1.3 Toxicity Screening (MTT Assay)

In order to test the toxicity of the AuNPs used in this project, the MTT assay was used to measure cell viability after incubation with AuNP samples. The toxicity of the three primary samples was initially screened in the h-TERT BJ1 human fibroblast cell line after 24, 48 and 72 hours incubation with the cells to determine any obvious issues (Figure 4-6). Subsequently, the toxicity of the covalent and ionic AuNP samples was screened in the more relevant MCF-7 breast cancer cell line after 24, 48, and 72 hours incubation with the cells (Figure 4-7). Results showed that the nine AuNP samples tested were not toxic to any cells up to 72 hours incubation.

N.B [Due to synthesis issues with the cAu_siRNA and cAu_Tat, siRNA these two covalent samples were not included in this toxicity screening. However they were later included in further MTT analyses using HeLa cells (presented in chapter 5, Figure 5-2) with no associated toxicity].
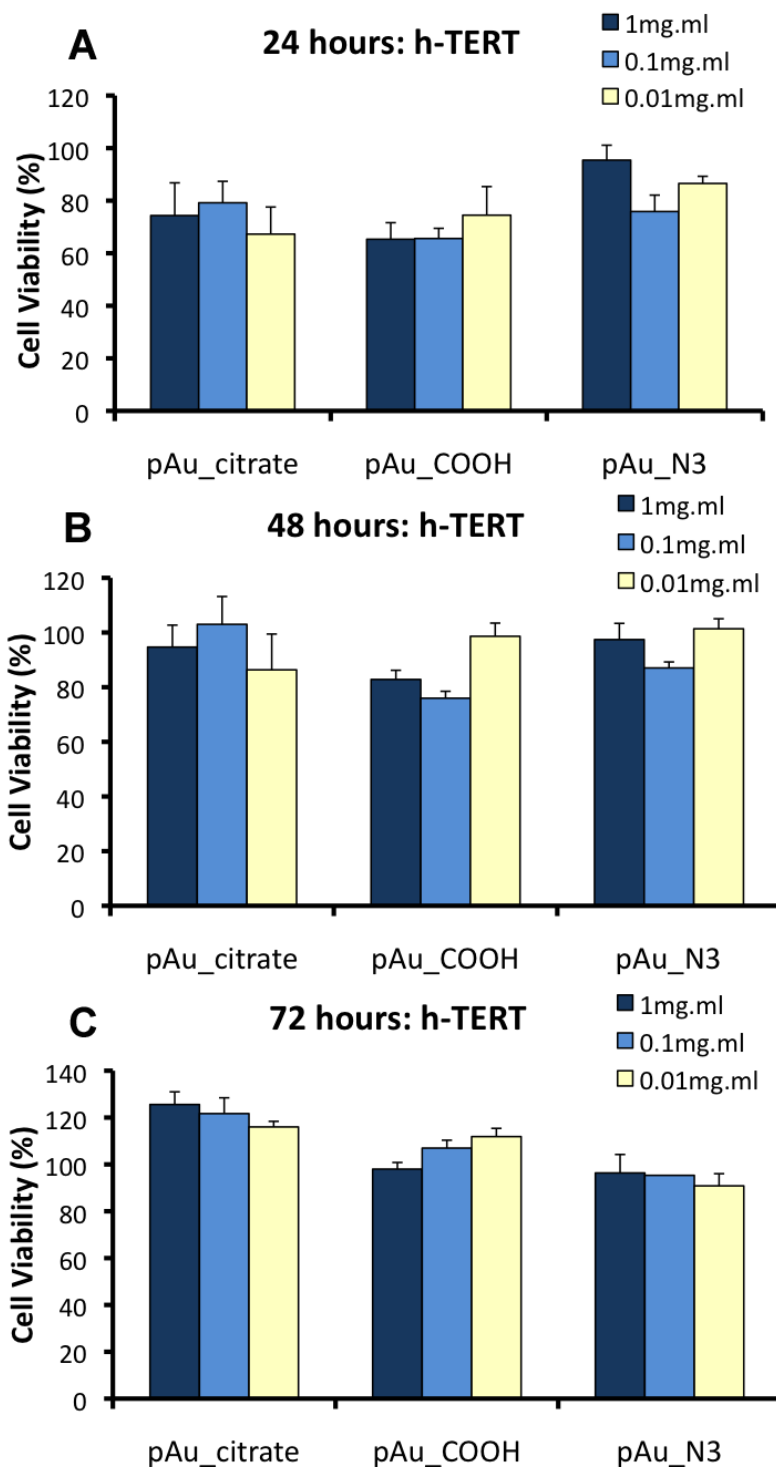
Figure 4-6 AuNP MTT toxicity screening in h-TERT cells
The MTT assay was used to determine the toxicity of the three primary AuNPs samples in h-TERT human fibroblast cells after 24 (A), 48 (B) or 72 hours (C). In this experiment, AuNPs were screened at concentrations of 1, 0.1 and 0.01mg.ml (error bars are SD, n=3).
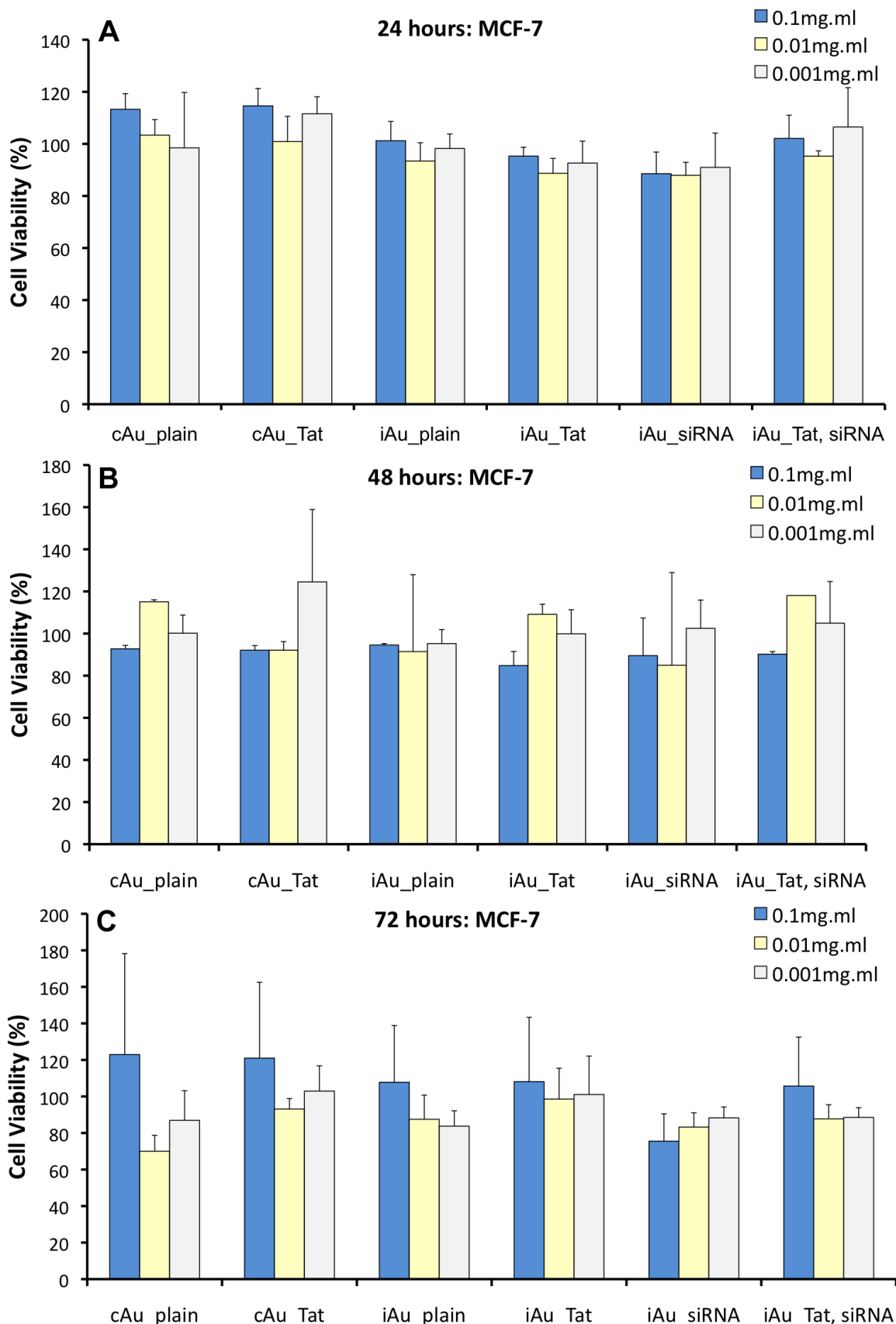
Figure 4-7 AuNP MTT toxicity screening in MCF-7 cells
The MTT assay was used to determine the toxicity of AuNPs from the covalent and ionic groups in MCF-7 human breast cancer cells after 24 (A), 48 (B) or 72 hours (C). In this experiment AuNP were screened at concentrations of 0.1, 0.01 and 0.001mg.ml (error bars are SD, n=3).

4.3.2 Uptake Analysis

Visualising cells by TEM following incubation with AuNPs allowed investigation of the (i) uptake level, (ii) time scale, and (iii) endocytotic method of particle uptake. TEM also allowed visualisation of any intracellular processing of particles after they had successfully traversed the cell membrane and gained entry into the cytoplasm.

4.3.2.1 TEM Experiment 1: Cell Uptake at 1 Hour (h-TERT)

The first TEM experiment performed was a 1 hour incubation of h-TERT human fibroblast cells with two of the primary AuNP samples; pAu_COOH and pAu_N3 (Figure 4-8). Results showed that after 1 hour high levels of each sample were cell-associated, with AuNPs mainly observed at the cell periphery, with few AuNPs actually being seen inside the cell membrane. This suggested early stage endocytosis at 1 hour. Notably, the difference in aggregation state previously illustrated between these two samples was again evident here, with pAu_COOH existing in a single-particle composition, and pAu_N3 existing as large aggregates of clumped particles. Endocytotic events, facilitating cellular internalisation of the samples, were captured for both AuNP species. In the case of pAu_COOH, membrane pits were observed forming and enclosing a small number of the single particles before transporting them internally within endocytotic vesicles (Figure 4-8 A). In contrast, pAu_N3, which contained aggregates too large to be internalised within pits, was observed being engulfed by larger membrane invaginations (Figure 4-8 D).
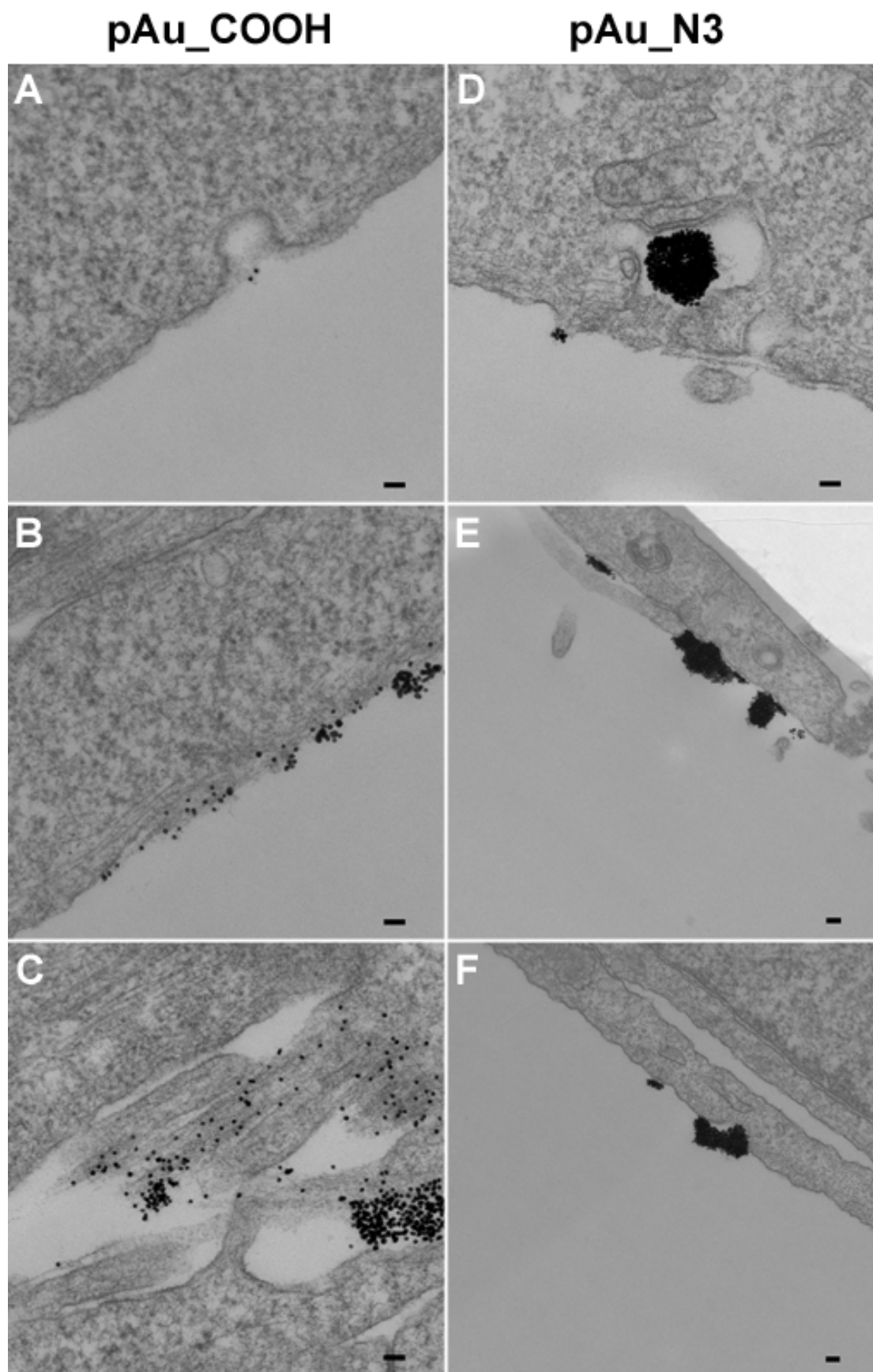
pAu_COOH   pAu_N3

Figure 4-8 Uptake of pAu_COOH and pAu_N3 into h-TERT cells after 1 hour
TEM images after 1 hour incubation with two of the primary AuNP species, pAu_COOH (A-C) and pAu_N3 (D-F). From these images it can be seen that pAu_N3 was aggregated into clumps, whereas pAu_COOH remained as single particles. At this 1 hour point, AuNPs were located at the cell surface in the early stages of endocytosis, a process captured in A and D [scale bars = 100nm].

4.3.2.2 TEM Experiment 2: Cell Uptake at 18 Hours (h-TERT)

Following the observation that endocytosis was in the early stage at 1 hour, subsequent TEM processing investigated the interaction of these two primary samples (pAu_COOH and pAu_N3) in h-TERT cells after a longer incubation time of 18 hours (Figure 4-9). Results showed that high levels of each sample were cell-associated, with pAu_COOH being mainly confined inside the cell, having traversed the membrane. This suggested 18 hours as an optimal time point to observe the AuNPs intracellularly, and was thus adopted for further experiments. At 18 hours, single particles of pAu_COOH were extensively noted inside membrane-enclosed vesicles within the cytoplasm (Figure 4-9 A-E). In addition, single particles of pAu_COOH were also seen out with any vesicular structure, appearing to be free in the cytoplasm (Figure 4-9 F). This may be explained by the fact that some vesicles full of single particles were observed to be bursting, releasing the particles within into the cytoplasm (Figure 4-9 D and E). In contrast, the aggregates of pAu_N3 were rarely seen inside the cell, suggesting that their larger size inhibited the process of endocytosis. Therefore, the pAu_N3 AuNP species was not deemed a suitable candidate to achieve the project goal of NP-mediated delivery of siRNA.

The TEM observations of pAu_COOH, (i.e. uptake into pits, subsequent internalisation, particle grouping in vesicles followed by bursting of these vesicles to release the particles into the cytoplasm) represents an ideal situation for NP-mediated delivery of siRNA, particularly since if NPs are free inside the cytoplasm, out with any endocytotic/lysosomic vesicle, it follows that their siRNA payload would be available to interact with the cytoplasmic RISC complex to induce silencing of the target gene.
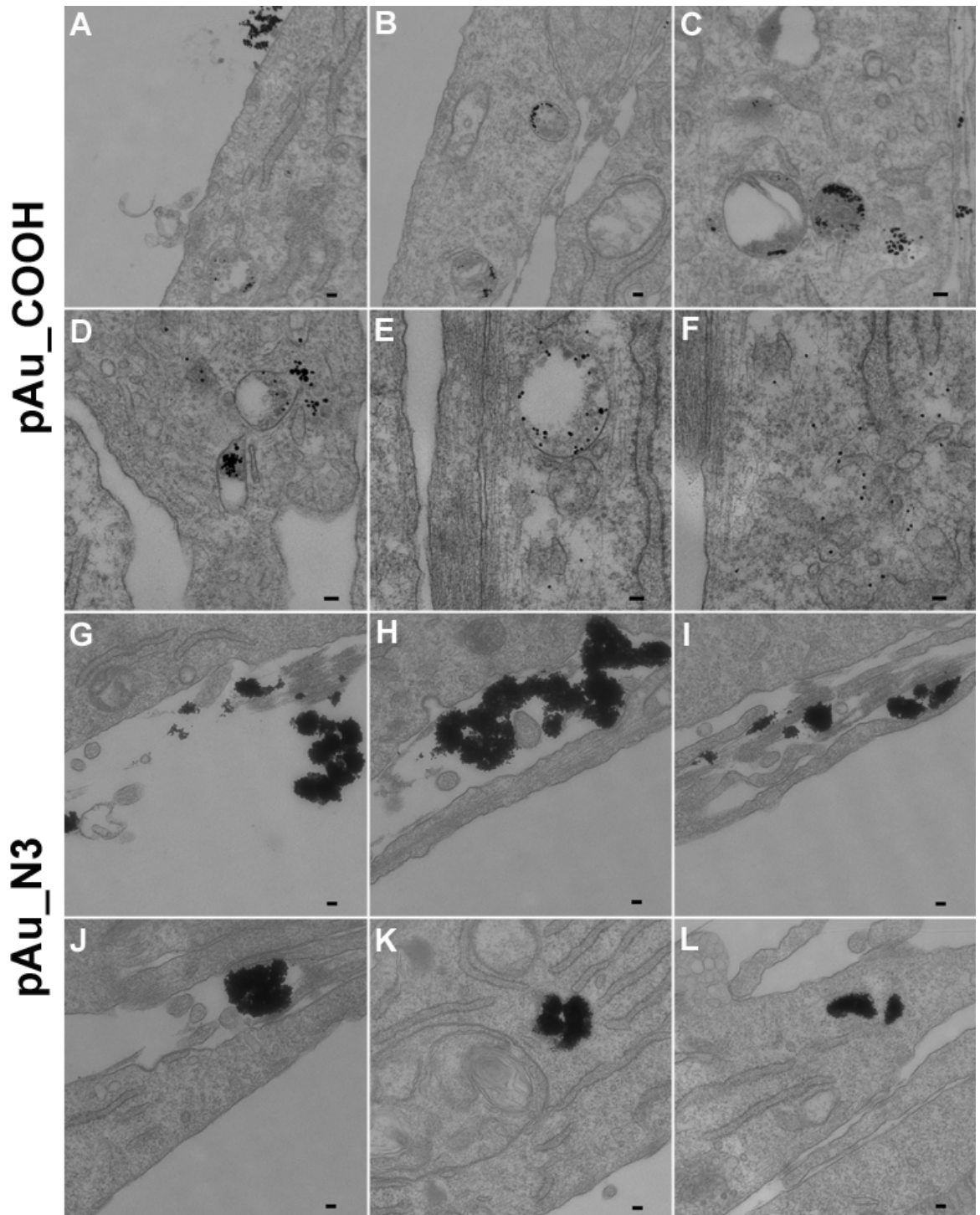
Figure 4-9 Uptake of pAu_COOH and pAu_N3 into h-TERT cells after 18 hours
TEM images after 18 hour incubation with two of the primary AuNP species; pAu_COOH (A-F) and pAu_N3 (G-L). The difference in sample aggregation-state is evident in these images, with pAu_N3 being highly aggregated and pAu_COOH remaining as single particles. pAu_N3 was mainly located at the cell surface, rarely being seen within the cytoplasm, indicating poor cellular uptake after 18 hours. Alternatively, pAu_COOH was mainly located inside the cytoplasm, either inside vesicles or free inside the cytosol, indicating very high cellular uptake after 18 hours, proving suitability to facilitate RNAi [scale bars = 100nm].

4.3.2.3 TEM Experiment 3: Cell Uptake of Ionic Samples at 1 & 48 Hours (MCF-7 Cancer Cells)

Following initial investigations into the cellular uptake of the primary AuNP samples (pAu_COOH and pAu_N3) into h-TERT fibroblasts, three AuNP samples from the ionic group were tested in MCF-7 breast cancer cells after 1 and 48 hours incubation (Figure 4-10), with similar results expected. However, TEM images in this case showed that no uptake of the ionic samples had occurred in MCF-7 cells after 1 or 48 hours (Figure 4-10). No cell-associated particles were seen, either on the surface or inside the cell. This experiment had involved a change of three variables in comparison to the previous TEM Experiment 2 (different cell type, AuNP samples and longer incubation time), thus it was not known what had caused the lack of uptake observed. Efforts now focused on elucidating which was the contributing factor.
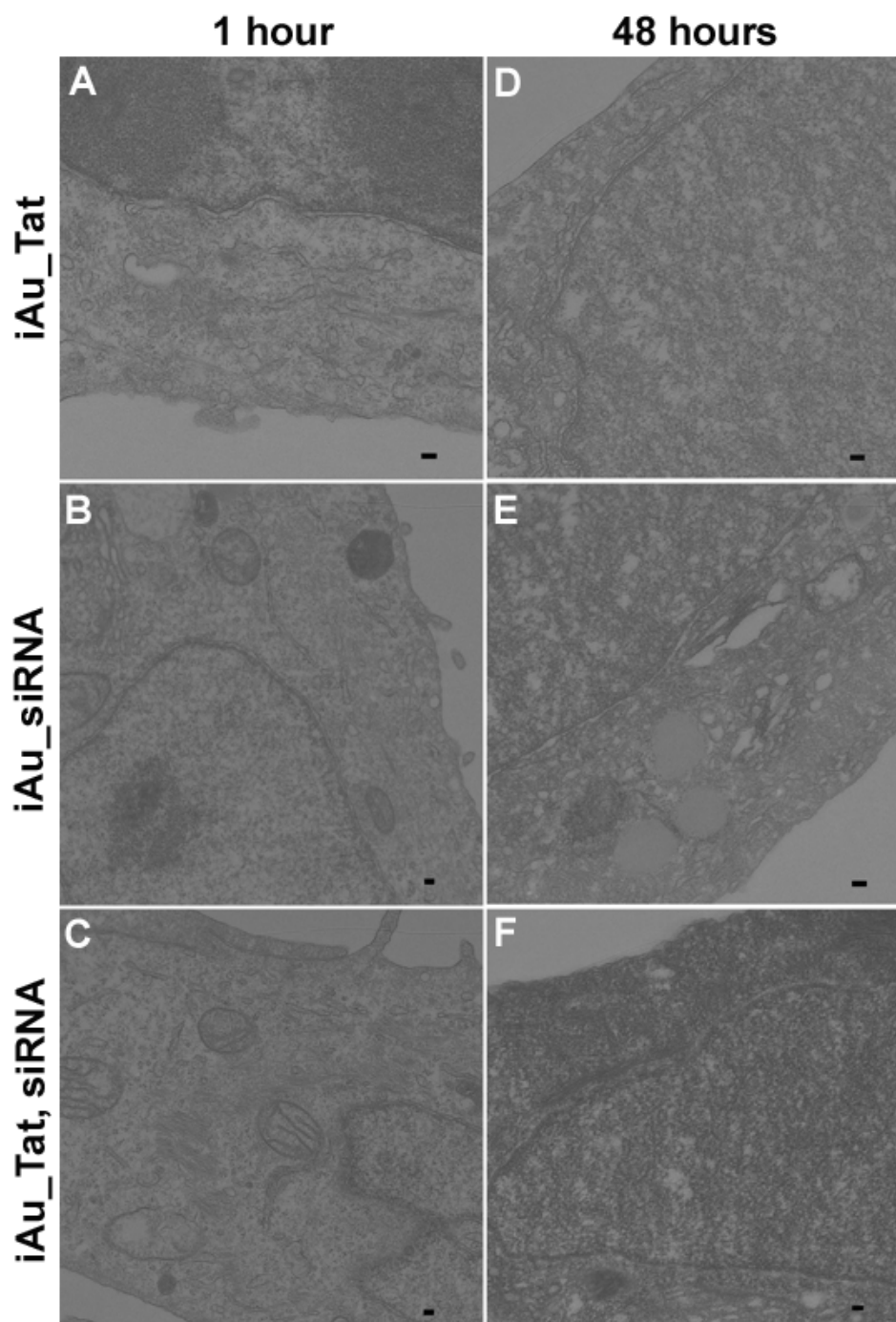
Figure 4-10 No uptake of ionic AuNPs into MCF-7 cells after 1 or 48 hours
TEM images after 1 or 48 hour incubation with three of the ionic AuNP species; iAu_Tat (A and D), iAu_siRNA (B and E) and iAu_Tat, siRNA (C and F). No AuNPs were seen in association with cells in any of the three treatment groups, indicating that no cellular uptake had occurred [scale bars = 100nm].

4.3.2.4 TEM Experiment 4: Cell Uptake of Ionic samples at 18 Hours (h-TERT & MCF-7)

In order to determine if cell type was a contributory factor, a comparison of the uptake levels of pAu_COOH and iAu_siRNA in both h-TERT and MCF-7 cells after 18 hours was carried out. Results showed that pAu_COOH was heavily uptaken into both cell types, whereas iAu_siRNA was poorly uptaken into both cell types (Figure 4-11A). This recommended that the lack of uptake seen in TEM Experiment 3 was in fact due to the new AuNP samples, rather than the new cell type, and suggested that the new ionic samples may have an inherent inability to be endocytosed into either cell type tested.

In addition to TEM analysis, ICP-MS was used to quantify the level of uptake of 10 different AuNP samples (the entire AuNP library, except from pAu_citrate) in both h-TERT and MCF-7 cells for comparison with the TEM results. The ICP-MS data supported results from TEM Experiment 4, and showed that pAu-COOH displayed much higher levels of uptake than iAu_siRNA in both cell types. The ICP-MS results also showed that the extremely high level of uptake displayed by pAu_COOH was significantly higher than all 8 members of the ionic and covalent groups, even those with Tat attached (Figure 4-11B).

A
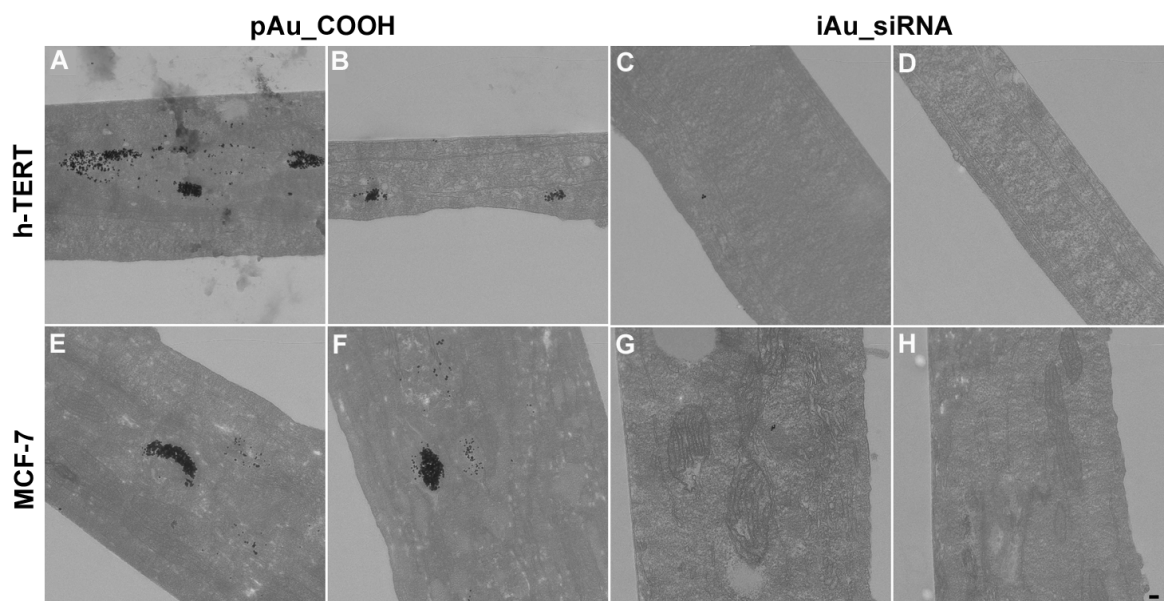
B
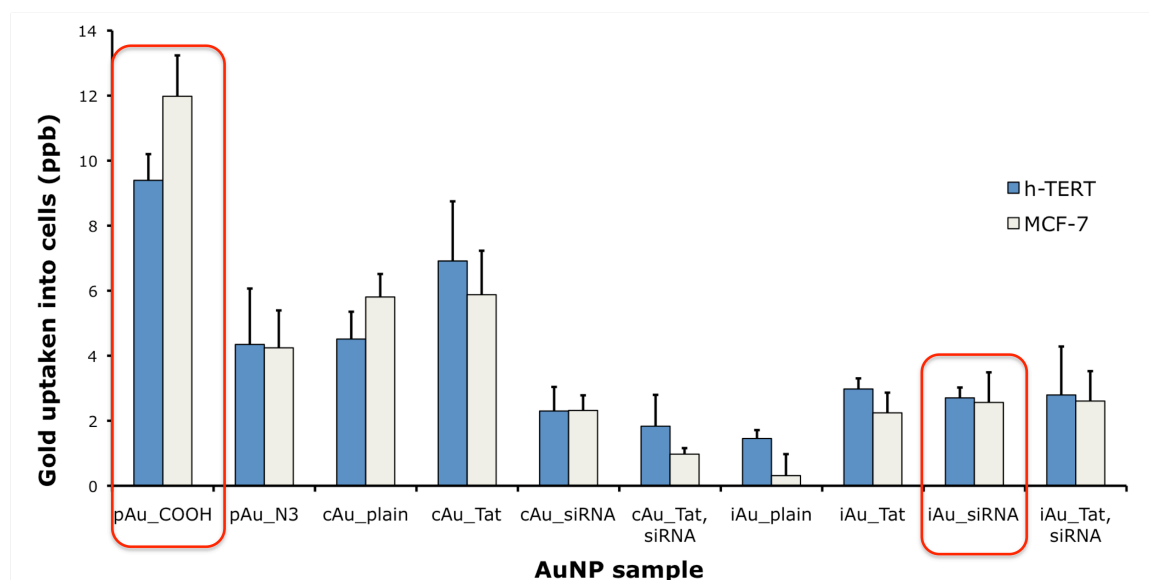
Figure 4-11 Uptake of pAu_COOH compared to covalent (cAu) and ionic (iAu) samples in h-TERT and MCF-7 cells after 18 hours (TEM and ICP-MS)
Figure A: TEM images of MCF-7 cells and h-TERT cells after 18 hours incubation with pAu_COOH (A, B, E and F) or iAu_siRNA (C, D, G and H). In accordance with previous TEM results, pAu_COOH displayed very high uptake in both h-TERT and MCF-7 cell types, with single particles being seen free inside the cytoplasm. In contrast, iAu_siRNA displayed very poor uptake in both cell types, and cell-associated particles were rarely observed [scale bar = 100nm]. Graph B: ICP-MS analysis of the cellular uptake of 10 AuNP species after 18 hours incubation with h-TERT and MCF-7 cells. The ICP-MS results supported the TEM, since pAu_COOH displayed a ~5-fold higher level of uptake compared to iAu_siRNA in both cell types (pAu_COOH and iAu_siRNA have been outlined in red in the ICP-MS graph for easy comparison to the TEM images in A.) (In Graph B, error bars are SD, n=3.)

4.3.2.5 TEM Experiment 5: Cell Uptake into HeLa Cells at 18 Hours (pAu-COOH, cAu_siRNA and cAu_Tat, siRNA)

Following literature reviews and collaborative work with other members of the Nanotruck project, HeLa cervical cancer cells were suggested for use as a cancer cell model to test c–myc RNAi. A final TEM assessment was carried out to determine the uptake of pAu-COOH, cAu_siRNA and cAu_Tat, siRNA into HeLa cells after 18 hours incubation. Results showed that all three AuNPs were heavily endocytosed into HeLa cells, being seen mainly within vesicles inside the cytoplasm (Figure 4-12). This very promising result suggested that it was feasible to hypothesise that covalent and ionic siRNA-functionalised AuNPs would be able to induce RNAi in HeLa cells, as the AuNPs were endocytosed. HeLa cells were thus selected as the optimal model cancerous cell type in which to test the c-myc knockdown capabilities of the siRNA-functionalised AuNPs involved in this project, as presented in chapter 5.
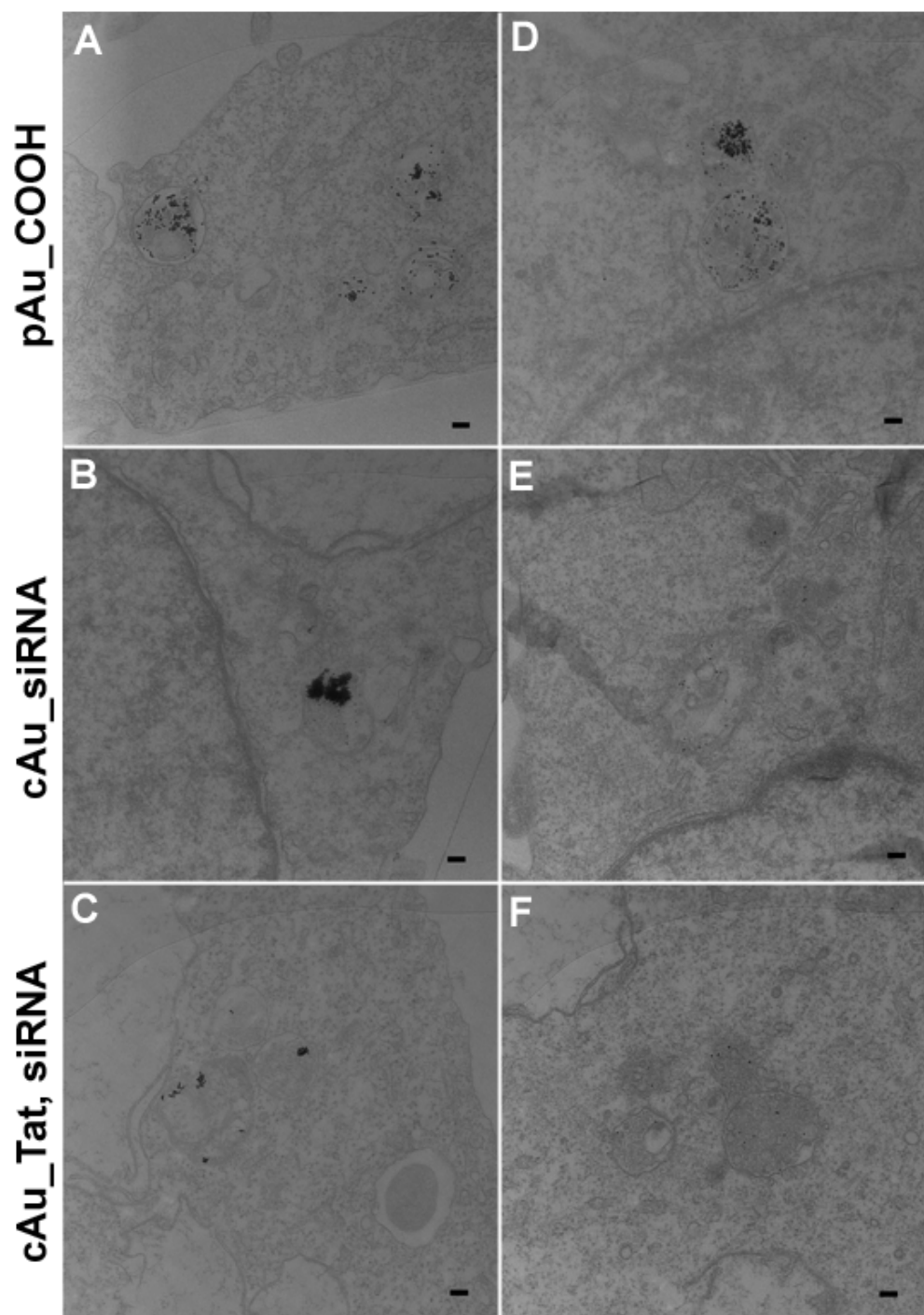
Figure 4-12 Uptake of pAu_COOH compared to cAu_siRNA (+/- Tat) in HeLa cells after 18 hours
TEM images after 18 hour incubation with pAu_COOH (A and D), cAu_siRNA (B and E) or cAu_Tat, siRNA (C and F). Results showed that all three AuNP species displayed very high uptake in HeLa cells [scale bars = 100nm].

4.4 Summary and Discussion

This chapter was mainly concerned with the initial experimental design for achieving RNAi in a cancer cell line and has outlined results from the initial biological screening of a group of 11 different AuNP samples. The performance of these samples in terms of NP characterisation, toxicity screening and cellular uptake was used to aid the design of functional optimal AuNP species for therapeutic RNAi.

4.4.1 AuNP Characterisation

The characterisation results showed that a significant difference in extent of particle aggregation existed between samples, ranging from samples composed of single, free AuNPs (cAu_siRNA), to samples composed of particles that were completely aggregated together into dense clumps (pAu_N3). This difference was most likely due to surface chemistry variations. The most obvious example of surface chemistry impacting particle aggregation would be the observation that samples carrying siRNA were in distinct single-particle form, whereas their control counterparts without siRNA suffered from aggregation. Therefore, it is conceivable that the negative charge given to particles through the attachment of negatively charged siRNA caused steric repulsion between particles, resulting in the low state of aggregation as observed by TEM. However, particles of pAu_citrate also appeared in the same single-particle format, and so this state is not exclusive to the involvement of the siRNA. Perhaps pAu_citrate also contained a charge strong enough to cause a similar state of steric repulsion between particles. To explain why some of the other samples became very heavily aggregated (pAu_N3), perhaps they lacked a charge strong enough to induce steric repulsion, or alternatively, it is feasible that some chemical surface groups provided attractive forces, causing a 'sticky' effect between particles.

In theory, using a Malvern Zetasizer is an ideal way to measure the size and zeta potential of NPs. However, there are some important technical factors that must be taken into careful consideration in order to correctly interpret the results. Firstly, the Zetasizer measures NP diameter through the use of dynamic light

scattering (DLS), which will read the size of the largest 'particle' in the suspension. Therefore, in a sample containing 20nm NPs aggregated into 100nm clumps, the Zetasizer will incorrectly record the NP diameter as being 100nm. Thus, in my opinion, DLS is only useful for measuring suspensions that you are either a) entirely sure are in a single particle state, with no aggregation and you are using DLS to measure single NP size, or b) you already know the single NP size of your suspension (e.g. via TEM), and you are using DLS to determine if any particle aggregation has occurred. In this case, TEM had confirmed NP size as 20nm. In comparison, DLS correctly measured the single NP size of all four ionic samples, and cAu_plain, to be 20nm. However, DLS also measured the single NP size of the other three covalent samples to be higher (up to 80nm for cAu_siRNA). This does not support the TEM images, as the two ionic samples without siRNA were aggregated, thus should have had a higher DLS size reading, and the covalent samples with siRNA attached appeared dispersed and therefore should have had a lower DLS size reading. The fact that the TEM and DLS results do not tie up exactly could be due to the temperamentality of using a Zetasizer, and also the danger that a TEM image may not be representative of the entire NP sample. On a more optimistic note, all eight of the covalent and ionic AuNP samples measured under 100nm in diameter by DLS, which is quite relatively accurate. Secondly, the format of the NP characterisation by TEM was given credibility due to the fact that samples consistently appeared in a similar size and state whenever they were investigated in the subsequent TEM cell uptake experiments.

In addition to size, the Zetasizer also measured the zeta potential of the eight covalent and ionic AuNPs, reporting samples to be between -20 and -50mV. Quite frequently in the field, a NP's zeta potential gets misconstrued to be a direct measurement of its electrical charge. However, this is not the case, and the main purpose of the zeta potential is to indicate a sample's colloidal stability. This is based on the rule that if a sample has a zeta potential higher than 30mV or lower than -30mV, it is considered stable, as the strength of these charges will cause steric repulsion of the individual particles, preventing them from aggregating out of solution. On the other hand, if a sample has a zeta potential between 30 and -30mV, it is considered unstable, as this strength of charge is not enough to repel individual particles away from each other in

solution, leading to particle aggregation. Assuming this rule, only two out of the eight AuNP samples tested had zeta potentials strong enough (below -30mV) to classify them as being 'colloidally stable' (cAu_plain, and cAu_Tat). This does not reflect the aggregation states reported by TEM, as cAu_plain and cAu_Tat were not the least aggregated samples tested, and those that were the least aggregated (cAu_siRNA and iAu_siRNA) were measured to have zeta potentials in the 'unstable' region of between 30 and -30mV.

4.4.2 Toxicity Testing

MTT toxicity testing did not report any significant reduction in viability in either cell type (h-TERT and MCF-7) after incubation with the nine different AuNP samples. Significant levels of toxicity are generally considered to correspond to the production of ≤ 80% cell viability. Following treatment with the three primary AuNP samples, the minimum observed cell viability was 60% at 24 hours, and 80% at 48 and 72 hours. Following treatment with the covalent and ionic samples, the minimum observed cell viability was 80% for 24 and 48 hours, and 70% for 72 hours. In conclusion, the majority of the MTT data suggests that the AuNP design used in this project can be considered non-toxic to these cell types, up to 72 hours. Interestingly there were some data points reporting cell viability over 100% after AuNP-treatment. This could have been an indicator of AuNP-induced cell proliferation, but this was disproved by doing a detailed cell counting experiment using Coomassie blue, which showed that there was no difference in cell number between control and AuNP-treated cells (results not shown). In addition, it was confirmed that the AuNPs themselves were not being detected in the colorimetric MTT assay (thereby increasing readings of cell viability). It is more likely that viability readings over 100% represent an increase in cellular metabolic activity, stimulated as the cells begin to endocytose the AuNPs in the surrounding media.

4.4.3 Uptake Analysis

The five separate TEM experiments outlined in this chapter were crucial in determining the complex story of AuNP cell uptake. There are two main conclusions to be drawn from this work. The first is that pAu-COOH was superior to all other samples with regards to cell uptake levels, in all cell lines tested (h-TERT, MCF-7 and HeLa). The second conclusion is that HeLa cells were advanced at taking up siRNA-functionalised AuNPs compared to h-TERT and MCF-7 cells. Whilst further studies need to be carried out to provide definite answers to explain both of these observations, they do lead to the following considerations. 1) COOH could play an important role in endocytosis, possibly being able to promote binding to certain receptors or docking molecules commonly present on the membranes of various different cell lines. Therefore, functionalising NPs with COOH may be a useful strategy in order to increase cell uptake in a range of different cell types. 2) The fact that siRNA-functionalised AuNPs in this case could only be taken up into HeLa cells and not h-TERT or MCF-7 cells highlights the fact that NP-uptake is largely cell type-specific. This idea has been previously reported, and resonates the importance of testing new NP designs on a particle-by-particle basis, in a variety of different cell lines.

4.4.3.1 COOH

In comparison to other studies, increased cell uptake mediated by COOH is a poorly understood phenomenon that has been reported by a handful of other research groups. For example, Jiang *et al* found that carboxyl-functionalised NPs internalised more rapidly and accumulated to a much higher level than plain NPs in mesenchymal stem cells (MSCs) (Jiang *et al.*, 2011). This study used endocytosis inhibitors to elucidate that carboxyl NPs were internalised by the clathrin-mediated mechanism, whereas plain NPs were internalised by macropinocytosis. The authors concluded that NP uptake mediated by carboxyl-functionalisation indicated a specific interaction of the carboxyl group with receptors on the cell surface. In addition, Zhang *et al* reported that carboxylic coated quantum dots (QDs) were taken up in greater amounts than either PEG- or PEG-amine coated QDs in human epidermal keratinocytes (HEK) (Zhang and Monteiro-Riviere, 2009). However, in contrast to Jiang *et al,* endocytosis

inhibitors showed that carboxylic QDs were recognized by lipid rafts but not by clathrin or caveolae in HEK cells. Another study into QDs by Xiao *et al* reported that carboxylic QDs were internalised quickly and with large amount in both MCF-10A (human mammary non-tumourigenic) and MCF-7 (carcinoma) cells, whereas no detectable intracellular uptake was observed for either PEG- and PEG-amine QDs in the same cell types (Xiao *et al.*, 2010). The authors concluded that the endocytosis of carboxylic QDs was probably assisted by receptors specific to ligands with negative charges (such as COOH). Finally, Clift *et al* reported that COOH QDs displayed higher uptake levels than both organic- and NH$_2$ (PEG) QDs in J774.A1 (murine 'macrophage-like') cells (Clift *et al.*, 2008).

These studies support my data that COOH functionalisation increases cell uptake of NPs. As a whole, this body of research dispels the logical and widely believed idea that NPs with positively charged surface groups should display better endocytosis than NPs with negatively charged surface groups, due to electrostatic interactions with the negatively charged cell membrane. In contrast, negatively charged COOH seems to provide the highest levels of endocytosis, even over positively charged surface groups, such as amine. This implies that the process of endocytosis is much more complex than previously thought, where negatively charged COOH may have an ability to bind to specific cell surface receptors to mediate NP internalisation. However, such COOH-specific receptors have yet to be identified.

4.4.3.2 Cell Type

The second conclusion derived from the TEM experiments presented in this chapter (i.e. that siRNA-functionalised AuNPs were taken up into HeLa cells, but not h-TERT or MCF-7 cells), is more difficult to directly compare to similar studies due to the huge variety in study design present in the literature. In contrast to my data, some studies have reported NP uptake to be possible across multiple cell types. For example, Siu *et al* found that amphiphilic core-shell NPs consisting of a poly(methyl methacrylate) core with a branched PEI shell could transfect MCF-7, BEL 7404, C6, CHO-K1 and HeLa cells successfully (Siu *et al.*, 2012). Conversely, in a recent study into the uptake of two different NP formulations into three different cell types, Lunov *et al* reported that the (i)

extent of NP internalisation, (ii) kinetics of particle uptake, and (iii) particle uptake mechanism may grossly differ between cell types (Lunov *et al.*, 2011).

In contrast to the results of this chapter, MCF-7 cells have been successfully transfected with siRNA *via* NP-mediated delivery in other studies. This included Huang *et al,* who reported that PEG-PCL-PEI copolymeric NPs could be used to transfect MCF-7 cells with siRNA, which resulted in significant silencing of the firefly luciferase gene (as was previously transfected into the cells) (Huang *et al.*, 2011). Furthermore, Kean *et al* found that chitosans with positive charges displayed increased uptake in MCF-7 cells compared to PEI, although this transfection preference of a positive charge was not observed in COS-7 cells (Kean *et al.*, 2005). These studies exemplify that transfection and NP-mediated siRNA delivery is possible in MCF-7 cells, although they shed little light on why this cell type would not internalise the siRNA-functionalised AuNPs presented in this chapter.

In my opinion, differences in surface receptor expression is one of the most likely explanations as to why uptake of siRNA-functionalised AuNPs differed between cell types in this chapter. This theory is supported by numerous studies that have demonstrated the heterogeneity of receptor expression on the surface of different cell lines. For example, a study by Li *et al* investigated the expression of the folate receptor across 25 different cancer cell lines. Results showed that receptor expression was extremely variable across different cell types, and that out of the 25 tested, MCF-7 and HeLa cells were identified to have the highest levels of folate receptors compared to the other cell type, and were thus selected for siRNA delivery mediated by folate-functionalised NPs (Li *et al.*, 2009). In addition, McNamara II *et al* showed that chimeric RNAs could be targeted to certain cell types due to the differential expression of the cell-surface receptor PSMA across cell types. The authors reported that cell types lacking PSMA, such as PC-3 cells could not bind to the chimeric RNAs, whereas cell types that did express PSMA, such as LNCaP cells could bind and internalise the chimeric RNAs, which induced gene silencing by RNAi (Mcnamara *et al.*, 2006).

Certainly, in the studies by Li *et al* and Mcnamara *et al,* cell-specific uptake had been anticipated by including ligands for the target receptors in the NP design (folate and a PSMA-binding aptamer respectively), whereas in this chapter, cell-specific uptake was an unexpected result. However, these studies are a good example of the heterogeneity of cell surface receptor expression observed across different cell types, which lends feasibility to the idea that in this chapter, HeLa cells may have expressed some as-yet unidentified cell surface receptor that facilitated siRNA-functionalised AuNP uptake, and was not expressed in either h-TERT or MCF-7 cells explaining their lack of uptake. Rather than being detrimental to a goal of universal siRNA delivery across all cell types, Kean *et al* state that the differences in transfection ability observed between cell lines may prove to be an asset allowing researchers to preferentially transfect desired cell types with appropriate vectors (Kean *et al.*, 2005). This suggests that the HeLa cell specific uptake of siRNA-functionalised AuNPs reported in this chapter could in fact be an asset, possibly allowing selective targeting of cervical cancer cells.

4.4.3.3 Tat

The TEM and ICP-MS data both showed that the CPP Tat did not increase the cellular uptake of AuNPs, as it had been expected to do. Prior to speculation on the reasoning for this, several issues need to be resolved, including confirmation that the Tat remained bound to the NP during the uptake process. Some doubt was cast over this as the attachment of a CPP normally results in an increase in zeta potential negativity (as demonstrated for the CPP penetratin in chapter 3). This increase was not observed with the Tat-functionalised AuNP samples, and so testing should be carried out to confirm that the CPP did not become detached or denatured/inactivated in some way. Overall, however, the inability of Tat to enhance uptake was sidelined since AuNPs without Tat proved perfectly capable of being heavily endocytosed into cells (pAu_COOH in to all cell types, and all samples into HeLa).

4.5 Conclusion

In conclusion, due to their superior AuNP-uptake capabilities, HeLa cells were selected as a model cell line in which to test the c-myc knockdown capabilities of the covalent and ionic AuNP samples.

5 c-myc Knockdown in HeLa Cells

5.1 Introduction

One of the biggest barriers to NP-mediated delivery of siRNA for therapeutic RNAi is the cellular uptake of siRNA-functionalised NPs. As reported in Chapter 4, HeLa cells presented as an optimal cell line in which to test RNAi delivery vehicles, due to the fact that they endocytosed the siRNA-functionalised AuNPs more successfully than other cell types (h-TERT and MCF-7). This chapter uses HeLa cells to address the two remaining objectives of this part of the Nanotruck project; the c-myc knockdown capabilities of the covalent and ionic siRNA-functionalised AuNPs and the effect of c-myc knockdown on the cell cycle.

In order for NP-mediated RNAi to be achieved, siRNA-functionalised NPs must be able to cross the cell membrane and gain access to the cytoplasm. Once in the cytosol, the NP's siRNA payload can interact with the RISC complex, become incorporated and thus cause the destruction of endogenous mRNA molecules with complementarity to the NP-delivered siRNA. The destruction of the target mRNA in this manner prevents its translation into protein, effectively silencing gene expression. In the case of this project, a reduction in c-myc expression in cancer cells was intended to normalise the balance of the cell cycle. This intent was based on the role c-myc plays as a transcription factor to regulate the expression of many other genes involved in controlling the cell cycle (Dang, 2012; Luescher and Vervoorts, 2012). Since the overexpression of c-myc is a contributing factor in oncogenesis, reducing its expression *via* the destruction of its mRNA by RNAi was expected to normalise oncogene expression, returning the cell cycle to a healthy rate (Ponzielli *et al.*, 2005; Wang *et al.*, 2005).

The performance of the covalent and ionic siRNA-functionalised AuNPs was assessed in terms of their c-myc knockdown capability using the following three approaches;

(1) monitor the level of target mRNA by qRT-PCR

(2) measure the level of c-myc protein resulting from translation of target mRNA. If NP-mediated RNAi has been successful, levels of the target mRNA and protein should be significantly reduced.

(3) This is frequently where knockdown assessment ends, but a third important factor to assess is the cellular effect of the RNAi-induced target mRNA and protein knockdown. In this case, the desired effect of c-myc knockdown was to decrease the number of cancer cells entering S phase in the cell cycle, thus to decrease cell proliferation. A recommended technique was used to measure cell proliferation, which involved the substitution of thymidine with labeled uridine (BrdU) during the DNA replication stage in the cell cycle. Once BrdU had been incorporated, it was immunodetected with an anti-BrdU antibody. This allowed dividing cells to be fluorescently distinguished in cell populations.

During assessment of the c-myc knockdown capability of siRNA-functionalised AuNPs, a range of controls were introduced into experiments for comparison. These were primarily the use of Lipofectamine to deliver c-myc and nonsense siRNA to HeLa cells, as it is one of the most effective *in vitro* transfection agents currently available (not for clinical use due to high toxicity) and acts as a good positive control. Furthermore, naked c-myc and nonsense siRNA was applied to HeLa cells in order to compare the knockdown potential of siRNA when it is used without any suitable delivery vehicle (such as NPs or Lipofectamine).

5.2 Aims

This chapter aimed to knockdown the c-myc oncogene in HeLa cervical cancer cells, through the delivery of siRNA by AuNPs. Knockdown was assessed at the levels of mRNA, protein and effect on the cell cycle by qRT-PCR, Western blot and BrdU staining respectively. This completes the third and forth objectives of this project, as outlined at the beginning of Chapter 4.

1) potential cell toxicity

2) cellular uptake

3) c-myc knockdown

4) effect on cell cycle

5.3 Methods

5.3.1 qRT-PCR

HeLa cells were grown at 1 x 10^5 cells per well in a 24 well plate and allowed to adhere overnight. AuNP treatments were added (500μl at 0.2mg/ml) and incubated with the cells for 48 hours (control cells were incubated with media instead). Lipofectamine 2000 was used according to the protocol for HeLa cells supplied by Invitrogen (Form No. 18057N). For siRNA delivery by Lipofectamine and direct (naked) delivery, siRNA was used at 25 pmol per well. Due to their toxicity, Lipofectamine-siRNA complexes were removed after 6 hours and then the cells were allowed to complete the 48 hour incubation in culture media. Naked siRNA and all AuNP treatments were left in contact with the cells for the full 48 hour incubation period. After 48 hours, treatments were removed and RNA was extracted using an RNeasy Mini Kit. Reverse transcription was performed using a QuantiTect Rev. Transcription kit. Each qRT-PCR reaction contained 10ng of cDNA. Three technical replicas were used for each of three biological replicas. A 7500 Real-time PCR System was used with Taqman master mix and Abi Prism 96-well plates as supplied by Applied Biosystems. Primers and probes for c-myc and GAPDH were supplied by Eurofins MWG Operon and their sequences are listed in Table 5-1, together with the c-myc siRNA sequence that was used in this project to induce RNAi. The binding sites of the c-myc siRNA and the c-myc qRT-PCR primers and probes are highlighted within the c-myc mRNA transcript displayed in Figure 5-1.

Name	Sequence
c-myc siRNA	GCGAGGATATCTGGAAGAAAT
c-myc forward	TCAAGAGGTGCCACGTCTCC
c-myc reverse	TCTTGGCAGCAGGATAGTCCTT
c-myc probe	FAM-CAGCACAACTACGCAGCGCCTCC-TAMRA
GAPDH forward	GAAGGTGAAGGTCGGAGTC
GAPDH reverse	GAAGATGGTGATGGGATTTC
GAPDH probe	VIC-CAAGCTTCCCGTTCTCAGCC-TAMRA

Table 5-1 Sequences of c-myc siRNA and Taqman qRT-PCR primers and probes
This table lists the sequences of the c-myc siRNA and the qRT-PCR probes and primers for c-myc and GAPDH. The colours correspond to binding sites within the c-myc mRNA transcript as shown in Figure 5-1.

```
ORIGIN
        1 gacccccgag ctgtgctgct cgcggccgcc accgccgggc cccggccgtc cctggctccc
       61 ctcctgcctc gagaagggca gggcttctca gaggcttggc gggaaaaaga acggagggag
      121 ggatcgcgct gagtataaaa gccggttttc ggggctttat ctaactcgct gtagtaattc
      181 cagcgagagg cagagggagc gagcgggcgg ccggctaggg tggaagagcc gggcgagcag
      241 agctgcgctg cgggcgtcct gggaagggag atccggagcg aataggggggc ttcgcctctg
      301 gcccagccct cccgctgatc ccccagccag cggtccgcaa cccttgccgc atccacgaaa
      361 ctttgcccat agcagcgggc gggcactttg cactggaact tacaacaccc gagcaaggac
      421 gcgactctcc cgacgcgggg aggctattct gcccatttgg ggacacttcc ccgccgctgc
      481 caggacccgc ttctctgaaa ggctctcctt gcagctgctt agacgctgga ttttttcgg
      541 gtagtggaaa accagcagcc tcccgcgacg atgcccctca acgttagctt caccaacagg
      601 aactatgacc tcgactacga ctcggtgcag ccgtatttct actgcgacga ggaggagaac
      661 ttctaccagc agcagcagca gagcgagctg cagcccccgg cgcccagcga ggatatctgg
      721 aagaaattcg agctgctgcc caccccgccc ctgtccccta gccgccgctc cgggctctgc
      781 tcgccctcct acgttgcggt cacacccttc tcccttcggg gagacaacga cggcggtggc
      841 gggagcttct ccacggccga ccagctggag atggtgaccg agctgctggg aggagacatg
      901 gtgaaccaga gtttcatctg cgacccggac gacgagacct tcatcaaaaa catcatcatc
      961 caggactgta tgtggagcgg cttctcggcc gccgccaagc tcgtctcaga gaagctggcc
     1021 tcctaccagg ctgcgcgcaa agacagcggc agcccgaacc ccgcccgcgg ccacagcgtc
     1081 tgctccacct ccagcttgta cctgcaggat ctgagcgccg ccgcctcaga gtgcatcgac
     1141 ccctcggtgg tcttccccta ccctctcaac gacagcagct cgcccaagtc ctgcgcctcg
     1201 caagactcca gcgccttctc tccgtcctcg gattctctgc tctcctcgac ggagtcctcc
     1261 ccgcagggca gccccgagcc cctggtgctc catgaggaga caccgcccac caccagcagc
     1321 gactctgagg aggaacaaga agatgaggaa gaaatcgatg ttgtttctgt ggaaaagagg
     1381 caggctcctg gcaaaaggtc agagtctgga tcaccttctg ctggaggcca cagcaaacct
     1441 cctcacagcc cactggtcct caagaggtgc cacgtctcca cacatcagca caactacgca
     1501 gcgcctccct ccactcggaa ggactatcct gctgccaaga gggtcaagtt ggacagtgtc
     1561 agagtcctga gacagatcag caacaaccga aaatgcacca gccccaggtc ctcggacacc
     1621 gaggagaatg tcaagaggcg aacacacaac gtcttggagc gccagaggag gaacgagcta
     1681 aaacggagct tttttgccct gcgtgaccag atcccggagt tggaaaacaa tgaaaaggcc
     1741 cccaaggtag ttatccttaa aaaagccaca gcatacatcc tgtccgtcca agcagaggag
     1801 caaaagctca tttctgaaga ggacttgttg cggaaacgac gagaacagtt gaaacacaaa
     1861 cttgaacagc tacggaactc ttgtgcgtaa ggaaaagtaa ggaaaacgat tccttctaac
     1921 agaaatgtcc tgagcaatca cctatgaact tgtttcaaat gcatgatcaa atgcaacctc
     1981 acaaccttgg ctgagtcttg agactgaaag atttagccat aatgtaaact gcctcaaatt
     2041 ggactttggg cataaaagaa cttttttatg cttaccatct tttttttttc tttaacagat
     2101 ttgtatttaa gaattgtttt taaaaaattt taagatttac acaatgtttc tctgtaaata
     2161 ttgccattaa atgtaaataa ctttaataaa acgtttatag cagttacaca gaatttcaat
     2221 cctagtatat agtacctagt attataggta ctataaaccc taattttttt tatttaagta
     2281 cattttgctt tttaaagttg attttttttct attgtttta gaaaaaataa aataactggc
     2341 aaatatatca ttgagccaaa tcttaaaaaa aaaaaaaa
```

Figure 5-1 Human c-myc mRNA sequence
Homo sapiens v-myc myelocytomatosis viral oncogene homolog (avian) (MYC) transcript is a 2379bp linear mRNA. The c-myc siRNA sequence used in this project is highlighted in yellow. The c-myc forward primer, reverse primer and probe used for qRT-PCR are highlighted in blue, grey and green respectively. (These c-myc siRNA and qRT-PCR sequences are listed in Table 5-1.) The c-myc mRNA transcript contains four exons as defined by the four different colours of text. Blue, green, red and black text indicates exons 1-4 respectively.

5.3.2 Protein Extraction

Cell culture and the addition of AuNPs/Lipofectamine was performed as in 5.3.1. After a 48 hour incubation the treatment media was removed, cells were trypsinised and pelleted by centrifugation. Cell pellets were resuspended in 50μl protein extraction buffer, left on ice for 15 min and then ultracentrifuged for 10 min at 14,000 rpm (4°C). The supernatant was transferred to a fresh eppendorf and stored at -80°C until ready to use. NB (A frozen protein pellet from Burkitts lymphoma Rayj cells (EBV+) was gifted from Joanna Wilson at the University of Glasgow for use as a c-myc positive control in Western blots.)

5.3.3 SDS-polyacrylamide gel electrophoresis (SDS-PAGE)

SDS-PAGE was used to separate proteins on the basis of size. SDS-PAGE was performed using Invitrogen Novex Mini Cell tank apparatus, and a PowerEase 500 power pack. Proteins were separated using NuPAGE 4-12% Bis-Tris gels (1.0mm x 15 well).

The total protein concentration of samples was quantified using a spectrophotometer (NanoDrop-1000 V3.7.1) following manufacturer's instructions. Samples were diluted to equal amounts of total protein (60ng for Hela cell samples and 10ng for Rayj EBV+ cell sample) and made up to 20μl with protein extraction buffer (with no inhibitors added). 7μl sample loading buffer was added and samples were incubated on a preheated heating block for 10 min at 70°C to denature proteins. During heating, the gel tank apparatus was assembled. The inner chamber was filled with inner chamber running buffer and the outer section of the tank was filled with normal running buffer. Combs were removed from the gel and empty wells were flushed with running buffer to remove any residual oils before sample loading. After heating, the total volume of each sample (27μl) was loaded onto the gel. 10μl protein ladder was loaded into the first lane of gel. Gel was run at 200V, 120mA, and 25W until the colour of the sample-loading buffer had reached the bottom of the gel.

5.3.4 Western Blotting

Following SDS-PAGE, proteins were transferred onto a nitrocellulose membrane for immunodetection. The gel was removed from plastic cassette and the wedge at the bottom edge of the gel was cut off. Gel was immersed in cold transfer buffer while transfer apparatus was assembled. Membrane was soaked in methanol for 10 sec, distilled water for 5 min and transfer buffer for 5 min. The rest of the transfer apparatus (pads and filter paper) was also soaked in transfer buffer and the transfer system was assembled in the following order, from cathode to anode: 2x sponge pads, 3x filter paper, gel containing proteins, transfer membrane, 3x filter paper, 3x sponge pads. The transfer cassette was completed with its lid, put into the tank and clamped into place. The tank was sat on ice, filled with transfer buffer, and proteins were transferred onto the nitrocellulose membrane at 25V, 120mA, and 3W for 1 hour.

5.3.5 Immunodetection of Proteins

Following Western blotting, proteins were visualised by enhanced chemical luminescence (ECL). Nitrocellulose membranes were removed from the transfer cassette and placed in a small container. To block non-specific binding sites membranes were incubated in blocking buffer for 1 hour on a plate shaker at room temperature, or overnight at 4°C. Primary antibodies were diluted in 5% (w/v) dried milk/ PBS-T to an appropriate dilution. Membranes were incubated in primary antibody on shaker for 1 hour at room temperature, or overnight at 4°C. Membranes received 3 x 10 min washes in PBS-T on shaker. Secondary IgG horseradish peroxidase-conjugated antibodies (HRP-conjugated IgG) were diluted in 5% (w/v) dried milk/ PBS-T to an appropriate dilution. Membranes were incubated in HRP-conjugated IgG for 1 hour at room temperature on shaker. Membranes received 3 x 10 min washes in PBS-T on shaker.

HRP-immunolabelled proteins were visualised using the ECL system. ECL reagents were mixed in a 1:1 ratio and then poured over the nitrocellulose membrane. The membrane was incubated in this detection mix for 5 min in the dark. The membrane was then removed from container, excess detection mix

was removed and the membrane was exposed to Kodak X-ray film in a lightproof cassette and developed using an X-Omat Processor.

5.3.6 Stripping of Nitrocellulose Membranes

To strip nitrocellulose membranes of bound antibodies, membranes were immersed in transfer buffer, and then incubated in stripping buffer for 10 min at room temperature, on shaker. Membranes were then washed in PBS-T, and blocked and re-probed with primary antibody as required.

5.3.7 Antibodies for Probing Nitrocellulose Membranes

To detect the c-myc protein, the primary antibody was Anti-c-myc antibody, raised in mouse (Abcam), used at 1:500 dilution in 5% (w/v) milk in PBS-T. The secondary antibody was anti-mouse IgG-HRP, raised in goat (Santa Cruz Biotech), used at 1:4000 dilution in 5% (w/v) milk in PBS-T.

To detect the GAPDH protein, the primary antibody was Anti-GAPDH antibody, raised in rabbit (Epitomics), used at 1:10,000 dilution in 5% (w/v) milk in PBS-T. The secondary antibody was anti-rabbit IgG-HRP, raised in goat (Santa Cruz Biotech), used at 1:4000 dilution in 5% (w/v) milk in PBS-T.

5.3.8 BrdU Staining

HeLa cells were seeded at 1 x 10^5 cells per well on glass coverslips in a 24 well plate and allowed to adhere overnight. AuNP/Lipofectamine treatments were added as in 5.3.1 and incubated for 48 hours (control cells were incubated with media alone). Cells were washed in PBS and incubated with 1ml of 100μM BrdU for 1.5 hours. Cells were washed in PBS, fixed in 4% formaldehyde, permeabilised, blocked in PBS/1%BSA and then incubated with anti-BrdU/DNase (1:100), followed by biotinylated anti-mouse secondary antibody (1:50), followed by streptavidin-FITC (1:50), in conjunction with rhodamine-phalloidin to stain actin. Cells were washed with PBS between each step.

5.3.9 Statistics

Statistical analysis was performed in SPSS. For the qRT-PCR data, the covalent AuNP group, the ionic AuNP group and the lipo/naked control group were all analysed independently by one-way ANOVA with Dunnett's test (n=3). For the BrdU data, the number of BrdU positive cells in 10 fields of view per treatment was quantified using Image J software, and analysed by one-way ANOVA with Dunnett's test (n=10). In all figures, * = $p < 0.05$, ** = $p < 0.01$. *** = $p < 0.001$.

5.4 Results

5.4.1 MTT Cell Toxicity Screening

In order to assess any cellular toxicity caused by the AuNPs, the viability of HeLa cells after incubation with each AuNP for 48 hours was measured using the MTT assay. Results showed that the HeLa cells remained highly viable after a 48 hour incubation with each AuNP species (Figure 5-2). In the majority of cases, cells remained over 80% viable, which is considered to indicate a very low level of NP toxicity. Slightly higher toxicity was caused by AuNPs with ionically attached siRNA (iAu_siRNA and iAu_Tat, siRNA), which reduced cellular viability to ~70%. In comparison, AuNPs with covalently attached siRNA (cAu_siRNA and cAu_Tat, siRNA) retained over 90% cellular viability. This batch of eight AuNPs can be considered generally non-toxic to cells, with the covalent attachment of siRNA proving a less toxic design than the ionic attachment of siRNA.
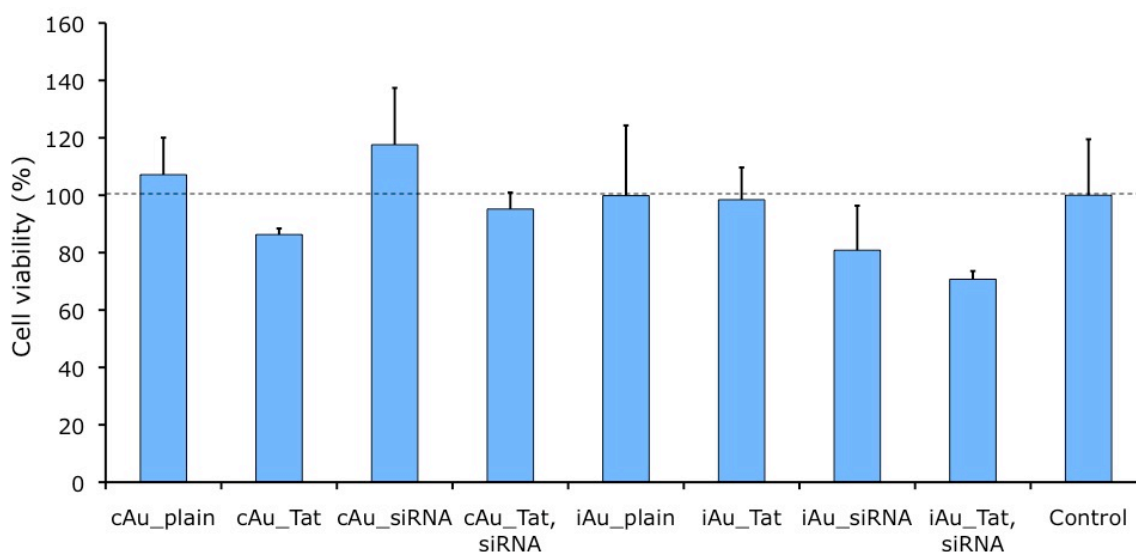
Figure 5-2 AuNP MTT toxicity screening in HeLa cells
The eight AuNP samples were screened following a 48 hour incubation with Hela cells.
Control cells, treated with only media, were taken to represent 100% viability, and the
viability of the eight nanoparticle treated samples was expressed as the percentage viability
relative to the control. A line has been drawn at 100% viability to aid easy comparison
between the control and the eight nanoparticle treated samples.

5.4.2 qRT-PCR

The level of c-myc mRNA was quantified by qRT-PCR after a 48 hour incubation with each of the eight AuNP species, in order to compare their c-myc knockdown capabilities. Results showed that the highest c-myc knockdown was achieved when the siRNA was covalently attached to the AuNP: cAu_siRNA caused a 39% knockdown, and cAu_Tat, siRNA caused a 42% knockdown. In comparison, when the siRNA was ionically attached to the AuNP, the c-myc knockdown was much lower: iAu_siRNA caused a 13% knockdown, and iAu_Tat, siRNA caused no knockdown at all. This suggested that covalent siRNA attachment was more effective than ionic siRNA attachment. In addition, results indicated that the inclusion of Tat did not significantly improve the knockdown efficiency of AuNPs. Due to the lack of requirement for Tat, it was concluded that out of the eight species investigated, cAu_siRNA was the optimal AuNP design for the delivery of c-myc siRNA to HeLa cells (Figure 5-3B).
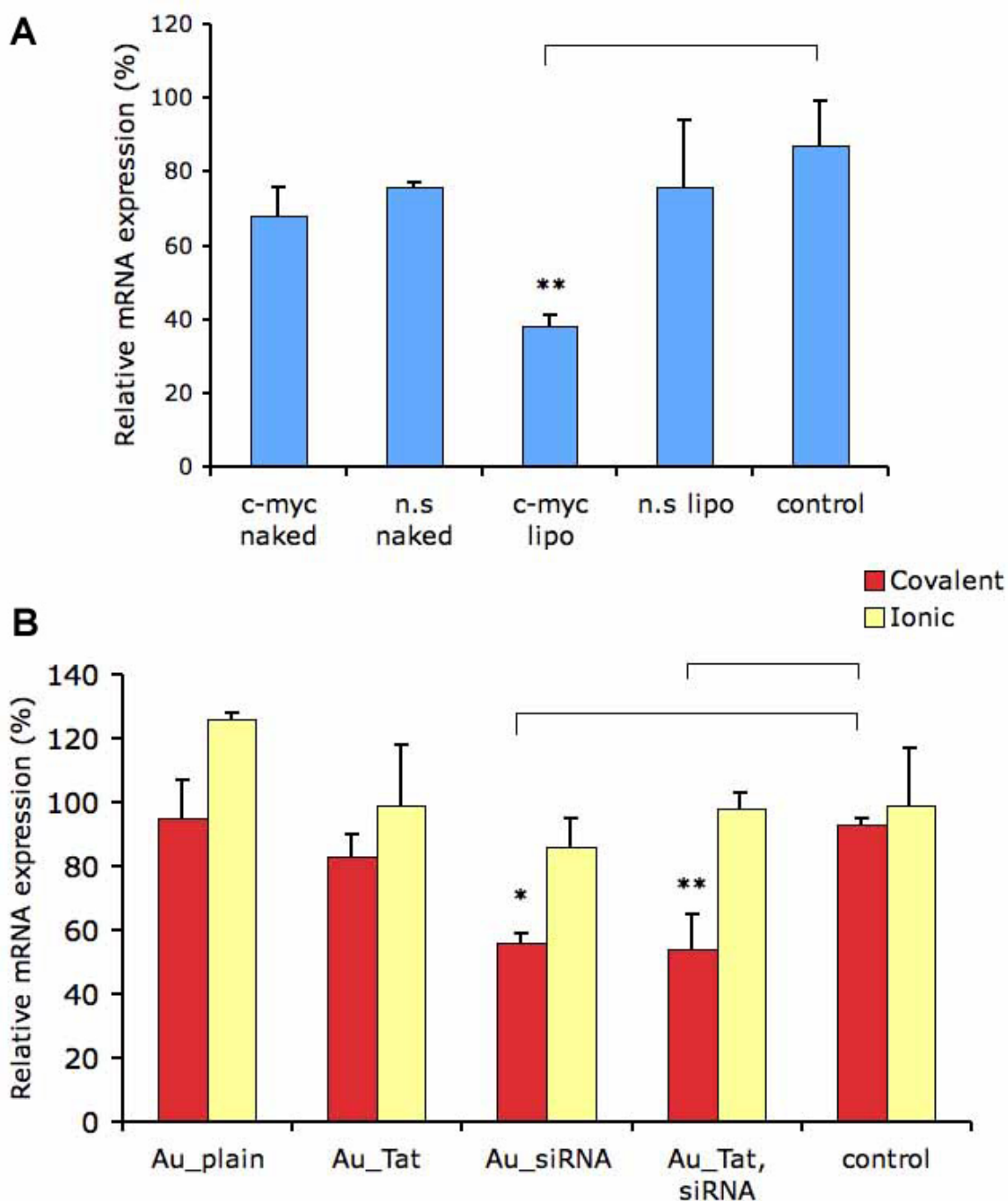
Figure 5-3 c-myc mRNA knockdown in HeLa cells, as assessed by qRT-PCR
This figure shows the level of c-myc mRNA (normalised to GAPDH) as assessed by Taqman quantitative real-time PCR (qRT-PCR). Graph A shows the level of c-myc mRNA after treatment with c-myc or nonsense (n.s) siRNA, either delivered directly onto the cells (naked), or delivered to the cells using Lipofectamine (lipo). Graph B shows the level of c-myc mRNA after treatment with the eight AuNP species. In both graphs, the control represents cells treated with media alone. All treatments were incubated with the cells for 48 hours. Please note that AuNPs with covalent siRNA attachment (red bars) produced a higher knockdown than AuNPs with ionic siRNA attachment (yellow bars). (* = p < 0.05, ** = p < 0.01 as analysed by one-way ANOVA with Dunnett's test in SPSS. Error bars are SD, *n*=3.)

5.4.3 Western Blotting

Cellular protein was investigated by Western blot in order to check if the 40% knockdown of c-myc mRNA induced by a 48 hour incubation with cAu_siRNA (as reported by qRT-PCR) was detectable at protein level. Only two AuNP species were selected for the Western blots; cAu_siRNA, and the corresponding negative control cAu_plain. These were compared against c-myc or nonsense (n.s) siRNA delivered to the cells by Lipofectamine. The density of the c-myc protein bands was normalised to the density of the GAPDH protein bands for each sample, and expressed graphically using Image J analysis. Results show that expression of the c-myc protein was reduced by 40% when c-myc siRNA was delivered by nanoparticles (cAu_siRNA) and by 80% when delivered by Lipofectamine (c-myc lipo). Expression of the c-myc protein was not effected by either of the two negative controls (cAu_plain or n.s lipo), supporting the fact that the c-myc knockdown is specific to the c-myc siRNA, and not caused by the presence of either AuNPs or Lipofectamine (Figure 5-4).

N.B [During the optimisation of the Western blot procedure, protein from the Rayj EBV+ cell line (known to overexpress c-myc) was employed as a positive control to which the other HeLa samples could be compared.]
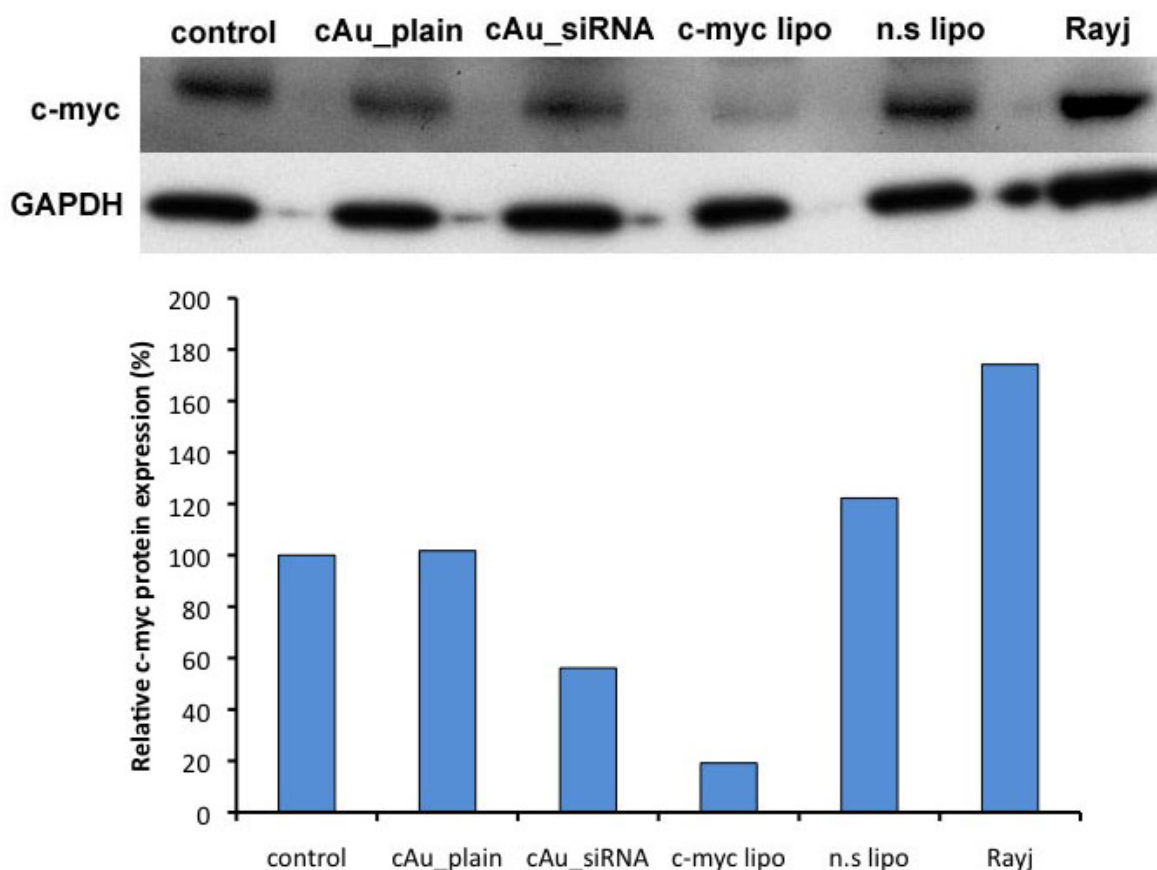
Figure 5-4 c-myc protein knockdown in HeLa cells, as assessed by Western blot
HeLa cells were incubated with each treatment for 48 hours, after which the level of
expressed c-myc protein was measured by Western blot. The density of each c-myc band
was normalised to the density of the corresponding GAPDH band (to allow for any
differences in loading volume) and results were expressed graphically as the percentage of
c-myc protein expression relative to the control sample (control cells treated with media
only). Results showed that cAu_siRNA produced a 40% knockdown in c-myc protein.

5.4.4 BrdU Staining

In order to determine if the 40% reduction in c-myc expression reported at both the mRNA and protein levels by qRT-PCR and Western blot respectively was having an effect on the speed of the cell cycle, BrdU staining was employed to fluorescently label dividing cells. The BrdU method allows 5-bromo2'-deoxy-uridine (BrdU) to be incorporated into the DNA in place of thymidine, during the process of DNA replication occurring in dividing cells. This incorporation allows dividing cells to be fluorescently visualised by subsequent immunodetection using a monoclonal antibody against BrdU.

As in the Western blot experiment, only two AuNP samples were investigated, cAu_siRNA and the corresponding negative control cAu_plain. These treatments were compared to c-myc or nonsense (n.s) siRNA delivered by Lipofectamine. Results show that a similar number of dividing cells were evident in the control cell culture and in those treated with the negative controls (cAu_plain and n.s lipo). In contrast, the number of dividing cells was significantly reduced in cell cultures when c-myc siRNA was delivered by nanoparticles (cAu_siRNA) and by Lipofectamine (c.m lipo) (Figure 5-5). This demonstrated that the reduction in the level of c-myc expression achieved by treatment with cAu_siRNA acted to inhibit cells entering the S phase of the cell cycle, thus decreasing cell proliferation.
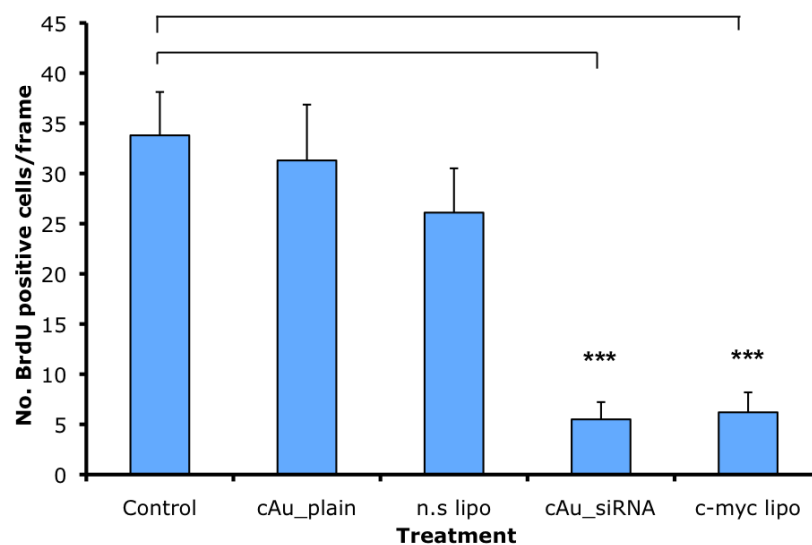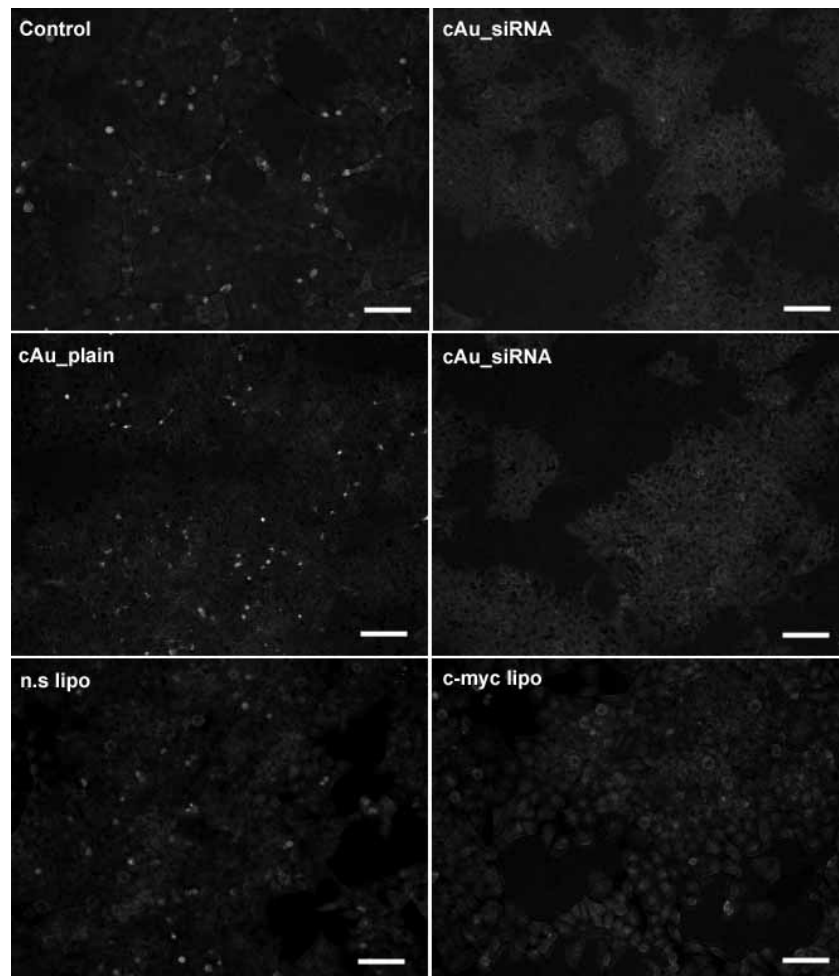
Figure 5-5 Proliferation of HeLa cells as assessed by BrdU staining
Cells treated with c-myc siRNA, either delivered by covalent attachment to AuNPs (cAu_siRNA) or by Lipofectamine (c-myc lipo) are presented in the right hand side of A (two images are provided for cAu_siRNA). Untreated cells (control), cells treated with AuNPs without any siRNA attached (cAu_plain) and cells treated with nonsense siRNA delivered by Lipofectamine (n.s lipo) are presented on the left hand side of A [scale bars = 100μm]. The number of BrdU positive cells in 10 fields of view per treatment was quantified in Image J and presented graphically (B). (*** = p < 0.001 as analysed by one-way ANOVA with Dunnett's test in SPSS. Error bars are SD, n=10.)

5.4.5 TEM

TEM was used to visualise the AuNPs inside HeLa cells to gain insight into the level and method of cellular uptake, and intracellular location of the internalised nanoparticles. AuNP samples with c-myc siRNA covalently attached, with and without Tat (cAu_siRNA and cAu_Tat, siRNA) were chosen for investigation by TEM as they produced the best c-myc knockdown as assessed by qRT-PCR. Furthermore, it was hoped that TEM would provide clarification as to the inclusion of Tat, as results to date suggested it was not enhancing uptake as originally expected. Results showed that both AuNP species were uptaken into HeLa cells, although from these images it appears that Tat did not increase uptake, and as such, was not necessary for inclusion in the nanoparticle design.
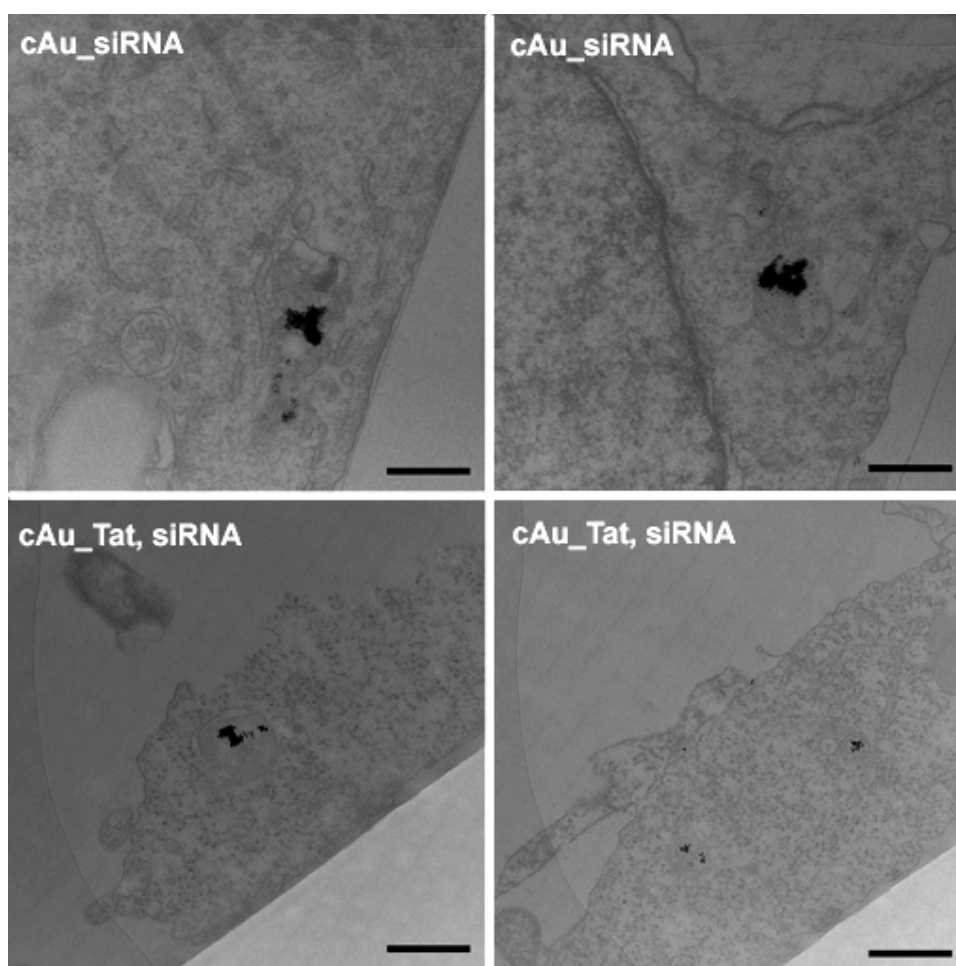
Figure 5-6 Uptake of AuNPs into HeLa cells as assessed by TEM
TEM images indicate AuNPs with siRNA covalently attached in HeLa cells after 18 hours incubation. The top two images show AuNPs without Tat, and the bottom two images show AuNPs with Tat. AuNPs were seen in the cytoplasm, where it is envisaged that their siRNA payload becomes incorporated into the RISC complex to cause gene silencing through RNA interference (RNAi) [scale bars = 500nm].

5.5 Summary and Discussion

This chapter has demonstrated knockdown of the c-myc oncogene in HeLa cells through RNAi, facilitated by the delivery of siRNA by AuNPs. Two alternative approaches for chemically attaching siRNA to AuNPs were investigated, and results conclude that the covalent attachment is favorable compared to the ionic attachment. The inclusion of Tat in the AuNP design did not significantly improve knockdown efficiency, and this is believed to be due to the fact that Tat did not appear to enhance cell uptake of AuNPs.

The reason for the higher knockdown levels observed when siRNA was attached covalently rather than ionically may be due to the fact that the Au-S covalent bonds between the thiolated siRNA and the AuNP core are stronger than the electrostatic bonds between the siRNA and the positively charged R_4N group on the outside of the particle. Therefore, due to weaker bonding, perhaps the ionically attached siRNA became dissociated from the AuNP before it could be successfully delivered to the cytoplasm to interact with RISC. Or alternatively, perhaps the presence of the positively charged R_4N group inactivated RISC in some way, possibly by preventing correct siRNA loading into the enzymatic complex.

5.5.1 The Unsuccessful Ionic Approach

In comparison to the literature, Ghosh *et al* used a similar ionic design strategy whereby AuNPs were functionalised with the amino acid lysine in order to ionically bind DNA plasmids for delivery to monkey kidney cells (Cos-1) (Ghosh *et al.*, 2008). This study utilised ionic binding between the positive charges of the amine groups within the lysine residues and the negatively charged DNA plasmid to achieve very high transfection efficiencies. The success of the ionic AuNP design demonstrated by Ghosh *et al* suggests that the similar positively charged R_4N surface groups used in this thesis should also have facilitated successful delivery of siRNA. However, results in this chapter proved that the ionic design was unsuccessful with regards to c-myc knockdown by RNAi. There are a number of possible reasons to explain why ionic attachment to AuNPs should enable the delivery and expression of plasmid DNA but not the delivery of c-myc siRNA for

RNAi, including 1) the electrostatic interaction of siRNA largely differs from that of plasmid DNA (Patil *et al.*, 2008; Gary *et al.*, 2007), and 2) following delivery, plasmid DNA does not require any involvement with the RISC complex for molecular functionality. The study by Ghosh *et al* concluded that AuNPs functionalised with lysine were ~28 fold superior than polylysine in reporter gene expression, suggesting that NPs functionalised with cationic surface groups may be more successful than the use of cationic polymers for ionic delivery strategies. In contrast to this, and despite the poor performance reported for polylysine, cationic polymers are commonly used in polyplex formation for siRNA cellular delivery, which is useful for comparison to this chapter.

The polyplex delivery strategy involves the formation of nanometer-sized ionic complexes (polyplexes) through noncovalent interaction between negatively charged siRNA and positively charged macromolecular vectors such as polymers, dendrimers and lipids (Salcher and Wagner, 2010). A recent polyplex study by Ornelas-Megiatto *et al* is relevant to this discussion of why ionic attachment of siRNA to the R_4N (quaternary ammonium) surface group proved unsuccessful for c-myc knockdown in HeLa cells. Ornelas-Megiatto *et al* compared polyplexes composed of either ammonium or phosphonium positively charged polymers, for their ability to deliver siRNA to HeLa cells in order to silence the luciferase gene. Results showed that ammonium polymers achieved 25% knockdown with 85% cell viability, whereas phosphonium polymers achieved 65% knockdown with 100% viability (Ornelas-Megiatto *et al.*, 2012). Based on these findings, the authors concluded that ammonium polymers were not the best choice of vector for siRNA delivery since they displayed higher toxicity and weaker nucleotide binding than other types of cationic polymers. In theory, these undesirable transfection properties associated with ammonium polymers could also hold true for the R_4N group that was used to ionically attach siRNA to AuNPs species described in this thesis. If so, it supports the idea that the poor knockdown capabilities of the ionic AuNPs could indeed have been caused by weak binding strength between the R_4N group and the siRNA, as previously suggested. However, in contrast to the findings of Ornelas-Megiatto *et al,* it seems unlikely that the R_4N group was the cause of any toxicity associated with the ionic AuNP samples, since the MTT assay showed that iAu_plain and iAu_Tat displayed no toxicity despite also having the R_4N group attached.

Aside from implicating weak binding and toxicity to explain the poor transfection properties of ammonium polymers, Ornelas-Megiatto *et al* did not consider that the cationic polymers used to bind siRNA could cause inhibition of the RISC complex. This lack of consideration is probably because the authors hypothesised that the siRNA payload became released from the cationic polymer upon entry into the cell, and therefore the two molecules would not be in contact during siRNA incorporation into RISC. Whether the R_4N group interfered with RISC in this chapter remains to be determined. Learning from the findings of Ornelas-Megiatto *et al*, perhaps ionic siRNA attachment to NPs will be more successful if cationic surface groups based on phosphonium are used instead of the R_4N quaternary ammonium group featured in this project, since they may provide stronger electrostatic interactions, thereby preventing the siRNA from becoming dissociated before it reaches the cell.

5.5.2 The Successful Covalent Approach

The particular type of covalent bond employed in this project, (i.e. the gold-thiol interaction) is a far stronger attachment than ionic bonding (Pissuwan *et al.*, 2011). In addition, it has been described as a dynamic bond allowing disassociation under reductive conditions such as the high glutathione concentrations in the cell cytoplasm (Lytton-Jean *et al.*, 2011; Meister and Anderson, 1983). Therefore it seems likely that c-myc knockdown was achieved because covalent attachment of siRNA provided two main advantages to delivery; 1) extracellular strength, and 2) intracellular release.

The c-myc knockdown achieved by the AuNPs with siRNA covalently attached echoes the success of previous studies that have achieved gene knockdown using functionalised NPs. For example, siRNA-delivering cationic NPs reduced the expression of Mcl-1 in carcinoma cells, causing an 81% reduction in cell viability (Chang *et al.*, 2011). In addition, conjugated polymer NPs delivered siRNA to reduce the expression of actin by 94% in HeLa cells (Moon *et al.*). In 2004, Wang *et al* demonstrated 80% knockdown of c-myc in breast cancer cells after transfection with a siRNA-encoding plasmid, demonstrating an alternative approach to siRNA delivery, growing in popularity due to its longer lasting

silencing (Wang *et al.*, 2005). In the example of Wang *et al*, Lipofectamine facilitated the plasmid transfection, although several more recent studies have used NPs to deliver siRNA-encoding plasmids for RNAi (Guo *et al.*; Mukerjee *et al.*). In comparison of this long-term plasmid approach, this chapter has shown that the knockdown produced by covalent AuNP siRNA delivery is in effect after 48 hours, but how long it would last *in vivo* is an issue that remains to be determined.

The majority of previous knockdown studies report a higher level of target gene knockdown than the 40% c-myc knockdown presented here, but this higher knockdown was often associated with a higher level of cellular toxicity (Chang *et al.*, 2011). Obviously killing cancer cells by RNAi appears as a desirable end goal to siRNA delivery. However, this chapter has shown that a 40% oncogene knockdown is indeed sufficient to induce a significant reduction in cancer cell proliferation, whilst avoiding cell death. This suggests that complete silencing of oncogenes may not actually be necessary for successful cancer therapy. Therefore, perhaps the end goal in future RNAi therapy should instead be to normalise the abhorrent expression levels of oncogenes rather than to stop their expression completely.

5.5.3 The Lack of Tat Influence

The CPP Tat was included in the AuNP design strategy as it was expected to increase cell uptake of the particles, thereby increasing their c-myc knockdown efficiency. However, the qRT-PCR data revealed that the inclusion of Tat did not significantly increase the level of c-myc knockdown. Uptake analysis by TEM and ICP-MS indicated that this lack of effect is due to the fact that Tat did not actually enhance the cell uptake of AuNPs. This finding could be possibly due to inaccessibility or dissociation of Tat. To discuss the former, some studies have shown that if the PEG chains on a NP surface are longer than the functional molecules, the activity of the functional molecules can be reduced due to their inaccessibility to the cell since they are hidden within the PEG layer. This danger was highlighted in a review by (Lytton-Jean *et al.*, 2011), which discussed that a study using AuNPs co-loaded with SH-PEG$_{5000}$-PAMA$_{7500}$ and SH-siRNA only achieved 65% luciferase knockdown in HuH-7 cells (Oishi *et al.*, 2006), whereas a

study that used AuNPs co-loaded with much shorter SH-PEG$_{400}$ and SH-siRNA achieved 70% luciferase knockdown in HeLa cells (Giljohann *et al.*, 2009). Lytton-Jean *et al* suggested that the improvement in knockdown efficiency was due to the use of shorter PEG chains, since it allowed more of the siRNA molecules to be accessible to the cell for RISC interaction. In comparison to these similar studies using PEGylated AuNPs, the PEG$_8$ chains used in this chapter were much smaller than either PEG$_{5000}$-PAMA$_{7500}$ or PEG$_{400}$, making them less likely to hide adjacent functional molecules from cellular recognition.

In this project, the 13 amino acid long Tat peptide was ~6.5nm in length, the 21 nucleotide long siRNA was ~10.5nm in length and the 8 monomer long PEG polymer was ~3.5nm in length. Therefore, it is unlikely that Tat was inaccessible to the cells, due to the fact that 1) the PEG chains were smaller than Tat and 2) Tat was attached to the ends of the PEG molecules rather than to the NP core. Alternatively, the most likely theory to explain why Tat did not improve uptake is that it became dissociated from the AuNP during transit from grant partners. This theory was suggested in chapter 4, since the Zetasizer results showed no difference in zeta potential between particles with or without Tat.

An interesting point worth discussing as to the use of Tat for enhancing siRNA delivery, is that it has recently emerged that infection with the HIV-1 Tat virus (from which the Tat CPP is derived) can inhibit RNAi in mammalian cells (Qian *et al.*, 2009). Although Tat was not shown to inhibit RNAi in this project, it is an important consideration in the design of future CPP-mediated siRNA delivery strategies for RNAi; as are peptide dissociation, and cellular inaccessibility within large PEG layers.

5.6 Conclusion

This study has been the first to directly compare ionic vs. covalent attachment of siRNA to NPs for RNAi. Results have demonstrated that c-myc knockdown by RNAi can be achieved in HeLa cells through the delivery of siRNA covalently attached to AuNPs. This has proven to be a more effective design strategy than either a) ionically attached siRNA, or b) the inclusion of Tat. The novel AuNPs presented in this thesis demonstrated low cellular toxicity, facilitated c-myc

knockdown and as a result, reduced cell proliferation in cancerous HeLa cells (as summarised in Table 5-2). Therefore they exemplify the achievable potential of NP-mediated RNAi in future cancer therapy.

Sample Acronym	Main findings
pAu_citrate	Used only in toxicity testing (low toxicity)
pAu_COOH	• Sample with best cell uptake properties • Desplayed high uptake into all cell types tested (h-TERT, MCF-7 & HeLa)
pAu_N3	• Aggregated
cAu_plain	Used only in toxicity testing (low toxicity)
cAu_Tat	• Low uptake in MCF-7 cells
cAu_siRNA	• Low uptake in h-TERT or MCF-7 cells • High uptake into HeLa cells • Sample with optimal knockdown properties • Produced 39% knockdown in c-myc mRNA • Produced 40% knockdown in c-myc protein • c-myc knockdown reduced cell proliferation
cAu_Tat, siRNA	• Low uptake in h-TERT or MCF-7 cells • High uptake into HeLa cells • Produced 40% knockdown in c-myc mRNA
iAu_plain	Used only in toxicity testing (low toxicity)
iAu_Tat	Used only in toxicity testing (low toxicity)
iAu_siRNA	• Low uptake into h-TERT or MCF-7 cells • High uptake into HeLa cells • Produced 13% knockdown in c-myc mRNA
iAu_Tat, siRNA	• Low uptake into h-TERT or MCF-7 cells • High uptake into HeLa cells • Knockdown unsuccessful (0%)

Table 5-2 Summary of main findings
This table summarises the main findings for each of the 11 AuNP species investigated in this thesis. The four main test criteria, as outlined at the start of chapter 4, were potential cell toxicity, cellular uptake, c-myc knockdown and effect on the cell cycle. Out of the 11 samples, pAu_COOH was found to display the best cellular uptake properties, and cAu_siRNA was found to be the optimal sample for c-myc knockdown. (This table has been colour-coordinated with Figure 4-2, where primary samples are displayed in green, covalent samples are displayed in violet and ionic samples in orange.)

6 Discussion

6.1 Introduction

Advances in biomedicine have identified many novel types of therapeutic molecules that have the potential to cure disease. These include newly identified small molecule drugs, and oligonucleotides for gene replacement therapy and RNAi. However, at present systemic delivery remains the major hurdle to widescale clinical use of these therapeutics. It is proposed that NPs will over come this hurdle by acting as multifunctional delivery vehicles to transport molecular cargo into diseased cells within the body. This thesis has investigated two different NP design strategies to assess their potential for use as therapeutic delivery vehicles; 1) the use of a magnetic field (MF) and a CPP (penetratin) to increase the delivery of iron oxide magnetic NPs (mNPs) to cells grown in tissue-equivalent 3D collagen gels, and 2) gold NPs (AuNPs) for the delivery of siRNA to silence the c-myc oncogene for cancer treatment. The main conclusions from this work were that;

- a MF facilitated movement of iron mNPs through 3D tissue-equivalent cell-seeded collagen gels, targeting the mNPs to the embedded fibroblast cells, whilst the CPP penetratin enhanced the cellular uptake of mNPs within this 3D model. This led to the conclusion that synergistic use of both together (i.e. the MF and penetratin) could provide an excellent platform for NP mediated delivery in 3D tissues.

- AuNPs delivered covalently attached siRNA to HeLa cells, mediating a 40% c-myc knockdown by RNAi. The COOH functional grouping was shown to significantly enhance cellular uptake, and the uptake of siRNA-functionalised AuNPs displayed cell-type specificity. Covalent attachment of siRNA proved more effective than ionic attachment of siRNA for RNAi.

This discussion will now consider how the findings from this thesis contribute towards the overall goal of achieving NP-mediated cancer treatment.

6.2 Selection of the Core NP Material

This thesis has investigated NPs composed of either gold (AuNPs) or iron (mNPs). Results within have suggested that both materials were excellent candidates with regards to production of therapeutic NPs. Two main criteria when considering cellular delivery vehicles were met, in that both metals displayed low cellular toxicity and high cellular uptake. However, both NP systems have also demonstrated that they offer further potential benefits. The main advantage of using iron for NP synthesis is that it provides magnetism to the NP enabling targeting *via* an externally applied magnetic field, as was exemplified in chapter 3. In addition, iron provides excellent *in vivo* imaging capabilities through the use of MRI. Alternatively, the main advantage of using gold for NP synthesis is that it can be used to bind thiolated molecules by exploiting the unique covalent bond that forms between gold and sulphur atoms. Chapter 5 has shown that the gold-sulphur covalent bond is highly advantageous to NP-mediated drug delivery, since it is stronger that other types of bonds, such as the electrostatic interactions involved in ionic attachment. The strength of this covalent gold-sulphur bond allows AuNPs to remain bound to their thiolated cargo up until and during cellular uptake, whereas in comparison weaker ionic bonds often become dissociated prior to cellular uptake. A further advantage of the gold-sulphur covalent bond is that it becomes dissociated within the reductive conditions of the intracellular environment, allowing for thiolated cargo molecules to become released from the AuNP once inside the cell. In addition, with regards to *in vitro* studies, during this project it was noticed that gold was more suitable for TEM since it is more electron dense than iron, whereas iron was more suitable for ICP-MS since it is more easily detectable than gold.

In my opinion, the findings from this thesis suggest that both iron and gold have very desirable but distinct properties that are advantageous to therapeutic NPs. Therefore, I propose that an excellent idea would be to utilise all of these benefits by making a chimeric NP out of both metals. A NP with an iron core would enable magnetic targeting and imaging by MRI, and a gold surface coating would facilitate the use of gold-sulphur covalent bonding of thiolated molecules. The potential of hybrid NPs composed of two different metals has already been

realised by materials chemists, and in their 2006 review, Cozzoli *et al* state that grouping inorganic materials with different properties in the same particle has been devised by several research groups (Cozzoli *et al.*, 2006). This review supports the use of such gold-iron chimeric NPs, concluding that providing a magnetically active core (e.g. iron) with a gold shell *via* a transmetalation reaction allows for the NP to display desirable magnetic properties (Park *et al.*, 2004), while simultaneously offering a suitable surface to which biomolecules can attach more easily (Cao *et al.*, 2001). Additional studies into gold-iron chimeric NPs include Umut *et al,* who have described the synthesis of multifunctional hybrid magnetic nanoparticles (HNPs) (Umut *et al.*, 2012) which conversely have a gold core and an iron shell. The authors state that iron provided the HNPs with magnetism whereas gold provided the HNPs with optical activities due to the fact that gold shows surface plasmon phenomena. Similarly, Bach *et al* have described the synthesis of NPs with an iron core and gold shell (Fe-Au/core-shell), stating that these hybrid metal NPs displayed superparamagnetic properties and could be functionalised by utilising gold-sulphur covalent bonding (Bach *et al.*, 2012).

6.3 Method of Administration

The literature suggests that NPs can be administered either locally or systemically. Local administration usually involves direct injection of NPs into the site of disease, (i.e. directly into a tumour), whereas systemic administration involves intravenous injection of NPs into the blood stream. It is understood that systemic delivery is necessary to treat disease sites deep within the body, and therefore this is the main goal of therapeutic NP delivery vehicles. To achieve systemic delivery, it is envisaged that after intravenous injection, NPs must circulate through the body within the blood stream until location of the disease site, upon which they should leave the blood stream *via* traversing the blood vessel wall and enter the surrounding tissue. Once at the disease target site, NPs must be able to selectively enter diseased cells and deliver their therapeutic payload intracellularly.

In regards to systemically administered therapeutic NPs for cancer treatment, it would appear that gold-iron chimeric NPs show great potential, as a magnetic

field may be employed to attract the NPs towards the disease site. This could be used as an adjunct to the enhanced permeability and retention (EPR) effect associated with solid tumours, which occurs with the systemic delivery of any type of NP formulation (Matsumura and Maeda, 1986). Fang *et al* describe the EPR effect as a unique pathophysiological phenomenon of solid tumours that allows biocompatible macromolecules (>40kDa) to accumulate selectively in the tumour (Fang *et al.*, 2012). The EPR effect is caused by the fact that tumours display increased vasculature, which is made permeable by (i) the presence of vascular mediators such as bradykinin and VEGF, (ii) the lack of a smooth muscle layer and (iii) large gaps between vascular endothelial cells. In addition, retention of macromolecules is mediated by impaired lymphatic clearance from the tumour interstitial space (Maeda *et al.*, 2003). Therefore, the EPR effect provides circulating NPs with an increased chance of being able to leave the blood stream and accumulate at the tumour site. Results from chapter 3 certainly suggest that this accumulation would be increased further through the use of a magnetic field as a relatively low field strength was shown to pull mNPs through the dense fibre network of the tissue-equivalent cell-seeded collagen gel model.

6.4 Cellular Uptake

Once at the target disease site, mediated by a combination of the EPR effect and magnetic targeting, therapeutic NPs must recognise and selectively enter diseased cells. TEM and ICP-MS results from chapter 4 have demonstrated that AuNPs displayed good cellular uptake properties, which was enhanced by the attachment of COOH and was cell-type specific if the AuNPs were functionalised with siRNA. The attachment of a CPP is still advisable, although this was not a necessary requirement to mediate cell uptake of AuNPs in this project. Despite the fact that Tat had no effect in this project, possibly due to molecular dissociation during transit, results from chapter 3 clearly demonstrated that the CPP penetratin was highly effective at enhancing the cell uptake of mNPs and is therefore recommended for use in future NP design strategies.

This thesis did not involve the use of NP targeting moieties, although this is advisable in an optimal design strategy for *in vivo* systemic delivery. The most

popular choices presented in the literature are folate, and the RGD tripeptide, which act to attract NPs to cancer cells that over express receptors for these targeting peptides. As discussed in chapter 4, the siRNA-functionalised AuNPs investigated in this project displayed very distinct cell-specific targeting, being internalised into HeLa cells, but not h-TERT or MCF-7 cells. Further investigation is required to determine if this effect was due to cell-type specific expression of certain surface receptors, which could be used to ensure specific uptake into only the target diseased cell type.

6.5 Therapy

Chapter 5 of this thesis demonstrated the successful NP-mediated delivery of siRNA to HeLa cells, which resulted in silencing of the c-myc oncogene and reduced cell proliferation. Therefore, this work has proven that RNAi is a very promising method of cancer treatment. However, one of the main problems facing the treatment of cancer is that it can be caused by many different genes. As discussed by Weinstein, it is hoped that due to the 'oncogene addiction' of many tumours, treating cancer by reducing the expression of one key oncogene, such as c-myc, will be sufficient to reverse tumourigenesis (Weinstein, 2002). Nevertheless, the problem still exists that each individual cancer may not be addicted to exactly the same oncogene. Therefore, it seems necessary that for clinical cancer treatment by RNAi to become a reality, its use must be designed on a patient-to-patient basis, according to the genetic profile of each cancer. Indeed, this idea is beginning to become well known as personalised therapy, and genetic profiling of cancer patients is already carried out to identify patients who would be more likely to respond to drugs due to the nature of the individual cancer. For example, 95% of chronic myelogenous leukemias are characterised by mutations involving the BCR-ABL fusion gene, leading to the expression of a leukemia-specific hybrid tyrosine kinase. Patients who have this mutation respond well to the powerful tyrosine kinase inhibitor, Imatinib (Saglio *et al.*, 2004). In addition, breast cancer patients are screened for abnormal expression of the HER2 gene, as cancers that are HER2+ are approved for treatment with Herceptin (Murphy and Fornier, 2010). Hopefully, if samples from tumour biopsies can be analysed by micro-array and compared against the patient's normal tissue, an expression profile of the patient's cancer genome

can be formed. This could then be used to identify any key oncogenes that are overexpressed, or alternatively, any tumour suppressor genes that are underexpressed. After screening in this manner, siRNA or expression plasmids could be selected for the identified abnormal genes, attached to a NP delivery vehicle and intravenously injected into the patient.

It could be envisaged that in a future clinical setting, this screening could be made routine for cancer patients. Specialised NP synthesis labs could be made available containing libraries of all the necessary molecular attachments including siRNAs, expression plasmids, targeting moieties (e.g. RGD/folate), CPPs (e.g. Tat/penetratin) and additional cancer drugs (eg. Imatinib/Herceptin). Following the cancer screening report, a team of oncologists, molecular biologists, nanoscientists and toxicologists could create the optimal multifunctional NP design tailored to that individual cancer. For example, a screening report may identify a breast cancer with overexpression of cell surface folate receptors, expression of the (as yet unidentified) cell surface receptors for COOH, c-myc overexpression, p53 mutation, and overexpression of cell surface HER2 receptors. Thus, in this example, an Fe-Au core/shell NP could be functionalised with folate for selective targeting of cancer cells, COOH to facilitate cell uptake of NPs, c-myc siRNA and a p53 expression plasmid to normalise gene expression and regain genetic control over the cell cycle, and Herceptin to reduce cell signaling and cell proliferation. This multifunctional NP design could be intravenously injected, targeted to the tumour site by an externally applied magnetic field (aided by the EPR effect), and deliver its therapeutic payload to the cancer cells. The gold core could also facilitate thermal ablation of the tumour by heating under NIR light.

6.6 The Consequence of Treatment

It is important to consider what the effects of such a NP treatment may be. Pelengaris and Khan discuss that based on data received from transgenic mouse models of tumourigenesis, deactivation of an initiating oncogene, such as c-myc, can have three possible cellular outcomes; apoptosis, redifferentiation or escape (as described in Figure 6-1) (Pelengaris and Khan, 2003). In the first two cases, apoptosis and redifferentiation lead to tumor reversal, and are therefore the

intended aim of administering a therapeutic NP for RNAi as described. This desirable outcome was exemplified by Jain *et al* who, reported that inactivation of c-myc caused osteogenic sarcoma cells to differentiate into mature osteocytes (Jain *et al.*, 2002). In light of this, perhaps the reduction in cell proliferation after c-myc RNAi reported in chapter 4 was mediated by redifferentiation of HeLa cells, although this was not determined. The less desirable third outcome is escape, where deactivation of the initiating oncogene has no effect on the cell and it escapes from treatment, resulting in no tumour reversal taking place. This can be explained by the fact that some cells within a tumour can gain lesions in additional oncogenes, lifting the previous addiction to the initiating oncogene. As some cancer cells may escape treatment in this manner, it lends further support to the benefits of NP multivalency, in order to attach siRNA molecules against a variety of different oncogenes to ensure tumour reversal (Paciotti *et al.*, 2006). Perhaps in designing future NP treatments the top 5 overexpressed oncogenes identified in tumour biopsy micro-array screening should all be attached to the delivery NP in order to maximize the chance of achieving tumour reversal.
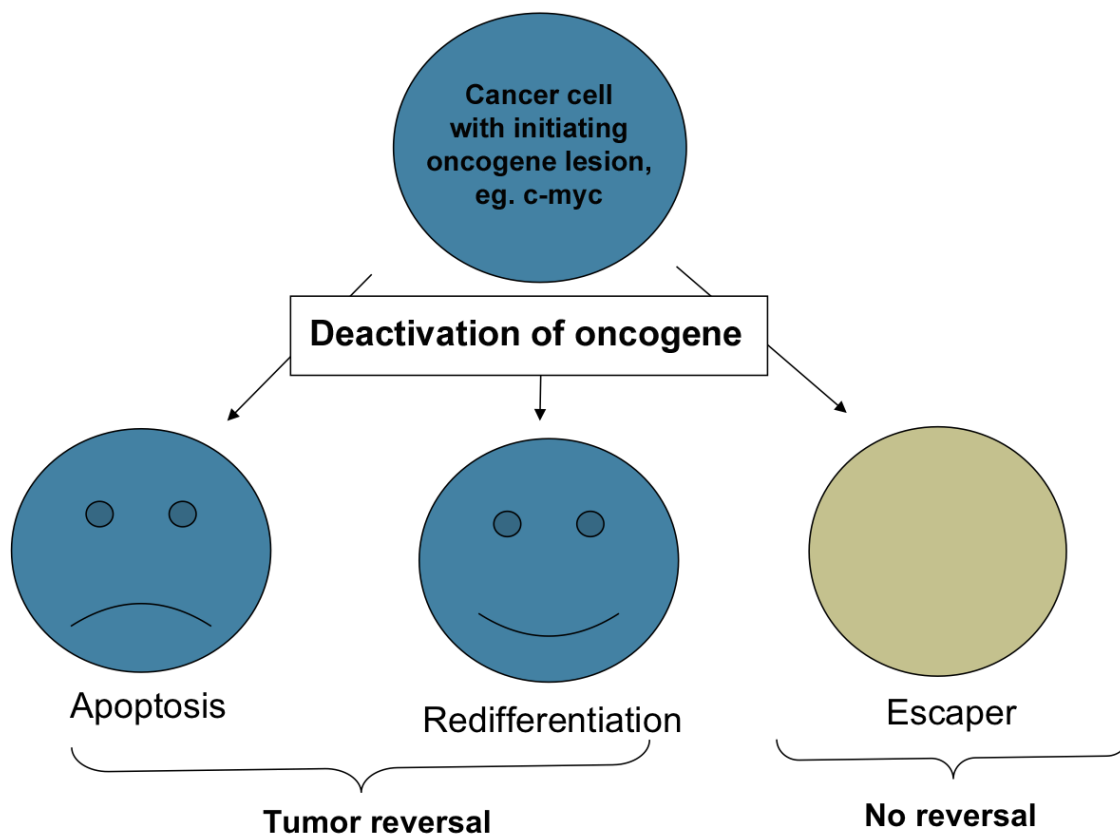
Figure 6-1 The possible outcomes of oncogene deactivation
Deactivation of oncogenes can result in desirable outcomes of cellular apoptosis or redifferentiation, which lead to tumour reversal. However, escaper cells can defy treatment, leading to no tumour reversal after oncogene deactivation. These escaper cells are likely to have obtained additional lesions in other oncogenes, reducing their addiction to the initiating oncogene. Image modified from (Pelengaris and Khan, 2003).

6.7 Dangers

This futuristic and theoretical approach to NP-mediated cancer treatment tries to maximize the opportunity for tumour reversal, by making multifunctional NPs as potent as possible and potentially deadly to cancer cells. Thus it is imperative to ensure that cell specific targeting is tightly controlled in developing this clinical treatment, as the effects would be dire if these potent therapeutic NPs were to gain entry into healthy cells. At present, the laws that govern NP entry into different cell types are poorly understood, as was demonstrated in chapter 4. NP cell uptake can occur in unexpected and unclear manners, such as the fact that COOH enhanced NP uptake and that the uptake of siRNA functionalised AuNPs was cell-type specific. Both of these findings were unexpected and as yet remain unexplained.

Considering the fact that the blood supply in the human body supplies over 200 different cell types, more needs to be known about their interactions with NPs to ensure safety. However, it is likely that most of these healthy cells and tissues will not encounter NPs since they should not be able to leave the blood circulation without the tumour associated EPR effect and the applied magnetic force at the tumour site. However, *in vivo* studies into NP biodistribution in mice have shown that while circulating NPs predominantly accumulate in the liver and spleen (Mykhaylyk *et al.*, 2001), reports have also suggested that the blood flow can take them to other organs such as the brain and heart (Jain *et al.*, 2008; Prijic and Sersa, 2011). Therefore investigations into NP interactions and toxicity within these organs and cell types should be prioritised.

It seems that the popular strategy of targeting NPs to cancer cells through the use of receptors that are overexpressed on cancer cells (e.g. the folate receptor) may not be advisable *in vivo*, since these receptor are also expressed on the surface of healthy cells, albeit to a lesser extent. This issue will have to be weighed up with consideration of how serious the effects would actually be of multifunctional NPs gaining low incident access into healthy cells.

6.8 Future work

Future work should now focus on clarifying some of the fundamental biological questions that remain unknown regarding the cellular interactions of NPs. This thesis has demonstrated the success of two different NP delivery design strategies *in vitro*, and whilst many of the observations discussed remain unexplained, they are well supported by the literature. In my opinion, the main areas to focus on are;

- clearly defining the mechanisms of NP endocytosis. This will include the identification of cell surface receptors responsible for unexplained cell uptake such as that induced by COOH, and comparison of the expression of these cell surface receptors across different cell types, to aid better prediction of cell-type specific NP uptake.

- Identifying new ways to tightly control the specificity of NP uptake into diseased cells, since perhaps overexpressed surface receptors, the EPR effect and magnetic targeting will not be enough to ensure the necessary 100% specificity of potent therapeutic NPs.

- Investigation into the long-term fate of NPs within the human body. For example, will NPs be filtered out by the kidney and excreted in the urine, or will they accumulate in certain organs such as the spleen and liver, resulting in long term toxicity problems over the course of months to years after treatment?

- Tissue-equivalent 3D cell culture models such as the collagen gels used in chapter 3 have been proven very effective for assessing the *in vivo* response to therapeutic NPs. Such 3D models are easier, quicker and less expensive than animal models and so should be utilised in future high throughput toxicity testing and assessment of NP delivery strategies.

6.9 Conclusion

There are currently many different options for designing therapeutic NP delivery vehicles. This thesis has demonstrated that NPs composed of iron or gold both performed very successfully as potential drug delivery vehicles. Therefore, results suggest that a chimeric Fe-Au core/shell NP design would utilise advantages associated with both metals, since an iron core would provide magnetic targeting and MRI imaging and a gold surface would facilitate the use of gold-sulphur bonding of thiolated molecules and thermal ablation under NIR light. Furthermore, this thesis has shown that NP-mediated RNAi is a promising method of cancer treatment, which can silence key oncogenes, such as c-myc, resulting in reduced proliferation of cancer cells. Due to the heterogeneous nature of cancer, it is envisaged that future RNAi treatment will be most successful if therapeutic NPs are individually tailored according to the expression profile of each cancer patient. This would herald a new age of personalised medicine.

List of References

Ahmad, M.Z., Akhter, S., Jain, G.K., Rahman, M., Pathan, S.A., Ahmad, F.J. Khar, R.K. (2010). Metallic nanoparticles: Technology overview & drug delivery applications in oncology. *Expert Opinion on Drug Delivery*, 7, 927-942.

Akhtar, S., Basu, S., Wickstrom, E. Juliano, R.L. (1991). Interactions of antisense DNA oligonucleotide analogs with phospholipid-membranes (liposomes). *Nucleic Acids Research*, 19, 5551-5559.

Alexiou, C., Jurgons, R., Schmid, R., Hilpert, A., Bergemann, C., Parak, F. Iro, H. (2005). In vitro and in vivo investigations of targeted chemotherapy with magnetic nanoparticles. *Journal of Magnetism and Magnetic Materials*, 293, 389-393.

Alonso, J.L. Goldmann, W.H. (2003). Feeling the forces: Atomic force microscopy in cell biology. *Life Sciences*, 72, 2553-2560.

Ameres, S.L., Martinez, J. Schroeder, R. (2007). Molecular basis for target rna recognition and cleavage by human risc. *Cell*, 130, 101-112.

Ang, D., Nguyen, Q.V., Kayal, S., Preiser, P.R., Rawat, R.S. Ramanujan, R.V. (2011a). Insights into the mechanism of magnetic particle assisted gene delivery. *Acta Biomaterialia*, 7, 1319-1326.

Ang, D., Tay, C.Y., Tan, L.P., Preiser, P.R. Ramanujan, R.V. (2011b). In vitro studies of magnetically enhanced transfection in cos-7 cells. *Materials Science & Engineering C-Materials for Biological Applications*, 31, 1445-1457.

Arap, W., Pasqualini, R. Ruoslahti, E. (1998). Cancer treatment by targeted drug delivery to tumor vasculature in a mouse model. *Science*, 279, 377-380.

Aulmann, S., Adler, N., Rom, J., Helmchen, B., Schirmacher, P. Sinn, H.P. (2006). C-myc amplifications in primary breast carcinomas and their local recurrences. *Journal of Clinical Pathology*, 59, 424-428.

Bach, L.G., Islam, M.R., Kim, J.H., Kim, H.G. Lim, K.T. (2012). Synthesis and characterization of poly(2-hydroxyethyl methacrylate)-functionalized fe-au/core-shell nanoparticles. *Journal of Applied Polymer Science*, 124, 4755-4764.

Balis, F.M. (2002). Evolution of anticancer drug discovery and the role of cell-based screening. *Journal of the National Cancer Institute*, 94, 78-79.

Barry, S.E. (2008). Challenges in the development of magnetic particles for therapeutic applications. *International Journal of Hyperthermia*, 24, 451-466.

Bell, E., Ivarsson, B. Merrill, C. (1979). Production of a tissue-like structure by contraction of collagen lattices by human-fibroblasts of different proliferative potential invitro. *Proceedings of the National Academy of Sciences of the United States of America*, 76, 1274-1278.

Bernstein, E., Caudy, A.A., Hammond, S.M. Hannon, G.J. (2001). Role for a bidentate ribonuclease in the initiation step of rna interference. *Nature*, 409, 363-366.

Beroukhim, R., Mermel, C.H., Porter, D., Wei, G., Raychaudhuri, S., Donovan, J., Barretina, J., Boehm, J.S., Dobson, J., Urashima, M., Mc Henry, K.T., Pinchback, R.M., Ligon, A.H., Cho, Y.-J., Haery, L., Greulich, H., Reich, M., Winckler, W., Lawrence, M.S., Weir, B.A., Tanaka, K.E., Chiang, D.Y., Bass, A.J., Loo, A., Hoffman, C., Prensner, J., Liefeld, T., Gao, Q., Yecies, D., Signoretti, S., Maher, E., Kaye, F.J., Sasaki, H., Tepper, J.E., Fletcher, J.A., Tabernero, J., Baselga, J., Tsao, M.-S., Demichelis, F., Rubin, M.A., Janne, P.A., Daly, M.J., Nucera, C., Levine, R.L., Ebert, B.L., Gabriel, S., Rustgi, A.K., Antonescu, C.R., Ladanyi, M., Letai, A., Garraway, L.A., Loda, M., Beer, D.G., True, L.D., Okamoto, A., Pomeroy, S.L., Singer, S., Golub, T.R., Lander, E.S., Getz, G., Sellers, W.R. Meyerson, M. (2010a). The landscape of somatic copy-number alteration across human cancers. *Nature*, 463, 899-905.

Beroukhim, R., Mermel, C.H., Porter, D., Wei, G., Raychaudhuri, S., Donovan, J., Barretina, J., Boehm, J.S., Dobson, J., Urashima, M., Mc Henry, K.T., Pinchback, R.M., Ligon, A.H., Cho, Y.J., Haery, L., Greulich, H., Reich, M., Winckler, W., Lawrence, M.S., Weir, B.A., Tanaka, K.E., Chiang, D.Y., Bass, A.J., Loo, A., Hoffman, C., Prensner, J., Liefeld, T., Gao, Q., Yecies, D., Signoretti, S., Maher, E., Kaye, F.J., Sasaki, H., Tepper, J.E., Fletcher, J.A., Tabernero, J., Baselga, J., Tsao, M.S., Demichelis, F., Rubin, M.A., Janne, P.A., Daly, M.J., Nucera, C., Levine, R.L., Ebert, B.L., Gabriel, S., Rustgi, A.K., Antonescu, C.R., Ladanyi, M., Letai, A., Garraway, L.A., Loda, M., Beer, D.G., True, L.D., Okamoto, A., Pomeroy, S.L., Singer, S., Golub, T.R., Lander, E.S., Getz, G., Sellers, W.R. Meyerson, M. (2010b). The landscape of somatic copy-number alteration across human cancers. *Nature*, 463, 899-905.

Berry, C.C. (2008). Intracellular delivery of nanopartides via the hiv-1 tat pepticle. *Nanomedicine*, 3, 357-365.

Berry, C.C., Cacou, C., Lee, D.A., Bader, D.L. Shelton, J.C. (2003). Dermal fibroblasts respond to mechanical conditioning in a strain profile dependent manner. *Biorheology*, 40, 337-345.

Berry, C.C., Charles, S., Wells, S., Dalby, M.J. Curtis, A.S.G. (2004a). The influence of transferrin stabilised magnetic nanoparticles on human dermal fibroblasts in culture. *International Journal of Pharmaceutics*, 269, 211-225.

Berry, C.C. Curtis, A.S.G. (2003). Functionalisation of magnetic nanoparticles for applications in biomedicine. *Journal of Physics D-Applied Physics*, 36, R198-R206.

Berry, C.C., Harianawalw, H., Loebus, J., Oreffo, R.O.C. De La Fuente, J. (2009a). Enhancement of human bone marrow cell uptake of quantum dots using tat peptide. *Current Nanoscience*, 5, 390-395.

Berry, C.C., Shelton, J.C. Lee, D.A. (2009b). Cell-generated forces influence the viability, metabolism and mechanical properties of fibroblast-seeded collagen get constructs. *Journal of Tissue Engineering and Regenerative Medicine*, 3, 43-53.

Berry, C.C., Wells, S., Charles, S., Aitchison, G. Curtis, A.S.G. (2004b). Cell response to dextran-derivatised iron oxide nanoparticles post internalisation. *Biomaterials*, 25, 5405-5413.

Borg, A., Baldetorp, B., Ferno, M., Olsson, H. Sigurdsson, H. (1992). C-myc amplification is an independent prognostic factor in postmenopausal breast-cancer. *International Journal of Cancer*, 51, 687-691.

Bosselmann, S. Williams, R.O. Has nanotechnology led to improved therapeutic outcomes? *Drug Development and Industrial Pharmacy*, 38, 158-170.

Bourhis, J., Le, M.G., Barrois, M., Gerbaulet, A., Jeannel, D., Duvillard, P., Ledoussal, V., Chassagne, D. Riou, G. (1990). Prognostic value of c-myc protooncogene overexpression in early invasive-carcinoma of the cervix. *Journal of Clinical Oncology*, 8, 1789-1796.

Braun, G.B., Pallaoro, A., Wu, G.H., Missirlis, D., Zasadzinski, J.A., Tirrell, M. Reich, N.O. (2009). Laser-activated gene silencing via gold nanoshell-sirna conjugates. *Acs Nano*, 3, 2007-2015.

Brust, M., Walker, M., Bethell, D., Schiffrin, D.J. Whyman, R. (1994). Synthesis of thiol-derivatized gold nanoparticles in a 2-phase liquid-liquid system. *Journal of the Chemical Society-Chemical Communications*, 801-802.

Buerli, T., Pellegrino, C., Baer, K., Lardi-Studler, B., Chudotvorova, I., Fritschy, J.-M., Medina, I. Fuhrer, C. (2007). Efficient transfection of DNA or shrna vectors into neurons using magnetofection. *Nature Protocols*, 2, 3090-3101.

Bumcrot, D., Manoharan, M., Koteliansky, V. Sah, D.W.Y. (2006). Rnai therapeutics: A potential new class of pharmaceutical drugs. *Nature Chemical Biology*, 2, 711-719.

Cao, Y.W., Jin, R. Mirkin, C.A. (2001). DNA-modified core-shell ag/au nanoparticles. *Journal of the American Chemical Society*, 123, 7961-7962.

Castanotto, D. Rossi, J.J. (2009). The promises and pitfalls of rna-interference-based therapeutics. *Nature*, 457, 426-433.

Chandler, J., Robinson, N. Whiting, K. (2001). Handling false signals in gold-based tests. *IVD Technology*, 7, 34-45.

Chang, R.S., Suh, M.S., Kim, S., Shim, G., Lee, S., Han, S.S., Lee, K.E., Jeon, H., Choi, H.-G., Choi, Y., Kim, C.-W. Oh, Y.-K. (2011). Cationic drug-derived nanoparticles for multifunctional delivery of anticancer sirna. *Biomaterials*, 32, 9785-9795.

Chen Pc, M.S., Oyelere Ak, (2008). Gold nanoparticles: From nanomedicine to nanosensing. *Nanotechnology, Science and Applications*, 1, 45-66.

Chithrani, B.D., Stewart, J., Allen, C. Jaffray, D.A. (2009). Intracellular uptake, transport, and processing of nanostructures in cancer cells. *Nanomedicine-Nanotechnology Biology and Medicine*, 5, 118-127.

Cho, W.S., Cho, M.J., Jeong, J., Choi, M., Cho, H.Y., Han, B.S., Kim, S.H., Kim, H.O., Lim, Y.T. Chung, B.H. (2009). Acute toxicity and pharmacokinetics of 13 nm-sized peg-coated gold nanoparticles. *Toxicology and Applied Pharmacology*, 236, 16-24.

Christian, S., Pilch, J., Akerman, M.E., Porkka, K., Laakkonen, P. Ruoslahti, E. (2003). Nucleolin expressed at the cell surface is a marker of endothelial cells in angiogenic blood vessels. *Journal of Cell Biology*, 163, 871-878.

Clift, M.J.D., Rothen-Rutishauser, B., Brown, D.M., Duffin, R., Donaldson, K., Proudfoot, L., Guy, K. Stone, V. (2008). The impact of different nanoparticle surface chemistry and size on uptake and toxicity in a murine macrophage cell line. *Toxicology and Applied Pharmacology*, 232, 418-427.

Connor, E.E., Mwamuka, J., Gole, A., Murphy, C.J. Wyatt, M.D. (2005). Gold nanoparticles are taken up by human cells but do not cause acute cytotoxicity. *Small*, 1, 325-327.

Corchero, J.L. Villaverde, A. (2009). Biomedical applications of distally controlled magnetic nanoparticles. *Trends Biotechnol*, 27, 468-76.

Cozzoli, P.D., Pellegrino, T. Manna, L. (2006). Synthesis, properties and perspectives of hybrid nanocrystal structures. *Chemical Society Reviews*, 35, 1195-1208.

Crosera, M., Bovenzi, M., Maina, G., Adami, G., Zanette, C., Florio, C. Larese, F.F. (2009). Nanoparticle dermal absorption and toxicity: A review of the literature. *International Archives of Occupational and Environmental Health*, 82, 1043-1055.

Cui, D., Tian, F., Ozkan, C.S., Wang, M. Gao, H. (2005). Effect of single wall carbon nanotubes on human hek293 cells. *Toxicology Letters*, 155, 73-85.

Dallafavera, R., Bregni, M., Erikson, J., Patterson, D., Gallo, R.C. Croce, C.M. (1982). Human c-myc onc gene is located on the region of chromosome-8 that is translocated in burkitt-lymphoma cells. *Proceedings of the National Academy of Sciences of the United States of America-Biological Sciences*, 79, 7824-7827.

Dang, C.V. (2012). Myc on the path to cancer. *Cell*, 149, 22-35.

Daniel, M.C. Astruc, D. (2004). Gold nanoparticles: Assembly, supramolecular chemistry, quantum-size-related properties, and applications toward biology, catalysis, and nanotechnology. *Chemical Reviews*, 104, 293-346.

Darton, N.J., Hallmark, B., Han, X., Palit, S., Slater, N.K.H. Mackley, M.R. (2008). The in-flow capture of superparamagnetic nanoparticles for targeting therapeutics. *Nanomedicine: Nanotechnology, Biology and Medicine*, 4, 19-29.

Davis, M.E., Zuckerman, J.E., Choi, C.H.J., Seligson, D., Tolcher, A., Alabi, C.A., Yen, Y., Heidel, J.D. Ribas, A. (2010). Evidence of rnai in humans from systemically administered sirna via targeted nanoparticles. *Nature*, 464, 1067-U140.

De La Fuente, J.M., Andar, A., Gadegaard, N., Berry, C.C., Kingshott, P. Riehle, M.O. (2006a). Fluorescent aromatic platforms for cell patterning. *Langmuir*, 22, 5528-5532.

De La Fuente, J.M. Berry, C.C. (2005). Tat peptide as an efficient molecule to translocate gold nanoparticles into the cell nucleus. *Bioconjugate Chemistry*, 16, 1176-1180.

De La Fuente, J.M., Berry, C.C., Riehle, M.O. Curtis, A.S.G. (2006b). Nanoparticle targeting at cells. *Langmuir*, 22, 3286-3293.

De Nigris, F., Balestrieri, M.L. Napoli, C. (2006). Targeting c-myc, ras and igf cascade to treat cancer and vascular disorders. *Cell Cycle*, 5, 1621-1628.

Dejardin, T., De La Fuente, J., Del Pino, P., Furlani, E.P., Mullin, M., Smith, C.A. Berry, C.C. (2011). Influence of both a static magnetic field and penetratin on magnetic nanoparticle delivery into fibroblasts. *Nanomedicine*, 6, 1719-1731.

Del Pino, P., Munoz-Javier, A., Vlaskou, D., Rivera Gil, P., Plank, C. Parak, W.J. (2010). Gene silencing mediated by magnetic lipospheres tagged with small interfering rna. *Nano Letters*, 10, 3914-3921.

Deming, S.L., Nass, S.J., Dickson, R.B. Trock, B.J. (2000). C-myc amplification in breast cancer: A meta-analysis of its occurrence and prognostic relevance. *British Journal of Cancer*, 83, 1688-1695.

Derfus, A.M., Chen, A.A., Min, D.H., Ruoslahti, E. Bhatia, S.N. (2007). Targeted quantum dot conjugates for sirna delivery. *Bioconjugate Chemistry*, 18, 1391-1396.

Derossi, D., Joliot, A.H., Chassaing, G. Prochiantz, A. (1994). The 3rd helix of the antennapedia homeodomain translocates through biological-membranes. *Journal of Biological Chemistry*, 269, 10444-10450.

Deshayes, S., Morris, M.C., Divita, G. Heitz, F. (2005). Cell-penetrating peptides: Tools for intracellular delivery of therapeutics. *Cellular and Molecular Life Sciences*, 62, 1839-1849.

Dexter, D.L., Kowalski, H.M., Blazar, B.A., Fligiel, Z., Vogel, R. Heppner, G.H. (1978). Heterogeneity of tumor-cells from a single mouse mammary-tumor. *Cancer Research*, 38, 3174-3181.

Di Lullo, G.A., Sweeney, S.M., Korkko, J., Ala-Kokko, L. San Antonio, J.D. (2002). Mapping the ligand-binding sites and disease-associated mutations on the most abundant protein in the human, type i collagen. *Journal of Biological Chemistry*, 277, 4223-4231.

Discher, D.E., Mooney, D.J. Zandstra, P.W. (2009). Growth factors, matrices, and forces combine and control stem cells. *Science*, 324, 1673-1677.

Dobson, J. (2006a). Gene therapy progress and prospects: Magnetic nanoparticle-based gene delivery. *Gene Therapy*, 13, 283-287.

Dobson, J. (2006b). Magnetic nanoparticles for drug delivery. *Drug Development Research*, 67, 55-60.

Duesberg, P.H. Vogt, P.K. (1979). Avian acute-leukemia viruses mc29 and mh2 share specific rna sequences - evidence for a 2nd class of transforming genes. *Proceedings of the National Academy of Sciences of the United States of America*, 76, 1633-1637.

Dykxhoorn, D.M. Lieberman, J. (2005). The silent revolution: Rna interference as basic biology, research tool, and therapeutic. *Annual Review of Medicine*, 56, 401-423.

Eastwood, M., Mudera, V.C., Mcgrouther, D.A. Brown, R.A. (1998). Effect of precise mechanical loading on fibroblast populated collagen lattices: Morphological changes. *Cell Motility and the Cytoskeleton*, 40, 13-21.

Elbashir, S.M., Harborth, J., Lendeckel, W., Yalcin, A., Weber, K. Tuschl, T. (2001). Duplexes of 21-nucleotide rnas mediate rna interference in cultured mammalian cells. *Nature*, 411, 494-498.

Fang, J., Qin, H.B., Nakamura, H., Tsukigawa, K., Shin, T. Maeda, H. (2012). Carbon monoxide, generated by heme oxygenase-1, mediates the enhanced permeability and retention effect in solid tumors. *Cancer Science*, 103, 535-541.

Faraday, M. (1857). Experimental relations of gold (and other metals) to light. *Phil Trans R Soc London*, 14, 145-181
.

Ferlay, J., Shin, H.-R., Bray, F., Forman, D., Mathers, C. Parkin, D.M. (2010). Estimates of worldwide burden of cancer in 2008: Globocan 2008. *International Journal of Cancer*, 127, 2893-2917.

Fire, A., Xu, S.Q., Montgomery, M.K., Kostas, S.A., Driver, S.E. Mello, C.C. (1998). Potent and specific genetic interference by double-stranded rna in caenorhabditis elegans. *Nature*, 391, 806-811.

Fischer, H.C. Chan, W.C.W. (2007). Nanotoxicity: The growing need for in vivo study. *Current Opinion in Biotechnology*, 18, 565-571.

Furlani, E.P and Xue X. (2012). A model for predicting field-directed particle transport in the magnetofection process. *Pharmaceutical Research*, 29, 1366-1379.

Gao, S., Dagnaes-Hansen, F., Nielsen, E.J.B., Wengel, J., Besenbacher, F., Howard, K.A. Kjems, J. (2009). The effect of chemical modification and nanoparticle formulation on stability and biodistribution of sirna in mice. *Molecular Therapy*, 17, 1225-1233.

Gary, D.J., Puri, N. Won, Y.-Y. (2007). Polymer-based sirna delivery: Perspectives on the fundamental and phenomenological distinctions from polymer-based DNA delivery. *Journal of Controlled Release*, 121, 64-73.

Gersting, S.W., Schillinger, U., Lausier, J., Nicklaus, P., Rudolph, C., Plank, C., Reinhardt, D. Rosenecker, J. (2004). Gene delivery to respiratory epithelial cells by magnetofection. *Journal of Gene Medicine*, 6, 913-922.

Ghosh, P.S., Kim, C.-K., Han, G., Forbes, N.S. Rotello, V.M. (2008). Efficient gene delivery vectors by tuning the surface charge density of amino acid-functionalized gold nanoparticles. *Acs Nano*, 2, 2213-2218.

Giljohann, D.A., Seferos, D.S., Prigodich, A.E., Patel, P.C. Mirkin, C.A. (2009). Gene regulation with polyvalent sirna-nanoparticle conjugates. *Journal of the American Chemical Society*, 131, 2072-+.

Gilman, A. Philips, F.S. (1946). The biological actions and therapeutic applications of the b-chloroethyl amines and sulfides. *Science*, 103, 409-&.

Gondi, C.S. Rao, J.S. (2009). Concepts in in vivo sirna delivery for cancer therapy. *Journal of Cellular Physiology*, 220, 285-291.

Goodman, C.M., Mccusker, C.D., Yilmaz, T. Rotello, V.M. (2004). Toxicity of gold nanoparticles functionalized with cationic and anionic side chains. *Bioconjugate Chemistry*, 15, 897-900.

Goodman, T.T., Ng, C.P. Pun, S.H. (2008). 3-d tissue culture systems for the evaluation and optimization of nanoparticle-based drug carriers. *Bioconjugate Chemistry*, 19, 1951-1959.

Goodman, T.T., Olive, P.L. Pun, S.H. (2007). Increased nanoparticle penetration in collagenase-treated multicellullar spheroids. *International Journal of Nanomedicine*, 2, 265-274.

Grinnell, F. (2003). Fibroblast biology in three-dimensional collagen matrices. *Trends in Cell Biology*, 13, 264-269.

Grinnell, F., Ho, C.H., Lin, Y.C. Skuta, G. (1999a). Differences in the regulation of fibroblast contraction of floating versus stressed collagen matrices. *Journal of Biological Chemistry*, 274, 918-923.

Grinnell, F., Ho, C.H., Tamariz, E., Lee, D.J. Skuta, G. (2003). Dendritic fibroblasts in three-dimensional collagen matrices. *Molecular Biology of the Cell*, 14, 384-395.

Grinnell, F., Zhu, M.F., Carlson, M.A. Abrams, J.M. (1999b). Release of mechanical tension triggers apoptosis of human fibroblasts in a model of regressing granulation tissue. *Experimental Cell Research*, 248, 608-619.

Grothey, A. (2006). Future directions in vascular endothelial growth factor-targeted therapy for metastatic colorectal cancer. *Seminars in Oncology*, 33, S41-S49.

Guo, S., Huang, Y., Jiang, Q., Sun, Y., Deng, L., Liang, Z., Du, Q., Xing, J., Zhao, Y., Wang, P.C., Dong, A. Liang, X.-J. Enhanced gene delivery and sirna silencing by gold nanoparticles coated with charge-reversal polyelectrolyte. *Acs Nano*, 4, 5505-5511.

Hadjipanayi, E., Mudera, V. Brown, R.A. (2009). Close dependence of fibroblast proliferation on collagen scaffold matrix stiffness. *Journal of Tissue Engineering and Regenerative Medicine*, 3, 77-84.

Hajdu, S.I. (2011). A note from history: Landmarks in history of cancer, part 1. *Cancer*, 117, 1097-102.

Halaby, M.J. Yang, D.Q. (2007). P53 translational control: A new facet of p53 regulation and its implication for tumorigenesis and cancer therapeutics. *Gene*, 395, 1-7.

Halder, J., Kamat, A.A., Landen, C.N., Han, L.Y., Lutgendorf, S.K., Lin, Y.G., Merritt, W.M., Jennings, N.B., Chavez-Reyes, A., Coleman, R.L., Gershenson, D.M., Schmandt, R., Cole, S.W., Lopez-Berestein, G. Sood, A.K. (2006). Focal adhesion kinase targeting using in vivo short interfering rna delivery in neutral liposomes for ovarian carcinoma therapy. *Clinical Cancer Research*, 12, 4916-4924.

Hamilton, A.J. Baulcombe, D.C. (1999). A species of small antisense rna in posttranscriptional gene silencing in plants. *Science*, 286, 950-952.

Hanahan, D. Weinberg, R.A. (2000). The hallmarks of cancer. *Cell*, 100, 57-70.

Hanahan, D. Weinberg, R.A. (2011). Hallmarks of cancer: The next generation. *Cell*, 144, 646-674.

Harush-Frenkel, O., Debotton, N., Benita, S. Altschuler, Y. (2007). Targeting of nanoparticles to the clathrin-mediated endocytic pathway. *Biochemical and Biophysical Research Communications*, 353, 26-32.

Helson, L., Green, S., Carswell, E. Old, L.J. (1975). Effect of tumor necrosis factor on cultured human melanoma cells. *Nature*, 258, 731-732.

Hirsch, L.R., Stafford, R.J., Bankson, J.A., Sershen, S.R., Rivera, B., Price, R.E., Hazle, J.D., Halas, N.J. West, J.L. (2003). Nanoshell-mediated near-

infrared thermal therapy of tumors under magnetic resonance guidance. *Proceedings of the National Academy of Sciences of the United States of America*, 100, 13549-13554.

Hoshino, A., Manabe, N., Fujioka, K., Suzuki, K., Yasuhara, M. Yamamoto, K. (2007). Use of fluorescent quantum dot bioconjugates for cellular imaging of immune cells, cell organelle labeling, and nanomedicine: Surface modification regulates biological function, including cytotoxicity. *Journal of Artificial Organs*, 10, 149-157.

Howard, K.A. (2009). Delivery of rna interference therapeutics using polycation-based nanoparticles. *Advanced Drug Delivery Reviews*, 61, 710-720.

Howard, M.D., Jay, M., Dziublal, T.D. Lu, X.L. (2008). Pegylation of nanocarrier drug delivery systems: State of the art. *Journal of Biomedical Nanotechnology*, 4, 133-148.

Hu, S.S., Lai, M.M. Vogt, P.K. (1979). Genome of avian myelocytomatosis virus mc29: Analysis by heteroduplex mapping. *Proceedings of the National Academy of Sciences*, 76, 1265-1268.

Huang, C., Li, M., Chen, C.Y. Yao, Q.Z. (2008). Small interfering rna therapy in cancer: Mechanism, potential targets, and clinical applications. *Expert Opinion on Therapeutic Targets*, 12, 637-645.

Huang, W., Lv, M. Gao, Z.G. (2011). Synthesis of polyethylenimine grafted with copolymers of polyethylene glycol and polycaprolactone and its potential for sirna delivery. *Chinese Chemical Letters*, 22, 749-752.

Huang, X., Jain, P.K., El-Sayed, I.H. El-Sayed, M.A. (2007). Gold nanoparticles: Interesting optical properties and recent applications in cancer diagnostics and therapy. *Nanomedicine*, 2, 681-693.

Iwase, H., Shimada, M., Tsuzuki, T., Okeya, M., Kobayashi, K., Hibino, Y., Watanabe, H. Goto, H. (2006). A phase i study of s-1 administration and a 24-h infusion of cisplatin plus paclitaxel in patients with advanced gastric cancer. *Anticancer Research*, 26, 1605-1609.

Jain, M., Arvanitis, C., Chu, K., Dewey, W., Leonhardt, E., Trinh, M., Sundberg, C.D., Bishop, J.M. Felsher, D.W. (2002). Sustained loss of a neoplastic phenotype by brief inactivation of myc. *Science*, 297, 102-104.

Jain, T.K., Reddy, M.K., Morales, M.A., Leslie-Pelecky, D.L. Labhasetwar, V. (2008). Biodistribution, clearance, and biocompatibility of iron oxide magnetic nanoparticles in rats. *Molecular Pharmaceutics*, 5, 316-327.

Jarver, P. Langel, U. (2006). Cell-penetrating peptides - a brief introduction. *Biochimica Et Biophysica Acta-Biomembranes*, 1758, 260-263.

Ji, H., Wu, G., Zhan, X., Nolan, A., Koh, C., De Marzo, A., Hoang Mai, D., Fan, J., Cheadle, C., Fallahi, M., Cleveland, J.L., Dang, C.V. Zeller, K.I. (2011).

Cell-type independent myc target genes reveal a primordial signature involved in biomass accumulation. *Plos One*, 6.

Jiang, X., Musyanovych, A., Roecker, C., Landfester, K., Mailaender, V. Nienhaus, G.U. (2011). Specific effects of surface carboxyl groups on anionic polystyrene particles in their interactions with mesenchymal stem cells. *Nanoscale*, 3, 2028-2035.

Josephson, L., Tung, C.H., Moore, A. Weissleder, R. (1999). High-efficiency intracellular magnetic labeling with novel superparamagnetic-tat peptide conjugates. *Bioconjugate Chemistry*, 10, 186-191.

Juliano, R., Alam, M.R., Dixit, V. Kang, H. (2008). Mechanisms and strategies for effective delivery of antisense and sirna oligonucleotides. *Nucleic Acids Research*, 36, 4158-4171.

Kean, T., Roth, S. Thanou, M. (2005). Trimethylated chitosans as non-viral gene delivery vectors: Cytotoxicity and transfection efficiency. *Journal of Controlled Release*, 103, 643-653.

Kennerdell, J.R. Carthew, R.W. (1998). Use of dsrna-mediated genetic interference to demonstrate that frizzled and frizzled 2 act in the wingless pathway. *Cell*, 95, 1017-1026.

Kim, S.H., Mok, H., Jeong, J.H., Kim, S.W. Park, T.G. (2006). Comparative evaluation of target-specific gfp gene silencing efficiencies for antisense odn, synthetic sirna, and sirna plasmid complexed with pei-peg-fol conjugate. *Bioconjugate Chemistry*, 17, 241-244.

Kim, Y., Dalhaimer, P., Christian, D.A. Discher, D.E. (2005). Polymeric worm micelles as nano-carriers for drug delivery. *Nanotechnology*, 16, S484-S491.

Kirchner, C., Liedl, T., Kudera, S., Pellegrino, T., Javier, A.M., Gaub, H.E., Stolzle, S., Fertig, N. Parak, W.J. (2005). Cytotoxicity of colloidal cdse and cdse/zns nanoparticles. *Nano Letters*, 5, 331-338.

Kovtun, A., Heumann, R. Epple, M. (2009). Calcium phosphate nanoparticles for the transfection of cells. *Bio-Medical Materials and Engineering*, 19, 241-247.

Kozma, L., Kiss, I., Szakall, S. Ember, I. (1994). Investigation of c-myc oncogene amplification in colorectal-cancer. *Cancer Letters*, 81, 165-169.

Kuhn, S.J., Finch, S.K., Hallahan, D.E. Giorgio, T.D. (2006a). Proteolytic surface functionalization enhances in vitro magnetic nanoparticle mobility through extracellular matrix. *Nano Letters*, 6, 306-312.

Kuhn, S.J., Hallahan, D.E. Giorgio, T.D. (2006b). Characterization of superparamagnetic nanoparticle interactions with extracellular matrix in an in vitro system. *Annals of Biomedical Engineering*, 34, 51-58.

Kumar, A., Jena, P.K., Behera, S., Lockey, R.F., Mohapatra, S. Mohapatra, S. (2010). Multifunctional magnetic nanoparticles for targeted delivery. *Nanomedicine-Nanotechnology Biology and Medicine*, 6, 64-69.

Kurreck, J. (2009). Rna interference: From basic research to therapeutic applications. *Angewandte Chemie-International Edition*, 48, 1378-1398.

Lamkowsky, M.-C., Geppert, M., Schmidt, M.M. Dringen, R. (2012). Magnetic field-induced acceleration of the accumulation of magnetic iron oxide nanoparticles by cultured brain astrocytes. *Journal of Biomedical Materials Research Part A*, 100A, 323-334.

Leamon, C.P. Low, P.S. (1991). Delivery of macromolecules into living cells - a method that exploits folate receptor endocytosis. *Proceedings of the National Academy of Sciences of the United States of America*, 88, 5572-5576.

Lee, C.C., Mackay, J.A., Frechet, J.M.J. Szoka, F.C. (2005). Designing dendrimers for biological applications. *Nature Biotechnology*, 23, 1517-1526.

Lee, J.-S., Green, J.J., Love, K.T., Sunshine, J., Langer, R. Anderson, D.G. (2009a). Gold, poly(beta-amino ester) nanoparticles for small interfering rna delivery. *Nano Letters*, 9, 2402-2406.

Lee, J.H., Lee, K., Moon, S.H., Lee, Y., Park, T.G. Cheon, J. (2009b). All-in-one target-cell-specific magnetic nanoparticles for simultaneous molecular imaging and sirna delivery. *Angewandte Chemie-International Edition*, 48, 4174-4179.

Lee, J.S., Green, J.J., Love, K.T., Sunshine, J., Langer, R. Anderson, D.G. (2009c). Gold, poly(beta-amino ester) nanoparticles for small interfering rna delivery. *Nano Letters*, 9, 2402-2406.

Lee, P.C. Meisel, D. (1982). Adsorption and surface-enhanced raman of dyes on silver and gold sols. *Journal of Physical Chemistry*, 86, 3391-3395.

Li, L., Liu, J., Diao, Z., Shu, D., Guo, P. Shen, G. (2009). Evaluation of specific delivery of chimeric phi29 prna/sirna nanoparticles to multiple tumor cells. *Molecular Biosystems*, 5, 1361-1368.

Li, S.D., Chono, S. Huang, L. (2008). Efficient oncogene silencing and metastasis inhibition via systemic delivery of sirna. *Molecular Therapy*, 16, 942-946.

Li, Z.R., Van Calcar, S., Qu, C.X., Cavenee, W.K., Zhang, M.Q. Ren, B. (2003). A global transcriptional regulatory role for c-myc in burkitt's lymphoma cells. *Proceedings of the National Academy of Sciences of the United States of America*, 100, 8164-8169.

Liao, D.J. Dickson, R.B. (2000). C-myc in breast cancer. *Endocrine-Related Cancer*, 7, 143-164.

Lommatzsch, S.T. Aris, R. (2009). Genetics of cystic fibrosis. *Seminars in Respiratory and Critical Care Medicine*, 30, 531-538.

Love, J.C., Estroff, L.A., Kriebel, J.K., Nuzzo, R.G. Whitesides, G.M. (2005). Self-assembled monolayers of thiolates on metals as a form of nanotechnology. *Chemical Reviews*, 105, 1103-1169.

Lovric, J., Cho, S.J., Winnik, F.M. Maysinger, D. (2005). Unmodified cadmium telluride quantum dots induce reactive oxygen species formation leading to multiple organelle damage and cell death. *Chemistry & Biology*, 12, 1227-1234.

Lu, A.H., Salabas, E.L. Schuth, F. (2007). Magnetic nanoparticles: Synthesis, protection, functionalization, and application. *Angewandte Chemie-International Edition*, 46, 1222-1244.

Luescher, B. Vervoorts, J. (2012). Regulation of gene transcription by the oncoprotein myc. *Gene*, 494, 145-160.

Lunov, O., Syrovets, T., Loos, C., Beil, J., Delecher, M., Tron, K., Nienhaus, G.U., Musyanovych, A., Mailaender, V., Landfester, K. Simmet, T. (2011). Differential uptake of functionalized polystyrene nanoparticles by human macrophages and a monocytic cell line. *Acs Nano*, 5, 1657-1669.

Lytton-Jean, A.K.R., Langer, R. Anderson, D.G. (2011). Five years of sirna delivery: Spotlight on gold nanoparticles. *Small*, 7, 1932-1937.

Maeda, H., Fang, J., Inutsuka, T. Kitamoto, Y. (2003). Vascular permeability enhancement in solid tumor: Various factors, mechanisms involved and its implications. *International Immunopharmacology*, 3, 319-328.

Mah, C., Zolotukhin, I., Fraites, T.J., Dobson, J., Batich, C. Byrne, B.J. (2000). Microsphere-mediated delivery of recombinant aav vectors in vitro and in vivo. *Molecular Therapy*.

Manche, L., Green, S.R., Schmedt, C. Mathews, M.B. (1992). Interactions between double-stranded-rna regulators and the protein-kinase dai. *Molecular and Cellular Biology*, 12, 5238-5248.

Maniti, O., Blanchard, E., Trugnan, G., Lamaziere, A. Ayala-Sanmartin, J. (2012). Metabolic energy-independent mechanism of internalization for the cell penetrating peptide penetratin. *The international journal of biochemistry & cell biology*, 44, 869-75.

Marenzana, M., Pickard, D., Macrobert, A.J. Brown, R.A. (2002). Optical measurement of three-dimensional collagen gel constructs by elastic scattering spectroscopy. *Tissue Engineering*, 8, 409-418.

Matranga, C., Tomari, Y., Shin, C., Bartel, D.P. Zamore, P.D. (2005). Passenger-strand cleavage facilitates assembly of sirna into ago2-containing rnai enzyme complexes. *Cell*, 123, 607-620.

Matsumura, Y. Maeda, H. (1986). A new concept for macromolecular therapeutics in cancer-chemotherapy - mechanism of tumoritropic accumulation of proteins and the antitumor agent smancs. *Cancer Research*, 46, 6387-6392.

Mcnamara, J.O., Andrechek, E.R., Wang, Y., D Viles, K., Rempel, R.E., Gilboa, E., Sullenger, B.A. Giangrande, P.H. (2006). Cell type-specific delivery of sirnas with aptamer-sirna chimeras. *Nature Biotechnology*, 24, 1005-1015.

Meade, B.R. Dowdy, S.F. (2008). Enhancing the cellular uptake of sirna duplexes following noncovalent packaging with protein transduction domain peptides. *Advanced Drug Delivery Reviews*, 60, 530-536.

Medarova, Z., Pham, W., Farrar, C., Petkova, V. Moore, A. (2007). In vivo imaging of sirna delivery and silencing in tumors. *Nature Medicine*, 13, 372-377.

Medintz, I.L., Uyeda, H.T., Goldman, E.R. Mattoussi, H. (2005). Quantum dot bioconjugates for imaging, labelling and sensing. *Nature Materials*, 4, 435-446.

Meister, A. Anderson, M.E. (1983). Glutathione. *Annual Review of Biochemistry*, 52, 711-760.

Mertsching, H., Weimer, M., Kersen, S. Brunner, H. (2008). Human skin equivalent as an alternative to animal testing. *GMS Krankenhaushygiene interdisziplinar*, 3, Doc11.

Miller, G. (2006). Nanomaterials, sunscreens and cosmetics: Small ingredients, big riskd. *Friends of the Earth Australia Nanotechnology Project*.

Mirkin, C.A., Letsinger, R.L., Mucic, R.C. Storhoff, J.J. (1996). A DNA-based method for rationally assembling nanoparticles into macroscopic materials. *Nature*, 382, 607-609.

Moon, J.H., Mendez, E., Kim, Y. Kaur, A. Conjugated polymer nanoparticles for small interfering rna delivery. *Chemical Communications*, 47, 8370-8372.

Mukerjee, A., Shankardas, J., Ranjan, A.P. Vishwanatha, J.K. Efficient nanoparticle mediated sustained rna interference in human primary endothelial cells. *Nanotechnology*, 22, 10.

Murphy, C.G. Fornier, M. (2010). Her2-positive breast cancer: Beyond trastuzumab. *Oncology-New York*, 24, 410-415.

Mykhaylyk, O., Antequera, Y.S., Vlaskou, D. Plank, C. (2007). Generation of magnetic nonviral gene transfer agents and magnetofection in vitro. *Nature Protocols*, 2, 2391-2411.

Mykhaylyk, O., Cherchenko, A., Ilkin, A., Dudchenko, N., Ruditsa, V., Novoseletz, M. Zozulya, Y. (2001). Glial brain tumor targeting of magnetite

nanoparticles in rats. *Journal of Magnetism and Magnetic Materials*, 225, 241-247.

Mykhaylyk, O., Zelphati, O., Rosenecker, J. Plank, C. (2008). Sirna delivery by magnetofection. *Current Opinion in Molecular Therapeutics*, 10, 493-505.

Napoli, C., Lemieux, C. Jorgensen, R. (1990). Introduction of a chimeric chalcone synthase gene into petunia results in reversible co-suppression of homologous genes in trans. *Plant Cell*, 2, 279-289.

Nativo, P., Prior, I.A. Brust, M. (2008). Uptake and intracellular fate of surface-modified gold nanoparticles. *Acs Nano*, 2, 1639-1644.

Nederman, T. Twentyman, P. (1984). Spheroids for studies of drug effects. *Recent Results in Cancer Research*, 95, 84-102.

Niu, X.Y., Peng, Z.L., Duan, W.Q., Wang, H. Wang, P. (2006). Inhibition of hpv 16 e6 oncogene expression by rna interference in vitro and in vivo. *International Journal of Gynecological Cancer*, 16, 743-751.

Oberdorster, G., Oberdorster, E. Oberdorster, J. (2005). Nanotoxicology: An emerging discipline evolving from studies of ultrafine particles. *Environmental Health Perspectives*, 113, 823-839.

Odom, G.L., Banks, G.B., Schultz, B.R., Gregorevic, P. Chamberlain, J.S. (2010). Preclinical studies for gene therapy of duchenne muscular dystrophy. *Journal of Child Neurology*, 25, 1149-1157.

Ohrt, T., Merkle, D., Birkenfeld, K., Echeverri, C.J. Schwille, P. (2006). In situ fluorescence analysis demonstrates active sirna exclusion from the nucleus by exportin 5. *Nucleic Acids Research*, 34, 1369-1380.

Oishi, M., Nakaogami, J., Ishii, T. Nagasaki, Y. (2006). Smart pegylated gold nanoparticles for the cytoplasmic delivery of sirna to induce enhanced gene silencing. *Chemistry Letters*, 35, 1046-1047.

Ornelas-Megiatto, C., Wich, P.R. Frechet, J.M.J. (2012). Polyphosphonium polymers for sirna delivery: An efficient and nontoxic alternative to polyammonium carriers. *Journal of the American Chemical Society*, 134, 1902-1905.

Paciotti, G.F., Kingston, D.G.I. Tamarkin, L. (2006). Colloidal gold nanoparticles: A novel nanoparticle platform for developing multifunctional tumor-targeted drug delivery vectors. *Drug Development Research*, 67, 47-54.

Pan, Y., Neuss, S., Leifert, A., Fischler, M., Wen, F., Simon, U., Schmid, G., Brandau, W. Jahnen-Dechent, W. (2007). Size-dependent cytotoxicity of gold nanoparticles. *Small*, 3, 1941-1949.

Pankhurst, Q.A., Connolly, J., Jones, S.K. Dobson, J. (2003). Applications of magnetic nanoparticles in biomedicine. *Journal of Physics D-Applied Physics*, 36, R167-R181.

Park, J.I., Kim, M.G., Jun, Y.W., Lee, J.S., Lee, W.R. Cheon, J. (2004). Characterization of superpararnagnetic "Core-shell" Nanoparticles and monitoring their anisotropic phase transition to ferromagnetic "Solid solution" Nanoalloyse. *Journal of the American Chemical Society*, 126, 9072-9078.

Parveen, S. Sahoo, S.K. (2008). Polymeric nanoparticles for cancer therapy. *Journal of Drug Targeting*, 16, 108-123.

Patil, M.L., Zhang, M., Betigeri, S., Taratula, O., He, H. Minko, T. (2008). Surface-modified and internally cationic polyamidoamine dendrimers for efficient sirna delivery. *Bioconjugate Chemistry*, 19, 1396-1403.

Pawaiya, R.V.S., Krishna, L. Kumar, R. (2011). Genes responsible for cancer: A review. *Indian Journal of Animal Sciences*, 81, 783-802.

Pelengaris, S. Khan, M. (2003). The c-myc oncoprotein as a treatment target in cancer and other disorders of cell growth. *Expert Opinion on Therapeutic Targets*, 7, 623-642.

Petersen, S., Barchanski, A., Taylor, U., Klein, S., Rath, D. Barcikowski, S. (2011). Penetratin-conjugated gold nanoparticles - design of cell-penetrating nanomarkers by femtosecond laser ablation. *Journal of Physical Chemistry C*, 115, 5152-5159.

Pickard, M. Chari, D. (2010). Enhancement of magnetic nanoparticle-mediated gene transfer to astrocytes by 'magnetofection': Effects of static and oscillating fields. *Nanomedicine*, 5, 217-232.

Pissuwan, D., Niidome, T. Cortie, M.B. (2011). The forthcoming applications of gold nanoparticles in drug and gene delivery systems. *Journal of Controlled Release*, 149, 65-71.

Plank, C., Schillinger, U., Scherer, F., Bergemann, C., Remy, J.S., Krotz, F., Anton, M., Lausier, J. Rosenecker, J. (2003). The magnetofection method: Using magnetic force to enhance gene delivery. *Biological Chemistry*, 384, 737-747.

Polizu, S., Savadogo, O., Poulin, P. Yahia, L. (2006). Applications of carbon nanotubes-based biomaterials in biomedical nanotechnology. *Journal of Nanoscience and Nanotechnology*, 6, 1883-1904.

Ponzielli, R., Katz, S., Barsyte-Lovejoy, D. Penn, L.Z. (2005). Cancer therapeutics: Targeting the dark side of myc. *European Journal of Cancer*, 41, 2485-2501.

Prijic, S. Sersa, G. (2011). Magnetic nanoparticles as targeted delivery systems in oncology. *Radiology and Oncology*, 45, 1-16.

Qian, S., Zhong, X., Yu, L., Ding, B., De Haan, P. Boris-Lawrie, K. (2009). Hiv-1 tat rna silencing suppressor activity is conserved across kingdoms and counteracts translational repression of hiv-1. *Proceedings of the National Academy of Sciences of the United States of America*, 106, 605-610.

Qian, X., Peng, X.-H., Ansari, D.O., Yin-Goen, Q., Chen, G.Z., Shin, D.M., Yang, L., Young, A.N., Wang, M.D. Nie, S. (2008). In vivo tumor targeting and spectroscopic detection with surface-enhanced raman nanoparticle tags. *Nature Biotechnology*, **26**, 83-90.

Rand, T.A., Ginalski, K., Grishin, N.V. Wang, X. (2004). Biochemical identification of argonaute 2 as the sole protein required for rna-induced silencing complex activity. *Proceedings of the National Academy of Sciences of the United States of America*, **101**, 14385-14389.

Rao, G.C.S., Kumar, M.S., Mathivanan, N. Rao, M.E.B. (2004). Nanosuspensions as the most promising approach in nanoparticulate drug delivery systems. *Pharmazie*, **59**, 5-9.

Richard, J.P., Melikov, K., Vives, E., Ramos, C., Verbeure, B., Gait, M.J., Chernomordik, L.V. Lebleu, B. (2003). Cell-penetrating peptides - a reevaluation of the mechanism of cellular uptake. *Journal of Biological Chemistry*, **278**, 585-590.

Richards, D.G., Mcmillin, D.L., Mein, E.A. Nelson, C.D. (2002). Gold and its relationship to neurological/glandular conditions. *International Journal of Neuroscience*, **112**, 31-53.

Royalsociety 2004. Nanoscience and nanotechnologies: Opportunities and uncertainties. The Royal Society and The Royal Society of Engineers.

Saglio, G., Morotti, A., Mattioli, G., Messa, E., Giugliano, E., Volpe, G., Rege-Cambrin, G. Cilloni, D. 2004. Rational approaches to the design of therapeutics targeting molecular markers: The case of chronic myelogenous leukemia. *In:* BRADLOW, H. L. C. L. M. L. Z. K. (ed.) *Signal transduction and communication in cancer cells*.

Salcher, E.E. Wagner, E. (2010). Chemically programmed polymers for targeted DNA and sirna transfection. *Topics in current chemistry*, **296**, 227-49.

Santarius, T., Shipley, J., Brewer, D., Stratton, M.R. Cooper, C.S. (2010). Epigenetics and genetics a census of amplified and overexpressed human cancer genes. *Nature Reviews Cancer*, **10**, 59-64.

Sanvicens, N. Marco, M.P. (2008). Multifunctional nanoparticles - properties and prospects for their use in human medicine. *Trends in Biotechnology*, **26**, 425-433.

Sato, Y., Murase, K., Kato, J., Kobune, M., Sato, T., Kawano, Y., Takimoto, R., Takada, K., Miyanishi, K., Matsunaga, T., Takayama, T. Niitsu, Y. (2008). Resolution of liver cirrhosis using vitamin a-coupled liposomes to deliver sirna against a collagen-specific chaperone. *Nature Biotechnology*, **26**, 431-442.

Sawant, R. Torchilin, V. (2010). Intracellular transduction using cell-penetrating peptides. *Molecular Biosystems*, **6**, 628-640.

Sayes, C.M., Gobin, A.M., Ausman, K.D., Mendez, J., West, J.L. Colvin, V.L. (2005). Nano-c-60 cytotoxicity is due to lipid peroxidation. *Biomaterials*, 26, 7587-7595.

Schafer, D.A. (2002). Coupling actin dynamics and membrane dynamics during endocytosis. *Current Opinion in Cell Biology*, 14, 76-81.

Scherer, F., Anton, M., Schillinger, U., Henkel, J., Bergemann, C., Kruger, A., Gansbacher, B. Plank, C. (2002). Magnetofection: Enhancing and targeting gene delivery by magnetic force in vitro and in vivo. *Gene Therapy*, 9, 102-109.

Schiffelers, R.M., Ansari, A., Xu, J., Zhou, Q., Tang, Q.Q., Storm, G., Molema, G., Lu, P.Y., Scaria, P.V. Woodle, M.C. (2004). Cancer sirna therapy by tumor selective delivery with ligand-targeted sterically stabilized nanoparticle. *Nucleic Acids Research*, 32.

Schwarze, S.R. Dowdy, S.F. (2000). In vivo protein transduction: Intracellular delivery of biologically active proteins, compounds and DNA. *Trends in Pharmacological Sciences*, 21, 45-48.

Sheiness, D. Bishop, J.M. (1979). DNA and rna from uninfected vertebrate cells contain nucleotide-sequences related to the putative transforming gene of avian myelocytomatosis virus. *Journal of Virology*, 31, 514-521.

Shi, Y. (2003). Mammalian rnai for the masses. *Trends in Genetics*, 19, 9-12.

Singh, S.R., Grossniklaus, H.E., Kang, S.J., Edelhauser, H.F., Ambati, B.K. Kompella, U.B. (2009). Intravenous transferrin, rgd peptide and dual-targeted nanoparticles enhance anti-vegf intraceptor gene delivery to laser-induced cnv. *Gene Therapy*, 16, 645-659.

Siu, Y.S., Li, L., Leung, M.F., Lee, K.L.D. Li, P. (2012). Polyethylenimine-based amphiphilic core-shell nanoparticles: Study of gene delivery and intracellular trafficking. *Biointerphases*, 7, 16.

Smith, C.-A.M., Fuente, J.D.L., Pelaz, B., Furlani, E.P., Mullin, M. Berry, C.C. (2010). The effect of static magnetic fields and tat peptides on cellular and nuclear uptake of magnetic nanoparticles. *Biomaterials*, 31, 4392-4400.

Song, E.W., Zhu, P.C., Lee, S.K., Chowdhury, D., Kussman, S., Dykxhoorn, D.M., Feng, Y., Palliser, D., Weiner, D.B., Shankar, P., Marasco, W.A. Lieberman, J. (2005). Antibody mediated in vivo delivery of small interfering rnas via cell-surface receptors. *Nature Biotechnology*, 23, 709-717.

Song, H.P., Yang, J.Y., Lo, S.L., Wang, Y., Fan, W.M., Tang, X.S., Xue, J.M. Wang, S. (2010). Gene transfer using self-assembled ternary complexes of cationic magnetic nanoparticles, plasmid DNA and cell-penetrating tat peptide. *Biomaterials*, 31, 769-778.

Soutschek, J., Akinc, A., Bramlage, B., Charisse, K., Constien, R., Donoghue, M., Elbashir, S., Geick, A., Hadwiger, P., Harborth, J., John, M., Kesavan, V.,

Lavine, G., Pandey, R.K., Racie, T., Rajeev, K.G., Rohl, I., Toudjarska, I., Wang, G., Wuschko, S., Bumcrot, D., Koteliansky, V., Limmer, S., Manoharan, M. Vornlocher, H.P. (2004). Therapeutic silencing of an endogenous gene by systemic administration of modified sirnas. *Nature*, 432, 173-178.

Spremulli, E.N. Dexter, D.L. (1983). Human-tumor cell heterogeneity and metastasis. *Journal of Clinical Oncology*, 1, 496-509.

Su, C.-H., Sheu, H.-S., Lin, C.-Y., Huang, C.-C., Lo, Y.-W., Pu, Y.-C., Weng, J.-C., Shieh, D.-B., Chen, J.-H. Yeh, C.-S. (2007). Nanoshell magnetic resonance imaging contrast agents. *Journal of the American Chemical Society*, 129, 2139-2146.

Takeshita, F., Minakuchi, Y., Nagahara, S., Honma, K., Sasaki, H., Hirai, K., Teratani, T., Namatame, N., Yamamoto, Y., Hanai, K., Kato, T., Sano, A. Ochiya, T. (2005). Efficient delivery of small interfering rna to bone-metastatic tumors by using atelocollagen in vivo. *Proceedings of the National Academy of Sciences of the United States of America*, 102, 12177-12182.

Taub, R., Kirsch, I., Morton, C., Lenoir, G., Swan, D., Tronick, S., Aaronson, S. Leder, P. (1982). Translocation of the c-myc gene into the immunoglobulin heavy-chain locus in human burkitt-lymphoma and murine plasmacytoma cells. *Proceedings of the National Academy of Sciences of the United States of America-Biological Sciences*, 79, 7837-7841.

Torchilin, V.P. (2005). Recent advances with liposomes as pharmaceutical carriers. *Nature Reviews Drug Discovery*, 4, 145-160.

Tseng, Y.-L., Liu, J.-J. Hong, R.-L. (2002). Translocation of liposomes into cancer cells by cell-penetrating peptides penetratin and tat: A kinetic and efficacy study. *Molecular Pharmacology*, 62, 864-872.

Umut, E., Pineider, F., Arosio, P., Sangregorio, C., Corti, M., Tabak, F., Lascialfari, A. Ghigna, P. (2012). Magnetic, optical and relaxometric properties of organically coated gold,äimagnetite (au,äife3o4) hybrid nanoparticles for potential use in biomedical applications. *Journal of Magnetism and Magnetic Materials*, 324, 2373-2379.

Valentine, M.T., Perlman, Z.E., Gardel, M.L., Shin, J.H., Matsudaira, P., Mitchison, T.J. Weitz, D.A. (2004). Colloid surface chemistry critically affects multiple particle tracking measurements of biomaterials. *Biophysical Journal*, 86, 4004-4014.

Vanderkrol, A.R., Mur, L.A., Beld, M., Mol, J.N.M. Stuitje, A.R. (1990). Flavonoid genes in petunia - addition of a limited number of gene copies may lead to a suppression of gene-expression. *Plant Cell*, 2, 291-299.

Verma, A. Stellacci, F. (2010). Effect of surface properties on nanoparticle-cell interactions. *Small*, 6, 12-21.

Voltairas, P.A., Fotiadis, D.I. Michalis, L.K. (2002). Hydrodynamics of magnetic drug targeting. *Journal of Biomechanics*, 35, 813-821.

Waleh, N.S., Gallo, J., Grant, T.D., Murphy, B.J., Kramer, R.H. Sutherland, R.M. (1994). Selective down-regulation of integrin receptors in spheroids of squamous-cell carcinoma. *Cancer Research*, 54, 838-843.

Walker, F.O. (2007). Huntington's disease. *The Lancet*, 369, 218-228.

Wang, Y.H., Liu, S., Zhang, G., Zhou, C.Q., Zhu, H.X., Zhou, X.B., Quan, L.P., Bai, J.F. Xu, N.Z. (2005). Knockdown of c-myc expression by rnai inhibits mcf-7 breast tumor cells growth in vitro and in vivo. *Breast Cancer Research*, 7, R220-R228.

Weinstein, I.B. (2002). Cancer: Addiction to oncogenes - the achilles heal of cancer. *Science*, 297, 63-64.

Whitehead, K.A., Langer, R. Anderson, D.G. (2009). Knocking down barriers: Advances in sirna delivery. *Nature Reviews Drug Discovery*, 8, 129-138.

Widder, K.J., Senyei, A.E., Reich, S.D. Ranney, D.F. (1978a). Magnetically responsive microspheres as a carrier for site-specific delivery of adriamycin. *Proceedings of the American Association for Cancer Research*, 19, 17-17.

Widder, K.J., Senyei, A.E. Scarpelli, D.G. (1978b). Magnetic microspheres - model system for site specific drug delivery invivo. *Proceedings of the Society for Experimental Biology and Medicine*, 158, 141-146.

Wittung, P., Kajanus, J., Edwards, K., Haaima, G., Nielsen, P.E., Norden, B. Malmstrom, B.G. (1995). Phospholipid membrane permeability of peptide nucleic acid. *FEBS Lett*, 375, 27-9.

Wu, S.Y., Zhang, L.J., Zhong, J.H. Zhang, Z.L. (2010). Dual contrast magnetic resonance imaging tracking of iron-labeled cells in vivo. *Cytotherapy*, 12, 859-869.

Xiao, Y., Forry, S.P., Gao, X., Holbrook, R.D., Telford, W.G. Tona, A. (2010). Dynamics and mechanisms of quantum dot nanoparticle cellular uptake. *Journal of Nanobiotechnology*, 8, 13.

Zaki, N.M., Nasti, A. Tirelli, N. (2011). Nanocarriers for cytoplasmic delivery: Cellular uptake and intracellular fate of chitosan and hyaluronic acid-coated chitosan nanoparticles in a phagocytic cell model. *Macromolecular Bioscience*, 11, 1747-1760.

Zamore, P.D. (2006). Rna interference: Big applause for silencing in stockholm. *Cell*, 127, 1083-1086.

Zeller, K.I., Zhao, X., Lee, C.W.H., Chiu, K.P., Yao, F., Yustein, J.T., Ooi, H.S., Orlov, Y.L., Shahab, A., Yong, H.C., Fu, Y., Weng, Z., Kuznetsov, V.A., Sung, W.-K., Ruan, Y., Dang, C.V. Wei, C.-L. (2006). Global mapping of c-myc binding sites and target gene networks in human b cells. *Proceedings of the National Academy of Sciences of the United States of America*, 103, 17834-17839.

Zhang, H., Lee, M.-Y., Hogg, M.G., Dordick, J.S. Sharfstein, S.T. (2010). Gene delivery in three-dimensional cell cultures by superparamagnetic nanoparticles. *Acs Nano*, 4, 4733-4743.

Zhang, L.W. Monteiro-Riviere, N.A. (2009). Mechanisms of quantum dot nanoparticle cellular uptake. *Toxicological Sciences*, 110, 138-155.

Zimmermann, T.S., Lee, A.C.H., Akinc, A., Bramlage, B., Bumcrot, D., Fedoruk, M.N., Harborth, J., Heyes, J.A., Jeffs, L.B., John, M., Judge, A.D., Lam, K., Mcclintock, K., Nechev, L.V., Palmer, L.R., Racie, T., Rohl, I., Seiffert, S., Shanmugam, S., Sood, V., Soutschek, J., Toudjarska, I., Wheat, A.J., Yaworski, E., Zedalis, W., Koteliansky, V., Manoharan, M., Vornlocher, H.P. Maclachlan, I. (2006). Rnai-mediated gene silencing in non-human primates. *Nature*, 441, 111-114.

Zukiel, R., Nowak, S., Wyszko, E., Rolle, K., Gawronska, I., Barciszewska, M.Z. Barciszewski, J. (2006). Suppression of human brain tumor with interference rna specific for tenascin-c. *Cancer Biology & Therapy*, 5, 1002-1007.